PACIFIC EARTHQUAKE ENGINEERING RESEARCH CENTER

Effects of Large Velocity Pulses on Reinforced Concrete Bridge Columns

Greg L. Orozco
University of California, San Diego

and

Scott A. Ashford
University of California, San Diego

PEER 2002/23
APRIL 2002

Effects of Large Velocity Pulses on Reinforced Concrete Bridge Columns

Greg L. Orozco
Department of Structural Engineering
University of California, San Diego

Scott A. Ashford
Department of Structural Engineering
University of California, San Diego

Final report on research supported primarily by the
Earthquake Engineering Research Centers
Program of the National Science Foundation under
Award Number EEC-9701568

PEER Report 2002/23
Pacific Earthquake Engineering Research Center
College of Engineering
University of California, Berkeley

April 2002

ABSTRACT

The study of near-field effects has been ongoing since the 1971 San Fernando earthquake in California. However, not until the 1994 Northridge earthquake in the Los Angeles area and the 1995 Kobe earthquake in Japan, where fault ruptures occurred near high-density urban settings, did structural engineers take an interest in how large velocity pulses affect structures. The large velocity pulse is a characteristic of near-field motion, which is described as the cumulative effect of almost all of the seismic radiation concentrated in one location.

To study the effects of the large velocity pulse, three 22% scale bridge columns were tested at UC San Diego, each column having dimensions of 1830 mm (72 in.) in height and 410 mm (16 in.) in diameter. The bridge columns were subjected to a velocity pulse followed by a cyclic loading history. Two out of the three test specimens were loaded dynamically and the third statically.

By comparing the results of the three tests, it was observed that the high strain rate increased the strength of the bridge column by 10% to 15%. Another finding was that a plastic hinge length equal to the radius of the bridge column produced a better conversion from curvature to displacement. Finally, the velocity pulse had minimal effect on the overall performance of the bridge column.

ACKNOWLEDGMENTS

This work was supported in part by the Pacific Earthquake Engineering Research Center through the Earthquake Engineering Research Centers Program of the National Science Foundation under award number EEC-9701568. The opinions, findings, conclusions, and recommendations expressed herein are those of the authors and do not necessarily reflect the views of PEER.

CONTENTS

LIST OF FIGURES

LIST OF TABLES

LIST OF SYMBOLS

E_{dyn}	Dynamic modulus of elasticity of concrete
E_{stat}	Static modulus of elasticity of concrete
$\in$	Strain rate
f_{dyn}	Dynamic compressive strength of concrete
f_{stat}	Static compressive strength of concrete
f_{cm}	Mean static strength of concrete
$\varepsilon_{u,\ dyn}$	Dynamic ultimate compression strain of concrete
$\varepsilon_{u,\ stat}$	Static ultimate compression strain of concrete
$f_{s,\ dyn}$	Dynamic tensile strength of steel
$f_{s.stat}$	Static tensile strength of steel
κ	Coefficient of steel and strength type
$\varepsilon_{us,\ dyn}$	Dynamic ultimate tensile strain of steel
$\varepsilon_{us,\ stat}$	Static ultimate tensile strain of steel
K_i	Initial slope, yield stiffness
E_c	Modulus of elasticity of concrete
I_e	Effective moment of inertia
L	Height of the bridge column
K_2	Secondary slope, post-yield stiffness
Δ_y	Yield displacement
ϕ_y	Yield curvature as specified in the SEQMC output
Δ_P	Plastic displacement
ϕ_m	Maximum curvature
L_p	Plastic hinge length
d_b	Diameter of the longitudinal bar
f_y	Yield stress of the longitudinal bar
Δ	Total displacement

1 Introduction

The results of a research program to evaluate the performance of 22% scale single bridge columns subjected to a large velocity pulse are presented in this report. The main objective of the research program is to investigate strain rate effects in identical test specimens.

Near-source effects can be broken down into three types of pulses: acceleration, velocity, and displacement. The velocity pulse motion, sometimes referred to as "fling," represents the cumulative effect of almost all of the seismic radiation from the fault (Somerville, 1997). From a seismological perspective, the velocity pulse is more commonly found in earthquake records than compared to acceleration and displacement pulses. Although from the engineer's standpoint, the velocity pulse can be a better indicator of damage than the acceleration pulse, the damage potential is also dependent on the peak displacement during the pulse (Hall et al., 1995). The displacement pulse without the high velocity pulse does not have a high damage potential because the structure has time to react to the displacements.

After the 1971 San Fernando earthquake, engineers and seismologists realized the potential damage that may occur due to the effects of near-source ground motions on structures. The damage observed during the 1994 Northridge, California, and the 1995 Kobe, Japan, earthquakes proved the engineer's hypothesis that structures located within the near-field area had more severe damage than structures located outside of this zone. These earthquakes provided a wealth of new information about the behavior of engineered structures because the respective epicenters were in urban settings. Based on the data collected, building designers started studying the near-source effects on buildings. Their research and findings led to implementing design factors in the 1997 Uniform Building Code (UBC, 1997) that began to account for near-fault motions. Additional design factors to more accurately model near-source effects were implemented in the 2000 International Building Code. Bridge designers recognized the damage potential for buildings and concluded that bridges also need to be examined.

A study was conducted under the Pacific Earthquake Engineering Research (PEER) Center's first-year investigation of the Effects of Large Velocity Pulses on Bridge Columns. The study was a multi-university collaborative effort, which involved the University of California at San Diego (UCSD), Berkeley (UCB), and Irvine (UCI), and the University of Southern California (USC) and California Institute of Technology (Caltech). The original column design was completed at UCB for a shake table test with a mass on top of the column. To develop a suite of comparable information, the design was distributed to UCSD, UCI, and USC for further testing with different loading protocols, while Caltech performed analytical studies of the effects of velocity pulses on the bridge columns.

At UCSD, three circular bridge columns were tested at the Charles Lee Powell Structural Systems Research Laboratories. Each test had the same loading history but had a different loading rate. One test was performed with an actuator that had a quasi-static loading history, stopping at peaks in both the positive and negative directions. Another test was completed with an actuator at a rate of 0.33 m/s (13 in./s). A third test was completed on the shake table with a loading rate of 1 m/s (39 in/s). In this report, the quasi-static test is designated the "Slow Test," the test with the actuator loaded dynamically is called the "Fast Test," and the test on the shake table is referred to as the "Dynamic Test."

In addition to the first-year testing of the column, Kenneth Cox, a UCSD graduate researcher analyzed approximately 34 earthquake records that exhibited velocity pulses. The information in these records indicated that the mean pulse was 1 m/s (39 in./s).

In the following chapters, further discussion of the design and construction of the bridge columns, methodology of the pulse, and evaluation of the three tests are presented. A review of articles concerning near-fault ground motions, strain rate effects, and previous experimental results is included to provide background information.

2 Literature Review

This section features reviews of articles involving descriptions of near-fault ground motions, strain rate effects, and the effects of near-source large velocity pulses on structures. The review discusses why the articles are appropriate for the research, examines experiments and equations presented in the articles, and provides summaries of the data applicable to this report.

2.1 NEAR-SOURCE EFFECTS

The study of the near-source large velocity pulse, also known as "fling," is a fairly new topic in earthquake engineering. The first time engineers and seismologists realized that velocity pulses may exist in strong ground motion records was after the 1971 San Fernando, California, earthquake. Bertero et al. (1978) were some of the first to study velocity pulses and their effects on structures. After the 1994 Northridge and 1995 Kobe earthquakes, many engineers and seismologists began to study the components of velocity pulses. A particular cause of velocity pulses, known as "directivity," has been studied by Attalla et al. (1998), Hall and Aagaard (1998), Hall et al. (1995), and Somerville and Grave (1993). "

Somerville (1997) described the effects of rupture directivity with an empirical model and provided guidelines for the specifications of response spectra and time histories. Abrahamson (1998) discussed the large pulses in various velocity time histories. In this paper, directivity effects were explained by the rupture process and by wave propagation.

Directivity effects can be classified as forward, reverse, and neutral. Forward directivity is when the direction of the rupture propagates toward the site, while reverse directivity is when the rupture progresses away from the site. Neutral directivity is when the site is perpendicular to the ruptured fault. Within the research community, the term "directivity effects" has come to mean "forward directivity effects" because forward directivity is more likely to be responsible for the ground motions that cause damage. Figure 2.1 portrays the three zones of directivity, with the star representing the epicenter and the black line indicating the fault.

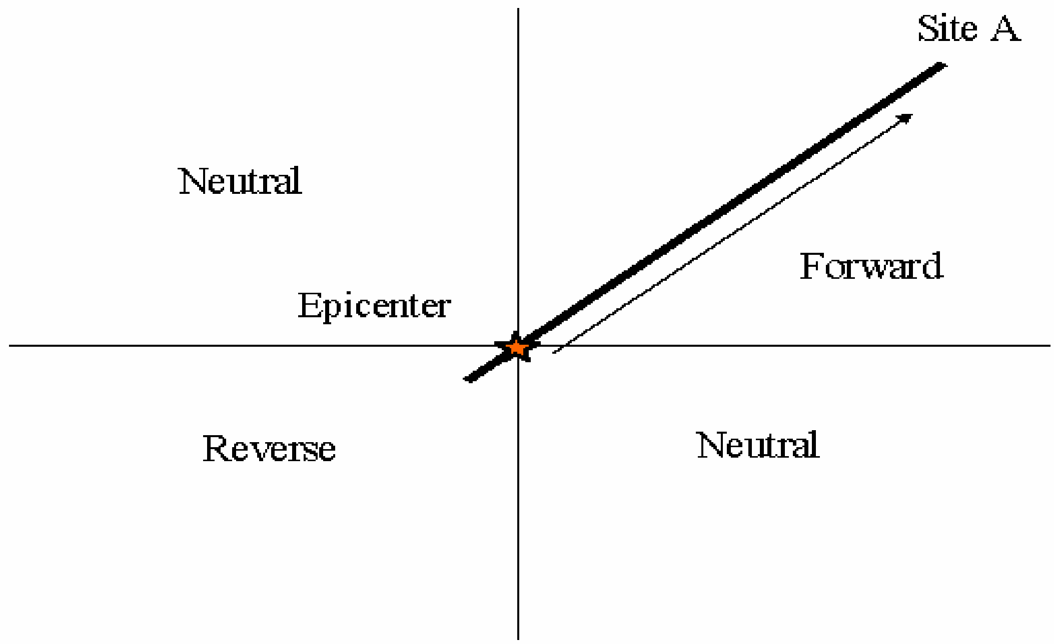

Fig. 2.1 Zones of directivity

The rupture often propagates at a velocity close to the velocity of shear wave radiation (Abrahamson 1998; Somerville 1997). The energy is accumulated in front of the propagating rupture and is expressed as a large velocity pulse. This energy propagation is similar to a sonic boom because the energy is concentrated in one site, Site A, as shown in Figure 2.2.

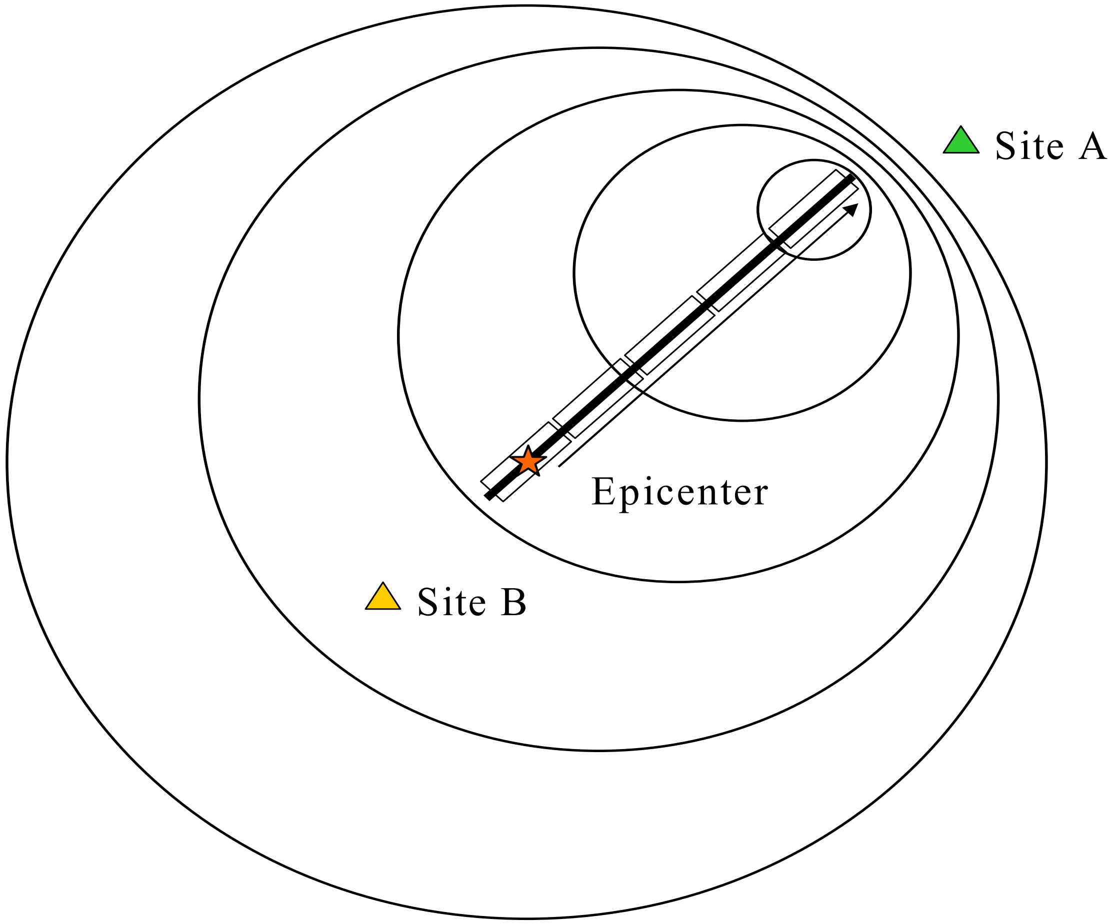

Fig. 2.2 An example of forward directivity effect on Site A

2.2 STRAIN RATE

When concrete and reinforcing steel are subjected to high strain rates, their properties experience an increase in the elastic modulus, the strength, and the yield strain. To date, there has been a limited amount of testing on strain rate effects combined with a lack of sufficient understanding of the behavior of the material. Researchers such as Mander et al. (1988), Bischoff and Perry (1995), Tedesco et al. (1993), Restrepo-Posada (1993), and Restrepo-Posada et al. (1994) have studied the effects of strain rate and have derived models and empirical formulas to explain the change in the properties.

Ammann and Nussbaumer (1995) presented empirical formulas and graphs, which correlate the increase due to the dynamic amplification factor of the material to strain rate and to static strength. They also limited the material properties to plain concrete with normal weight aggregate and reinforcing steel, which are the same criteria as used in this research. The 1995 paper presented a direct and practical approach for structural engineers who are faced with strain rate problems.

Ammann and Nussbaumer developed a set of equations that help to characterize strain rate effects on concrete and steel. The increase due to strain rate effects on the elastic modulus of concrete can be described as:

$$E_{dyn}/E_{stat} = (\in/\in_o)^{0.026} \text{with } \in_o = 30 \cdot 10^{-6} \text{ s}^{-1} \quad (2.1)$$

the compressive strength of concrete as:

$$f_{dyn}/f_{stat} = (\in/\in_o)^{1.026\alpha} \text{for } \in_o \leq 30 \text{ s}^{-1} \quad (2.2)$$

$$\alpha = 1/(5+3 \cdot f_{cm}/4) \quad (2.3)$$

and the ultimate compression strain of concrete as:

$$\varepsilon_{u,\,dyn}/\varepsilon_{u,\,stat} = (\in/\in_o)^{0.02} \text{ with } \in_o = 30 \cdot 10^{-6} \text{ s}^{-1} \quad (2.4)$$

The increase of concrete tensile strength due to strain rate effects was neglected because concrete has relatively small tensile strength. The increase in strength due to strain rate effects on steel tensile strength is defined as:

$$f_{s,\,dyn}/f_{s.stat} = 1 + \kappa \cdot \ln(\in/\in_o) \quad (2.5)$$

(mild steel $\kappa_{yield} = 12 / f_{yield\ stat}$ otherwise $\kappa = 1$), and the ultimate tensile strain is described as:

$$\varepsilon_{us,\,dyn}/\varepsilon_{us,\,stat} = (\in/\in_o)^{0.02} \text{ with } \in_o = 30 \cdot 10^{-6} \text{ s}^{-1} \quad (2.6)$$

The elastic modulus of steel is unaffected by the loading rate.

Al-Haddad (1995) studied the curvature ductility capacity of reinforced concrete sections under different rates of loading by comparing experimental results with a theoretical model. Al-Haddad performed a parametric study of ductility factors versus tension steel ratios for a rectangular reinforced concrete beam. The study was broken down further by varying the compression steel to tension steel ratios and modifying the rate of loading from static loading to a strain rate of 0.05/sec, and finally to a rate of 0.1/sec. Moment-curvature analysis of a section is generally performed under monotonically increasing loads that depict only the first quarter of a hysteretic loop of a plastic hinge rotation. Therefore, curvature-steel ratio comparisons neglect the calculation of an approximate plastic hinge length, which may lead to errors in the analysis of results.

Some researchers postulate that the overall strength of the testing specimen will level off as the strain rate increases. In the course of each study, new sets of relationships were derived.

The designer should exercise caution in utilizing these results because that test technique and method of analysis varies from researcher to researcher.

2.3 NEAR-SOURCE EFFECTS ON STRUCTURES

The study of the effects of near-source ground motions on structures has generally been limited to the effects on buildings. Bertero et al. (1978) studied buildings that were severely damaged during the 1971 San Fernando earthquake and the implications of pulses on pre-1971 aseismic design methods. Hall et al. (1995) performed an analytical study on a 20-story steel moment frame structure and a three-story base-isolated building in the Greater Los Angeles area. Iwan (1996), Attalla et al. (1998), and Hall and Aagaard (1998) completed further analytical studies on near-source effects on buildings.

Mayes and Shaw (1997) evaluated the response of 16 columns designed using the Caltrans Bridge Design Specifications to several seismic events involving near-fault ground motions. For analysis purposes, a bilinear hysteric loop was utilized to represent the column.

The 16 columns studied by Mayes and Shaw had heights ranging from 6.1 m to 15.2 m, with periods ranging from 0.7 sec to 3.8 sec. The columns were assumed to be fixed at the base and free at the top, with an axial load on the top of the column. The ANSR-II computer program with 5% viscous damping was utilized to model the column with bilinear hysteretic properties.

The initial stiffness of the column is calculated as:

$$K_i = 3E_cI_e/L^3 \tag{2.7}$$

and the secondary slope as:

$$K_2 = 0.03\ K_i \tag{2.8}$$

Strength and stiffness degradation and P-Δ effects were neglected in the model.

Mahin and Hachem (1998) presented an analytical investigation concentrating on the response of columns subjected to near-source ground motions. Both elastic and inelastic materials were examined with a series of simplified structures and ground motions. The columns used in this study were given the property of bilinear hysteretic behavior, whereas a finite element model was used to obtain a realistic inelastic response. Using the finite element model, a parametric study was conducted by varying the aspect ratio, reinforcement ratio, axial load, and input ground motion. Trends and results showed that the elastic models are acceptable, but that there are some uncertainties with an elastic period that is shorter than the duration of any damaging pulse in the records associated with fault rupture.

Researchers for both of the above investigations concluded that the elastic model predicts the peak response of the columns well, provided that the period is less than two times the predominate period of the excitation. It was also observed that the bilinear hysteretic properties performed relatively well subjected to recorded ground motions, but further research is needed on their response to synthetic ground motions. Both studies were based on limited work; thus further investigation should be carried out to fully understand near-source effects on bridges and their components.

3 Loading History

As part of the PEER Year-One study, UCSD analyzed 34 earthquake time histories showing a velocity pulse, in order to develop a mean peak velocity pulse to be used as input time histories for bridge column testing. The mean velocity pulse from the 34 earthquake records was determined to be 1 m/s (39 in./s). This chapter presents a limited discussion on the development of the velocity pulse and the input time histories of three tests.

As previously stated, UCSD performed three tests, each with a different rate of loading. Of the two tests using a hydraulic actuator, one is referred to as the "Slow Test," or "quasi-static test." The other, referred to as the "Fast Test," had an input peak velocity of 0.33 m/s (13 in./s). Finally, the shake table, or "Dynamic Test," had an input peak velocity of 1 m/s (39 in./s).

3.1 DEVELOPMENT OF THE VELOCITY PULSE

The development of the velocity pulse was intended to capture the average properties of duration, peak velocity, and shape in a simplified form for structural testing. The first step consisted of extracting a full cycle of each pulse from the 34 near-field earthquake records. Then an average pulse was constructed from the 34 pulses. Next, the records were modified to have the same number of data points and a time step that matched the average period, thus normalizing each pulse. Since the peak velocity value in the average pulse did not match the average peak from all of the records, the average pulse was scaled up to match the value of the average peak velocity. The program NONLIN, "Nonlinear Time-History Analysis," (Mathematics Archives) was used to obtain the displacement response of the bridge column under the scaled average velocity pulse at the ground surface. NONLIN solves for the response of bilinear, single-degree-of-freedom structures subjected to earthquake excitation. Although more complex models are available, the use of a simple model was considered appropriate for the simple pulse developed.

3.2 INPUT TIME HISTORIES

In an attempt to develop a collection of information, UCI shared with UCSD the loading history of one of the two tests UCI performed under the PEER Year-One velocity pulse investigation. The UCI loading history was without an initial pulse loading, but was composed of a cyclic loading history based on drift ratios of 0.5%, 1.0%, 1.5%, 2.0%, 3.0%, 4.0%, 5.0%, and 6.0%. Each drift ratio had three peaks in both the positive and negative directions. The input time histories for the tests at UCSD were a combination of the pulse developed by UCSD and the cyclic loading history from UCI. The combination of the velocity pulse with the traditional cyclic loading provides a simple means of comparing the results of the velocity pulse tests to the UCI non-pulse loading test, as well previous tests carried out at UCSD.

In the first test the input loading rate was applied in a quasi-static manner. This was accomplished by stopping the test at the peak displacements and at other points of interest during the test. The input time history in this Slow Test added two cycles of 7% drift ratios to ensure failure of the column. Figure 3.1 shows the displacement history of the Slow Test.

The input displacement time history used for the Fast Test was scaled to the peak achievable velocity of 0.33 m/s (13 in./s) for a 979 kN (220 kip) capacity actuator. Figure 3.2 shows the displacement time history used for the Fast Test.

The input displacement time history in the Dynamic Test was scaled to the peak velocity of the shake table of 1 m/s (39 in./s). The saw-toothed time history, as in the first two tests with an actuator, was smoothed into a sinusoidal time history to avoid infinite acceleration. Several seconds of zero displacement were added in between drift ratio magnitudes. The saw-toothed displacement time history for the Dynamic Test is plotted in Figure 3.3.

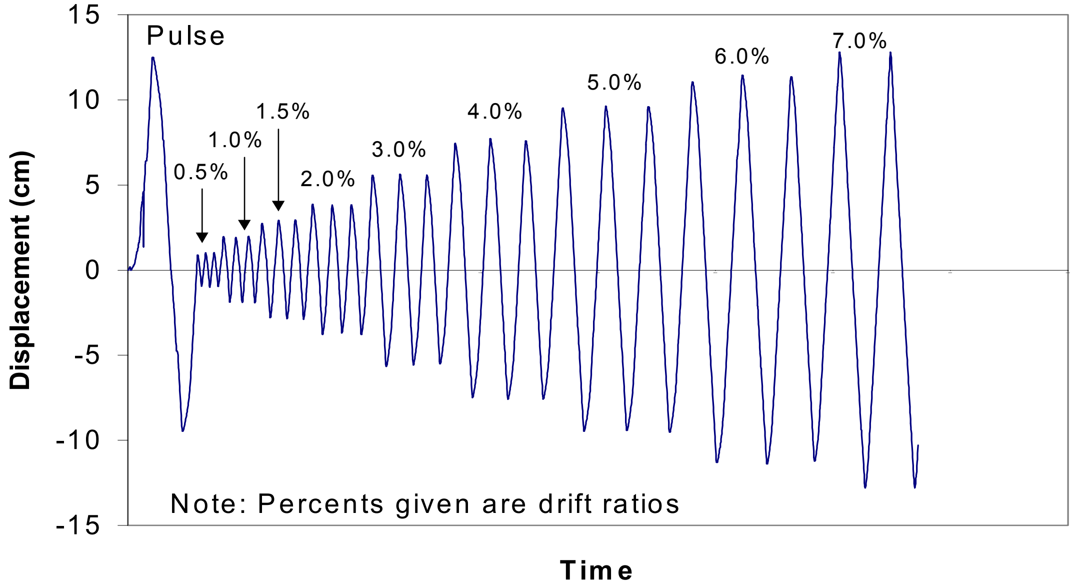

Fig. 3.1 Input time history for Slow Test

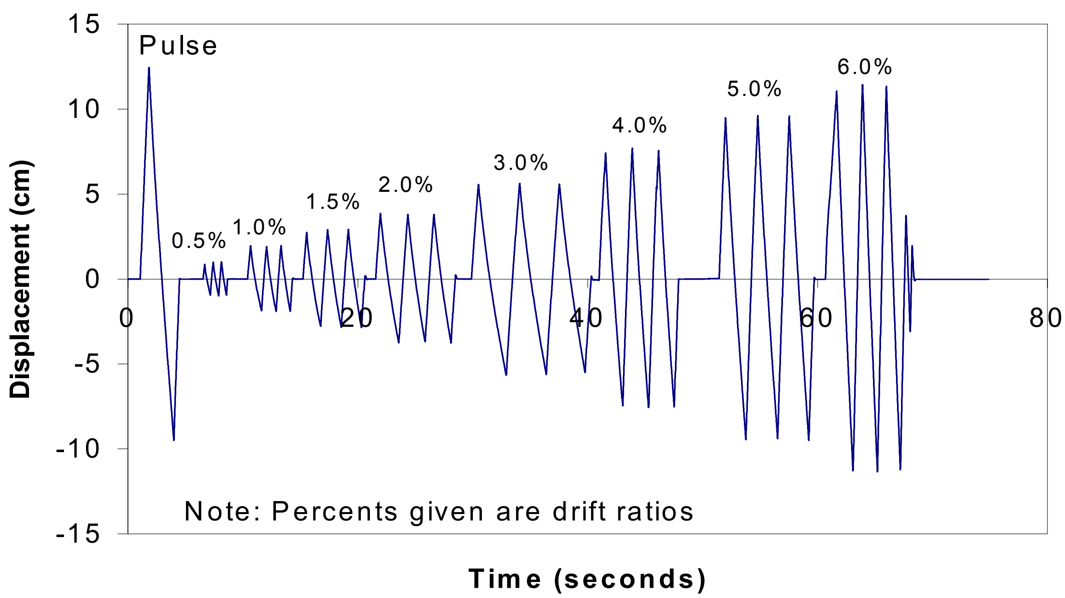

Fig. 3.2 Input time history for Fast Test

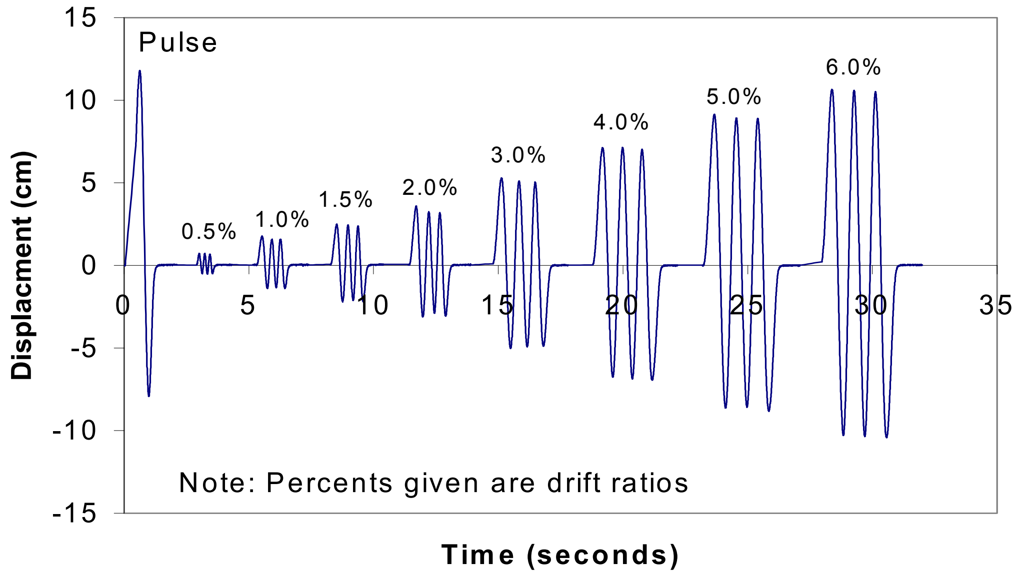

Fig. 3.3 Input time history for Dynamic Test

4 Test Design and Prediction

This chapter discusses the design methodology of the bridge column, the construction of the bridge column, the compressive strength of the concrete, and the tensile strength of the steel.

The design of the three bridge columns tested at UCSD was based on the bridge columns used for the UCB shake table tests. They were designed according to Caltrans ARS spectra and scaled to 22%. The axial load ratio and concrete strength were first assumed, then the axial load and mass were determined, and the bridge column was designed to provide enough strength to satisfy Caltrans ARS Spectra (Plot B) for the bridge column's period. An elevation view of the bridge column is seen in Figure 4.1.

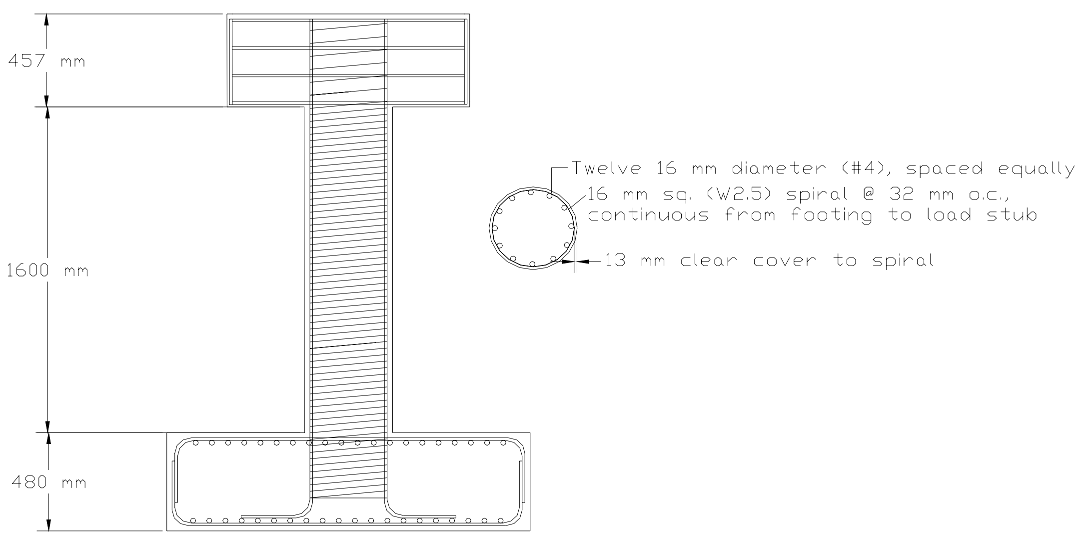

Fig. 4.1 Bridge column elevation

4.1 SIMILITUDE

An obvious goal of any experiment is to make the experimental results as applicable as possible to actual situations. To achieve this end, the concept of similitude is often used to convert the measurements of experimental testing to describe the behavior of full-sized structural systems. Experimental test data results are usually thought of as models and are used to study the phenomenon of interest under carefully controlled conditions. From these models, empirical formulas can be developed to specifically assess the characteristics of full-sized structures. Thus it is necessary to establish the relationship between the experimental model and the actual structure.

The loading rate varied for the three bridge columns tested at UCSD. The relationship for the applied loading rate to measured strain is based on the scale factor. For instance, the prototype column has a 1 m/s (39 in./s) loading rate; therefore a 22% scale column should have an applied rate of 0.22 m/s (8.6 in./s). In an attempt to study the effects of the strain rate based on the loading rate, the scaled loading rate was not utilized for the UCSD test specimens.

Specifically, for the three bridge columns tested at UCSD, the conversion from 22% scale specimens to full-size structure was not a consideration for this report. The intent of the research and this report was to build a database of information with the other PEER universities, not to study a specific bridge structure.

4.2 DESIGN OF THE BRIDGE COLUMN

The test specimen had a diameter of 410 mm (16 in.) that corresponds to an 1830 mm (72 in.) prototype bridge column diameter. In addition, the test specimen had a height of 1830 mm (72 in.) that corresponds to the prototype bridge column height of 8230 mm (324 in.). The height of the bridge column was measured from the top of the footing to the center of the load stub. The longitudinal reinforcing steel consisted of twelve 16 mm diameter (#4) bars that were spaced equally, which produced a steel/concrete ratio of 1.2%. The longitudinal steel had a yield strength of 416 MPa (Grade 60), conforming to ASTM 706 or equivalent, with a yield stress that should not exceed 520 MPa (75 ksi). The transverse reinforcement was 16 mm^2 (W2.5) ASTM with a yield strength of 555 MPa (Grade 80). The spiral was spaced at 32 mm (1.25 in.) on center continuous from the base of the footing to the top of the load stub. The concrete cover from the face of the bridge column to the face of the spiral was 13 mm (0.5 in.).

4.2.1 Design of the Footing

The footing design was based on the standard practice in the UCSD Powell Structural Lab. The footing was 1680 mm (66 in.) by 1680 mm (66 in.) and 480 mm (19 in.) in height. The reinforcement steel for the in-plane loading were 19 mm diameter (#6) U-shaped bars that had the dimensions of 1570 mm (62 in.) in width and 300 mm (12 in.) in height with a radius of 76 mm (3 in.) at the bend. The U-shaped bars were combined into 18 sets of oval shapes that had a height of 410 mm (16 in.) on-center. The 16 mm diameter (#5) straight bars in the out-of-plane loading direction were 1630 mm (64 in.) in length and placed in two rows of twenty. One row was placed in the top of the footing and the other row at the bottom of the footing. Finally, forty 10 mm diameter (#3) J-hooks that were 430 mm (16.75 in.) in height with a 100 mm (4 in.) arm were spaced equally throughout the footing.

4.2.2 Design of the Load Stub

Similar to the footing, the load stub design was based on the standard practice in the UCSD Powell Structural Lab. The load stub dimensions were 1118 mm (44 in.) by 610 mm (26 in.) and 457 mm (18 in.). The reinforcement steel was a set of four 13 mm diameter (#4) bars bent into a rectangle that had a length of 1060 mm (41.75 in.) on-center and a width of 603 mm (23.75 in.) on-center with a radius 25.4 mm (1 in.) at the bends. The first rectangle was tied in all corners 25.4 mm (1 in.) up on a 19 mm diameter (#6) straight bar with a length of 406 mm (16 in.). The next three rectangles were tied 114 mm (4.5 in.) on-center up from the first rectangle. In the plane of loading eight 19 mm diameter (#6) straight bars with a length of 1111 mm (43.75 in.) were spaced equally throughout the load stub. Finally, eight 19 mm diameter (#6) straight bars with a length of 654 mm (25.75 in.), were placed out-of-plane loading.

4.2.3 Concrete Mix Design

The following mix was designed to have a 28-day compressive strength of 27 MPa (4 ksi), but not to exceed 37.9 MPa (5.5 ksi). The mix content volume was designed for 0.76 cu m (1 cu yd) with a slump of 102 mm (4 in.) and consisted of:

9.5 mm (0.375 in.) pea gravel mix
962 kg (2120 lb) of WC sand (WC – Wash Concrete)
417 kg (920 lb) of 9.5 mm (0.375 in.) aggregate
345 kg (760 lb) of Type V cement
114 liters (30 gal) of water (total 167 liters (44.15 gal) @ plant)
1.12 liters (38 oz) of a water reducer admixture, WRDA 79

4.2.4 Construction of the Specimens

The procedure for building each bridge column specimen started by tying the bridge column and footing steel as specified in the design. The bridge column was then placed upright in the constructed footing. Next, the footing was poured to 480 mm (19 in.) in height. Following this, the load stub was built as specified in the design and tied to the top of the bridge column. Finally, the bridge column and load stub were poured together.

The slump was an average of 108 mm (4.25 in.) throughout both pours for the two tests with an actuator. The dynamic test had a slump of 114 mm (4.5 in.) for the footing, and the column and load stub had a slump of 178 mm (7 in.). The compression strength at 28 days, and on the day of the test for the footing, bridge column, and load stub that are presented in Tables 4.1 and 4.2.

Table 4.1 Concrete compressive strength of footing

Test	28 Day (MPa)	Day of the Test (MPa)
Slow Test	28.4	34.5
Fast Test	28.4	33.4
Dynamic Test	28.4	29.9

Table 4.2 Concrete compressive strength of bridge column and load stub

Test	28 Day (MPa)	Day of the Test (MPa)
Slow Test	29.0	34.4
Fast Test	29.0	30.2
Dynamic Test	31.8	32.1

A tension test was performed on the longitudinal bars and spiral reinforcing. The tensile test values for both the longitudinal bars are found in Table 4.3. During the spiral tensile tests, the spirals yielded at the grip, which did not provide a true yield value. This was due to the fact that the clamped down strength of the steel grips on the tension machine was too strong for the small size of the spirals. Therefore, the yield stress used for the analysis work was the specified yield strength of 555 MPa (Grade 80). The use of the specified yield strength of the spiral in the analysis was considered reasonable because the supplied yield strength of the longitudinal bars was within 7.5% maximum of the actual yield strength.

Table 4.3 Tensile strength of longitudinal bars

Test	Yield Stress (MPa)	Ultimate Stress (MPa)
Slow Test	446	737
Fast Test	446	737
Dynamic Test	428	705

4.3 INSTRUMENTATION SETUP

The primary instrumentation used on the bridge columns included strain gauges and string-activated potentiometers. Additional instrumentation beyond what was required was added as part of a performance based study. For this study, a large amount of extra linear potentiometers and strain gauges were added to the three specimens in order to measure the characteristics of the structure at various levels of damage. For further information on the performance based study, see Hose et al. (1999). Details of the instrumentation setup are discussed below.

4.3.1 Test Setup

The test setup for the Slow and Fast tests is shown in Figure 4.2. The test specimen was secured to the strong floor by eight 35 mm (1-3/8 in.), yield strength 1040 MPa (Grade 150) high-strength bars stressed to 667 kN (150 kips). A 979 kN (220 kip) capacity actuator, with a +/- 610 mm (24 in.) stroke, was attached in between the strong wall and load stub.

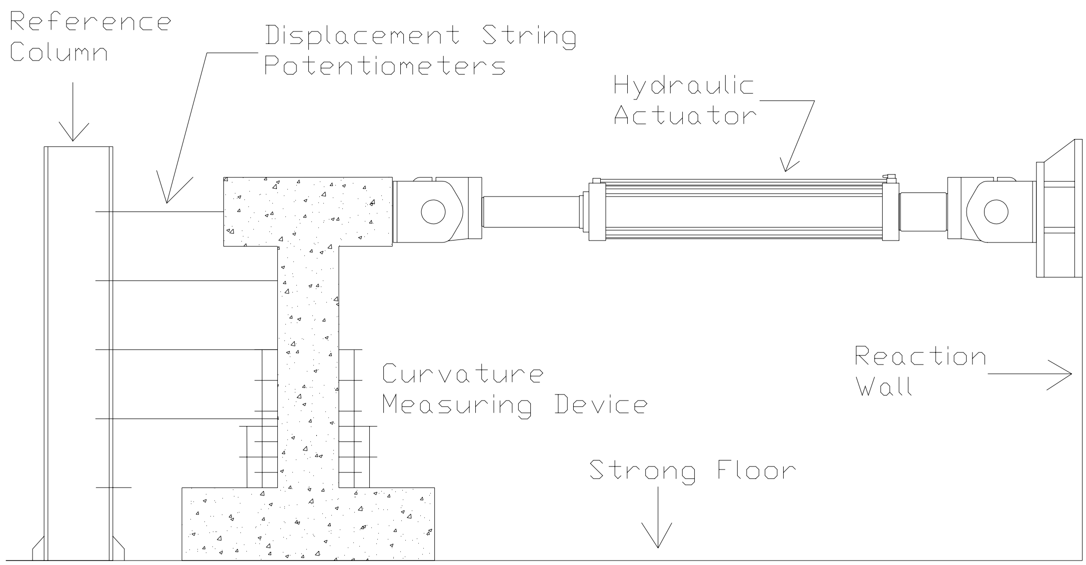

Fig. 4.2 Setup for Slow and Fast tests

A load-cell housed in the actuator measured the lateral load levels of the two tests. The tip-of-column lateral displacement was measured by a string linear potentiometer which was connected at mid-height of the load stub, or 1829 mm (72 in.) from the top of the footing. In addition, three more string linear potentiometers located at 457 mm (18 in.), 914 mm (36 in.), and 1372 mm (54 in.) from the top of the footing were attached to a reference column. Figure 4.3 depicts the elevations of the displacement string linear potentiometers.

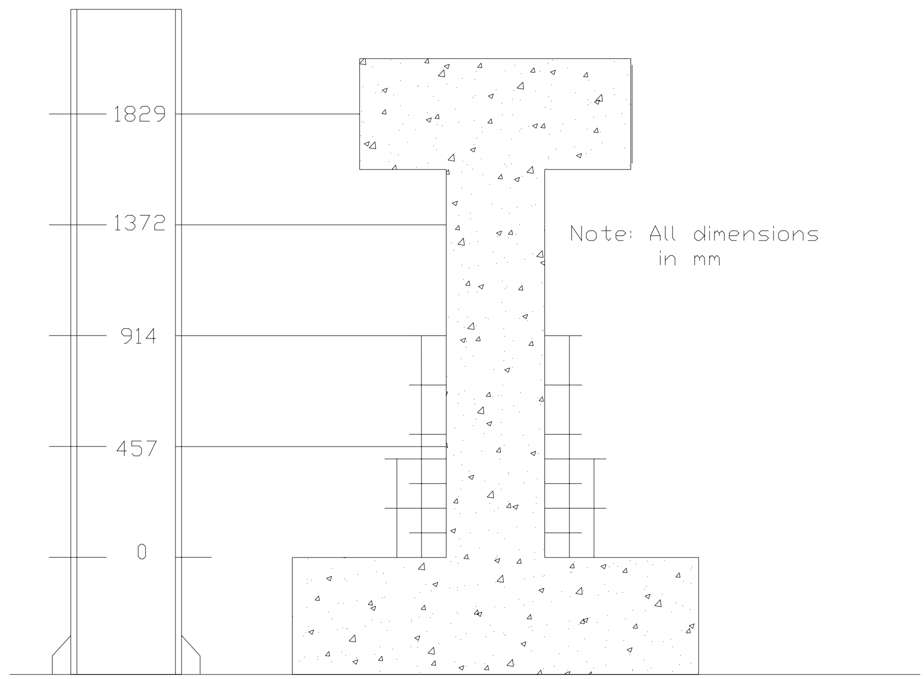

Fig. 4.3 Elevations of displacement string linear potentiometers for Slow and Fast tests

The setup for the Dynamic Test is shown in Figure 4.4. The test specimen was secured to the shake table by twenty 16 mm (5/8 in.), yield strength 250 MPa (Grade 36) threaded rods tightened to a snug fit with a quarter turn. There was no hydro-stone in between the base of the footing and the shake table. A 667 kN (150 kip) capacity actuator, with a +/- 254 mm (10 in.) stroke, was attached in between the strong wall and load stub. The top actuator was used to pin the load stub and prevent displacement.

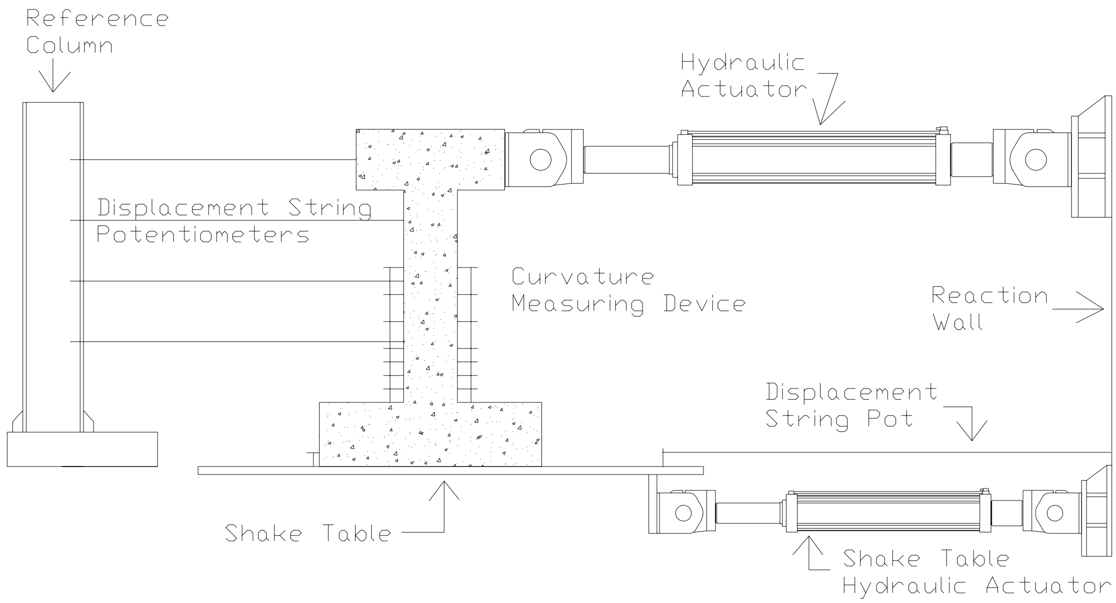

Fig. 4.4 Setup for Dynamic Test

The lateral load of the test was measured by a load-cell housed in the top actuator. The lateral displacements were measured by two means, the first being the internal transducer in the shake table, the second being a string linear potentiometer that was connected to the shake table. The internal load-cell in the actuator and a string linear potentiometer which was connected at mid-height of the load stub, or 1829 mm (72 in.) from the top of the footing, were used to verify that zero displacement at the top of the bridge column was achieved. Additional string linear potentiometers were attached to the column at three other locations: 356 mm (14 in.), 965 mm (38 in.), and 1372 mm (54 in.) from the top of the footing. Figure 4.5 shows the elevations of the displacement string linear potentiometers.

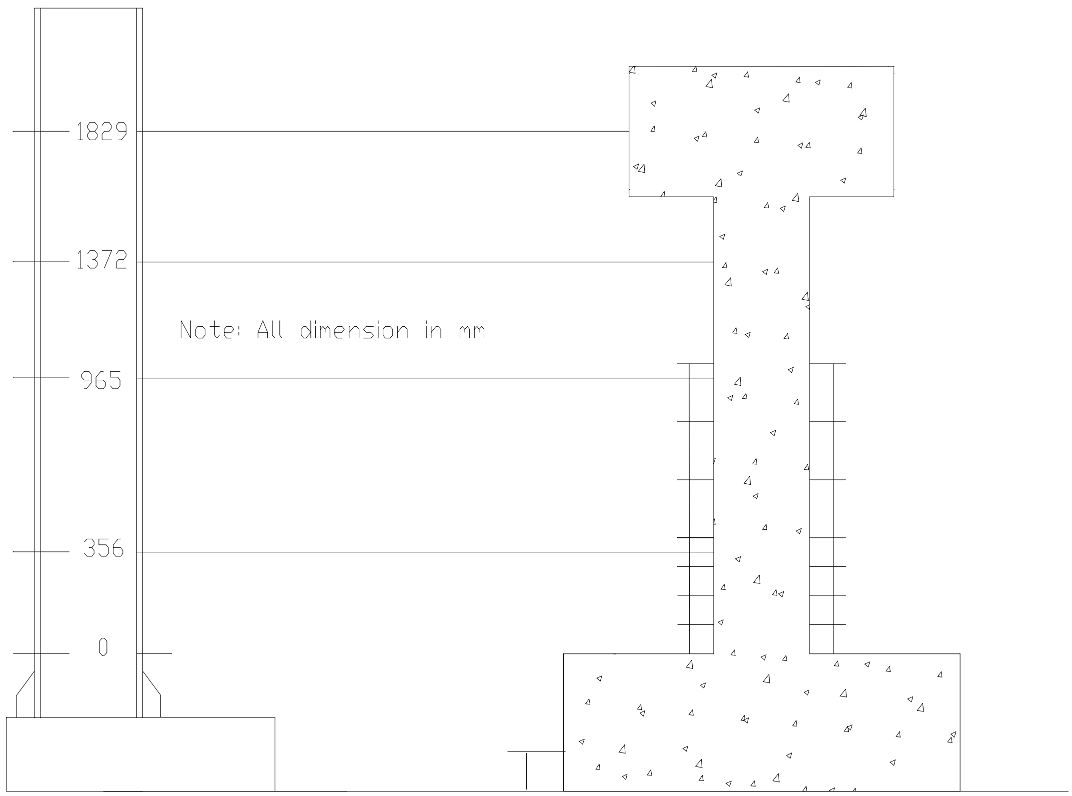

Fig. 4.5 Elevations of displacement string linear potentiometers for Dynamic Test

4.3.2 Curvature

A total of 22 linear potentiometers were placed on each of the bridge columns to measure the curvature distribution for the Slow and Fast Tests. For the in-plane curvature measurements, 18 linear potentiometers were installed on the bridge column in two rows with varying gauge lengths. The two rows with the different gauge lengths were an attempt to determine if a finer discretization of the gauge lengths would provide a better output versus a coarse discretization. Figure 4.6 shows the layout of the linear potentiometers for the in-plane curvature measurements. The remaining four linear potentiometers were placed in the out-of-plane loading direction, or perpendicular to the actuator, and measured strain penetration in the footing. The out-of-plane linear potentiometers had a gauge length of 203 mm (8 in.) and were spaced 203 mm (8 in.) apart.

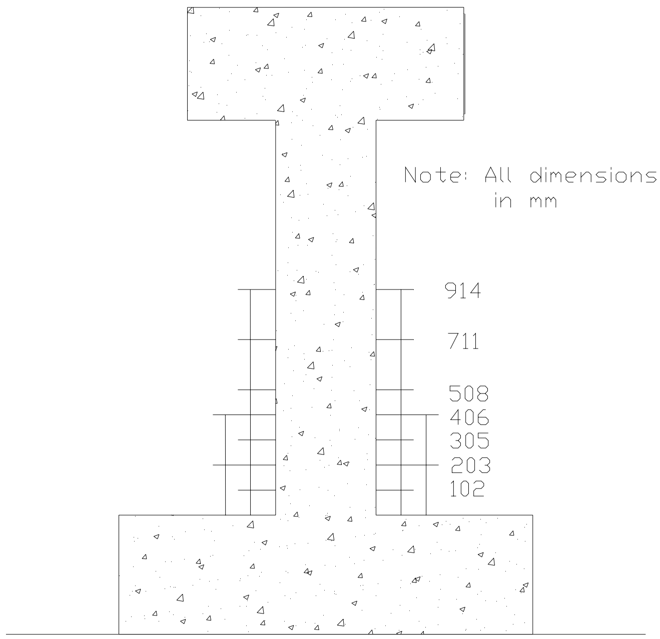

Fig. 4.6 Layout of linear potentiometers to measure curvature for in-plane loading for Slow and Fast tests

A total of 18 linear potentiometers were placed to measure curvature on the bridge column for the Dynamic Test. From the previous two tests with an actuator, it was observed that varying the gauge length provided similar output results in terms of precision in the measurement of the resulting curvature. Therefore, only 14 linear potentiometers were installed on the bridge column for the in-plane loading. Figure 4.7 shows the layout of the linear potentiometers for the in-plane loading. The remaining four linear potentiometers were placed in the out-of-plane loading direction in the same fashion as the previous test setup.

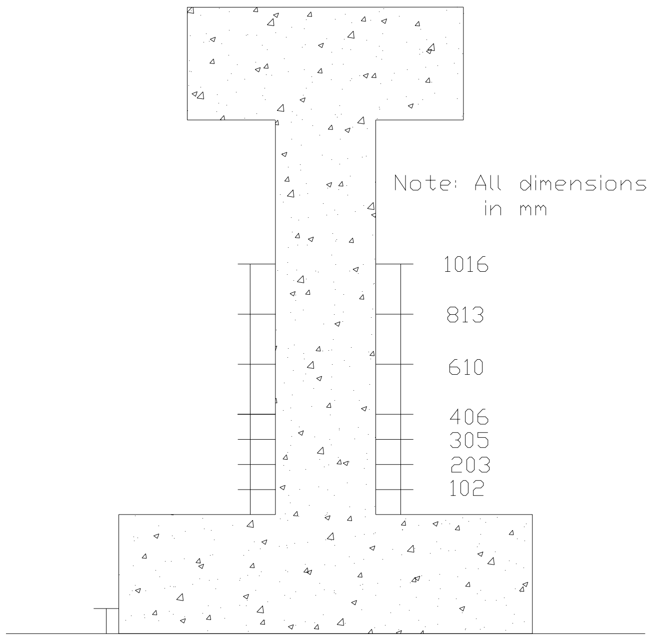

Fig. 4.7 Layout of linear potentiometers to measure curvature for in-plane loading for Dynamic Test

4.3.3 Strain Gauges

A total of 38 strain gauges were used to record the strains on the longitudinal bars and spirals of the bridge column and footing for the Slow and Fast tests. Twelve strain gauges were 5 mm (0.2 in.) high-yield gauges and the remaining gauges were 5 mm (0.2 in.) regular-yield gauges. Figure 4.8 depicts the locations and type of strain gauges on the longitudinal bars.

To record the strains on the spirals for the Slow and Fast Tests, 28 strain gauges were placed at various locations on the bridge column. All the strain gauges were 2 mm (0.08 in.) regular-yield gauges. Figure 4.9 shows the location of the strain gauges on the spirals.

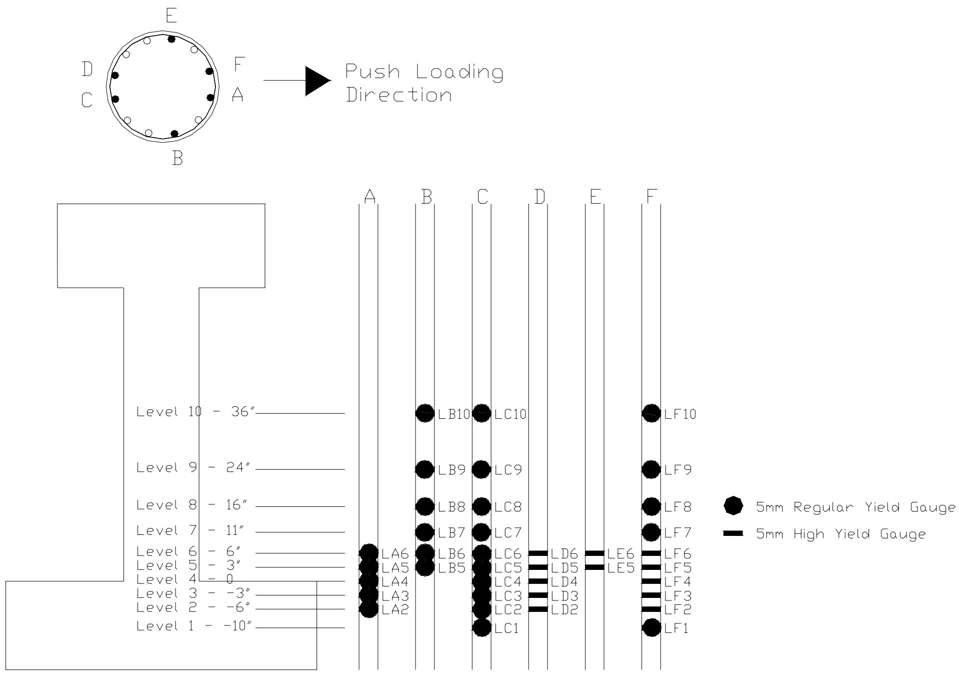

Fig. 4.8 Strain gauges on longitudinal bars for Slow and Fast tests

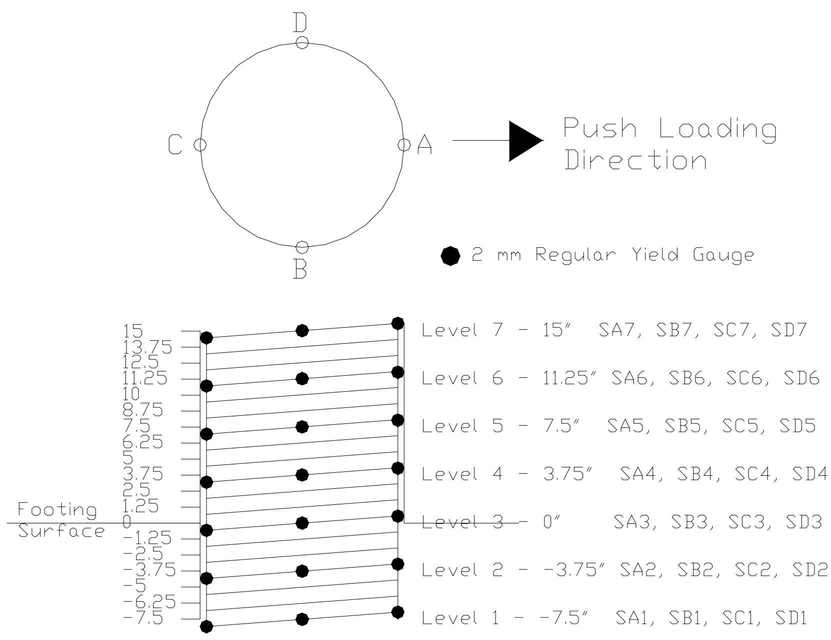

Fig. 4.9 Strain gauges on spirals for Slow and Fast tests

A total of 76 strain gauges were used to record the strains throughout the bridge column and footing for the Dynamic Test. There were 24 gauges attached to the longitudinal bars, which is less than the number used for the two actuator test specimens. Fewer strain gauges were used for this test because more strain gauges were placed on the spiral. This provided a means of obtaining more information about the strains in the hinge region. Figure 4.10 depicts the locations of the strain gauges on the longitudinal bars.

Figure 4.11 shows the location of the 52 strain gauges on the spirals for the Dynamic Test. For this test, 2 mm (0.08 in.) high-yield gauges in the hinge region were augmented by the 2 mm (0.08 in.) regular-yield gauges, which were placed through the test specimen.

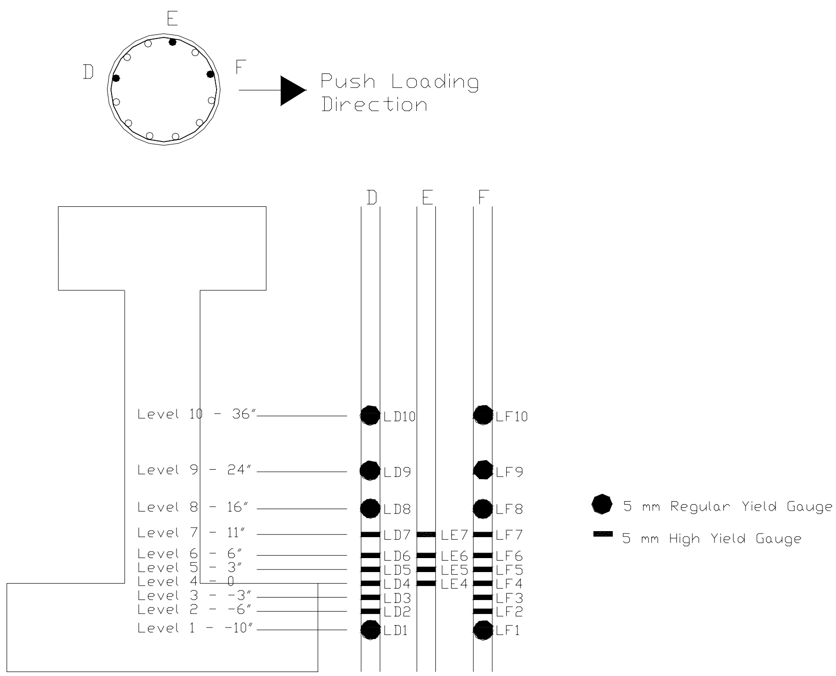

Fig. 4.10 Strain gauges on longitudinal bars for Dynamic Test

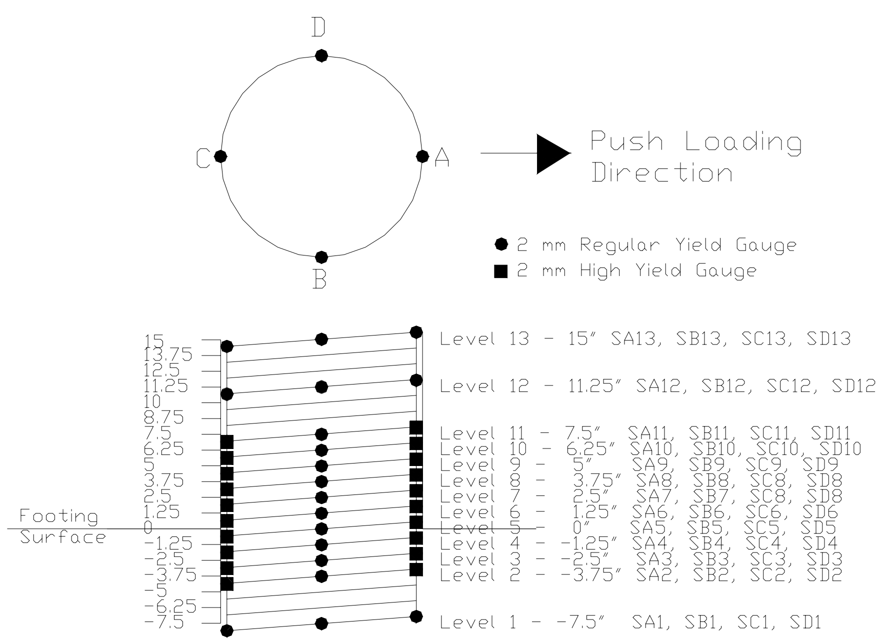

Fig. 4.11 Strain gauges on spirals for Dynamic Test

5 Test Results and Discussion

The first part of this chapter is a description of the observations of the bridge columns. This is followed by a discussion of the strain gauge data and dynamic amplification factors of the three tests at UCSD: the Slow, Fast, and Dynamic tests. Then a discussion of the basis of the prediction is included. In addition, this chapter compares the predicted results with the recorded responses of the three tests. Finally, this chapter compares the recorded responses of the three tests at UCSD with each other and the UCI Non-Pulse test.

5.1 OBSERVATIONS

This section presents the observations on how the bridge columns responded throughout the loading history. Owing to the input loading rate, no observations could be made during the whole loading history for the Fast and Dynamic tests; therefore, the detailed observations are for the response of the bridge column during the Slow Test. The observations for the Fast and Dynamic tests are only for the end of the response.

At the peak displacement of the first ramp of the pulse loading, minimum cracking was observed in both the compression and tension faces. In the out-of-plane faces, diagonal cracking varied from 30° to 60° angles. On the reverse pulse loading, the first flexural cracking was detected. Also, incipient spalling occurred, which exposed three spirals. Furthermore, a vertical bar in the tension face began to buckle.

Besides spiral yielding at 1% drift, little other damage was observed between 0.5% and 3% drift. At 4% drift, a noticeable kink in the spiral was detected in the compression faces. Furthermore, at 4% drift, a few vertical cracks ran up the bridge column where vertical bars were located.

At 5% drift, the hinge regions in both the tension and compression faces begin to take shape. The concrete cover in the hinge region, 114 mm (4.5 in.) up from the footing, was completely spalled off. Also, three more vertical bars began to buckle. At 6% drift, the hinge height increased 25 mm (1 in.) and deep cracks in the concrete core developed. Another vertical bar buckled in addition to a spiral fracturing in both the tension and compression faces. Finally, at 7% drift, three vertical bars fractured.

The end response of the Fast and Dynamic tests were observed to be similar. Few observations could be made during the Fast and Dynamic tests, so all observations for the two tests are for the end of the response. At the completion of the two tests, the plastic hinges were approximately 200 mm (8 in.) in height and 250 mm (10 in.) wide. The Fast Test had three longitudinal bars fracturing, while another two buckled about 65 mm (2.5 in.) up from the footing. In the Dynamic Test, two longitudinal bars fractured and three bars buckled near 65 mm (2.5 in.) up from the footing. Finally for both the Fast and Dynamic Tests, the spiral fractured in both plastic hinge regions roughly 65 mm (2.5 in.) up from the footing.

Presented in Figure 5.1 is an overall view of the bridge column for the Slow Test after the full pulse cycle loading. Figure 5.2 displays the plastic hinge for the Slow Test after the pulse loading. Figure 5.3 shows the plastic hinge length after the complete loading history for the Fast Test. Finally, Figure 5.4 is an overall view of the bridge column for the Dynamic Test during the pulse cycle loading.

Fig. 5.1 Overall view of bridge column of Slow Test past pulse loading

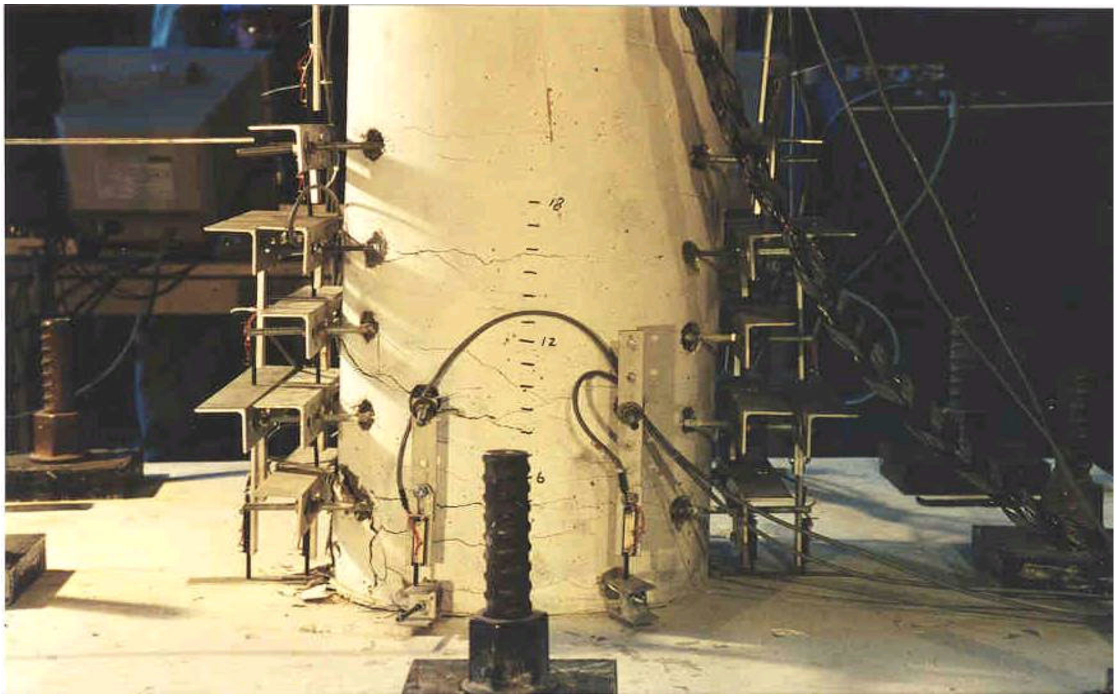

Fig. 5.2 Plastic hinge region after pulse loading for Slow Test

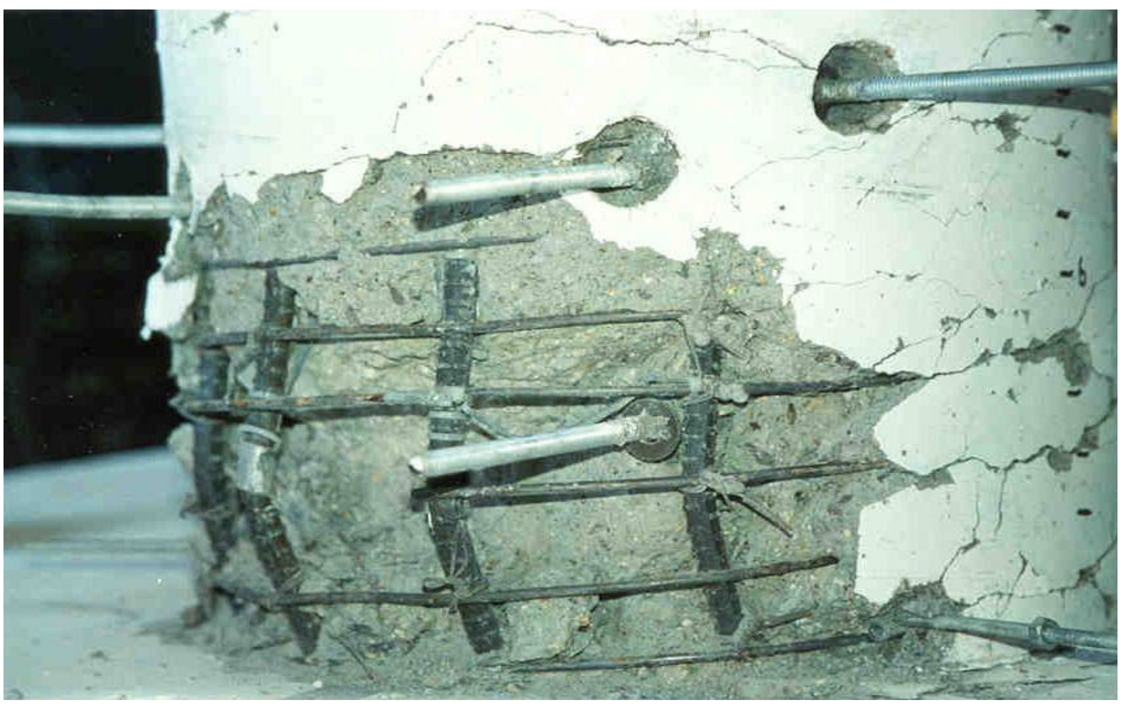

Fig. 5.3 Plastic hinge region after complete loading history for Fast Test

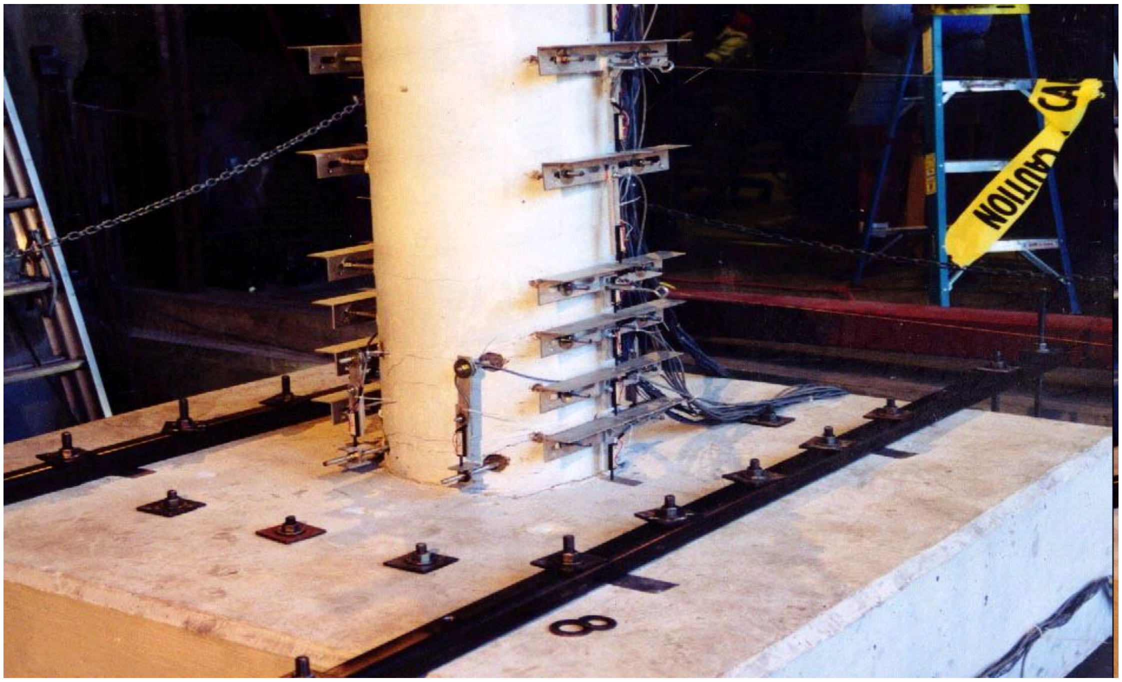

Fig. 5.4 Overall view after pulse loading for Dynamic Test

5.2 STRAIN GAUGE DATA

A key component to this research is evaluating the strain gauge data and quantifying the effects of strain rate. Strain rate effects cause the test specimen to have overstrength factors that are explained by dynamic amplification factors as discussed in Chapter 2 and represented by Equations 2.1 through 2.6. Strain rate is a major factor in understanding how the bridge columns performed throughout the three tests.

Sets of longitudinal bar strain data are provided in the Appendix for the Slow, Fast, and Dynamic tests. The strain gauge data presented in the Appendix were obtained from strain gauges located within the plastic hinge region for the first peak of the displacement drift ratio levels. Also, a partial series of the longitudinal bar strain time histories for the Fast and Dynamic tests are in the Appendix. The majority of the strain gauges that were located within the plastic hinge region exceeded the maximum value of the strain gauge. Thus, a limited set of data was obtained from the strain gauges.

From the surviving strain gauges in the hinge region for the Fast Test, 0.05/sec was calculated as an average strain rate, while the average strain rate of the Dynamic Test was approximately 0.1/sec. The average strain rate is calculated by taking approximately 4 gauges in the hinge region, then finding the slope of the strain gauge time history. The average strain rates of the two tests were used to calculate the dynamic amplification factors presented in Table 5.1 for the Fast Test and Table 5.2 for the Dynamic Test, using the equations presented in Section 2.2.

Table 5.1 Dynamic amplification factors for Fast Test

Material	Multiplier
E_{con}	1.2
ε_{con}	1.15
f'_{con}	1.2
f_{steel}	1.35

Table 5.2 Dynamic amplification factors for Dynamic Test

Material	Multiplier
E_{con}	1.25
ε_{con}	1.18
f'_{con}	1.25
f_{steel}	1.4

Similar to the longitudinal bar strain data, spiral strain profiles and partial sets of strain time histories are presented in the Appendix for the Slow, Fast, and Dynamic tests. The average strain rate values on the spirals for the Fast and Dynamic tests were low compared to the longitudinal bar strain rate; therefore, no dynamic amplification factors were calculated.

5.3 DYNAMIC TEST FORCE-DISPLACEMENT CORRECTION

In an attempt to check for uplift, a single displacement linear potentiometer was attached to the footing and shake table for the Dynamic Test. This displacement linear potentiometer did, in fact, record uplift during the test. However, since only one linear potentiometer was utilized, a limited data set was obtained. To capture the true displacement, a computer model was constructed using the program "Ruaumoko," (Carr 1996), to model the rigid rotation due to the uplifting in the footing. The true, or "corrected" displacement, was the total displacement measured from the shake table subtracted by the rigid rotation from the output of Ruaumoko.

The model was composed of line elements with infinite stiffness that represented the bridge column and footing. The threaded tie-down rods were modeled as elastic springs with gap elements. In tension, the springs were modeled with the threaded rod properties, while in compression, the spring had infinite stiffness. The infinite stiffness in compression was used to model the contact between the footing and shake table. A force time history was applied to the top of the bridge column that forced the footing to undergo the same vertical displacement in the computer model as in the measured uplift.

A relation was then derived from the computer output between the horizontal displacement at the top of the bridge column and the footing. The new relationship was applied to the measured uplift in the footing. Then a rigid rotation was developed between the footing uplift and the top of the bridge column. This produced a displacement at the top of the bridge column. Finally, the corrected displacement was calculated by subtracting the recorded displacement with the displacement at the top of the bridge column as previously presented. The force-displacement graphs for the Dynamic Tests included in Chapters 5 and 6 are with the corrected displacement.

5.4 COMPARISON OF PREDICTED AND RECORDED RESPONSE

A comparison of the recorded response of the Slow Test and predicted force-displacement is provided in Figure 5.5. The comparison of the recorded response of the Fast Test and predicted force-displacement is furnished in Figure 5.6. Finally, a comparison of the corrected response for the Dynamic Test and predicted force-displacement is provided in Figure 5.7.

5.4.1 Basis of the Prediction

The predicted performance of the bridge columns for the various load cases was based on a moment-curvature relationship derived from the program SEQMC, "SEQad Moment-Curvature Analysis" (SC Solutions, 1999). This computer program provides a moment-curvature analysis of reinforced concrete sections based on a confined concrete model developed by Mander et al. (1998), and prescribed reinforcing steel characteristics.

The Slow, Fast, and Dynamic tests had the same prediction for comparison purposes. The input strength of the concrete for the SEQMC program was based upon the 28-day compression test results and the steel strength was based on the yield strength. The values of the compressive strength of the concrete and yield strengths for both the longitudinal bars and spirals are found in Tables 4.1 through 4.3. The ideal moment was calculated based upon a strain of 0.004, and the strain at which spalling occurs was set at 0.007.

The moment-curvature analysis output from SEQMC was converted into a force-displacement prediction. The force was calculated by dividing the moment by the height of the bridge column, 1829 mm (72 in.). The curvature-to-displacement conversion was based upon a set of relations in Paulay and Priestley (1993).

The yield displacement can be written as:

$$\Delta_y = \phi_y L^2/3 \tag{5.1}$$

where Δ_y = yield displacement; ϕ_y = yield curvature as specified in the SEQMC output; and L = height of the bridge column = 1829 mm (72 in.). The plastic displacement can be written as:

$$\Delta_P = (\phi_m - \phi_y) L_p (L - L_p) \tag{5.2}$$

where ϕ_m = maximum curvature; and L_p = plastic hinge length. Paulay and Priestley stated that the plastic hinge is defined over the region in which the plastic curvature is assumed equal to the maximum plastic curvature. Estimation for the effective plastic hinge length may be expressed as:

$$L_p = 0.08L + 0.022 d_b f_y \text{ (MPa)} \tag{5.3}$$

where d_b = diameter of the longitudinal bar and f_y = yield stress of the longitudinal bar. Combining the yield displacement, Equation 5.1, and the plastic displacement, Equation 5.2, the total displacement is derived as:

$$\Delta = \Delta_y + \Delta_p \tag{5.4}$$

5.4.2 Discussion of Predicted and Recorded Response

For all three tests, the predicted force-displacement response compares relatively well to the response of the bridge column after the pulse loading. On the other hand, the predicted response poorly assessed the responses of the test specimens during loading. This is not surprising, since the strain rate effect was not considered in the material properties.

All comparisons in this report are based on the post-pulse loading. Both the Slow and Dynamic test results showed that the predicted force-displacement overestimated the yield response of the bridge columns. On the other hand, the Fast Test results matched the predicted force-displacement response closely until the last levels of lateral displacement. At l15 mm (4.5 in.) lateral displacement for the Slow Test, the predicted force-displacement overpredicts the recorded response by 10%. Again, at l15 mm (4.5 in.) lateral displacement, the predicted force-displacement overpredicts the Fast Test recorded response by 5%. Finally, at l15 mm (4.5 in.) lateral displacement for the Dynamic Test, the predicted force-displacement nearly predicts the corrected response. The differences between the predicted and the recorded responses were attributed to a combination of a smaller plastic hinge length and the use of low concrete strength in the predictions.

The plastic hinge length equation used in the predicted force-displacement response was derived for a monotonically increasing load, as opposed to a cyclic loading scenario used for the three tests. A plastic hinge length equaling the radius of the bridge column, 203 mm (8 in.) will produce a better conversion from curvature to displacement. The plastic hinge length was determined by isolating the plastic hinge length from Equations 5.1 through 5.4. The total displacement was the recorded displacement measured in the actuator from the Fast Test. The yield curvature, Φ_y, was calculated from an equation in Priestley *et al.* (1993);

$$\Phi_y = 2.45\ f_{s,\,dyn}/(E_s \cdot D) \tag{5.5}$$

where D = diameter of the column. The maximum curvature at the footing-column interface was estimated based upon the recording of the linear potentiometers on the bridge column. Paulay and Priestley (1993) stated that the radius of the bridge column might be used for an approximation of the plastic hinge length.

The Slow Test had a test-day strength of the concrete that was 20% higher than the 28-day strength used as the input value for the predicted response. The Fast Test results had an increase of 5% from the test-day concrete strength to a 28-day concrete strength. The major difference in the strength of the bridge column for the Fast Test was the result of strain rate effects. The average increase of dynamic amplification factors due to strain rate effects for the tensile and compressive strength is approximately 30% above the test-day strength.

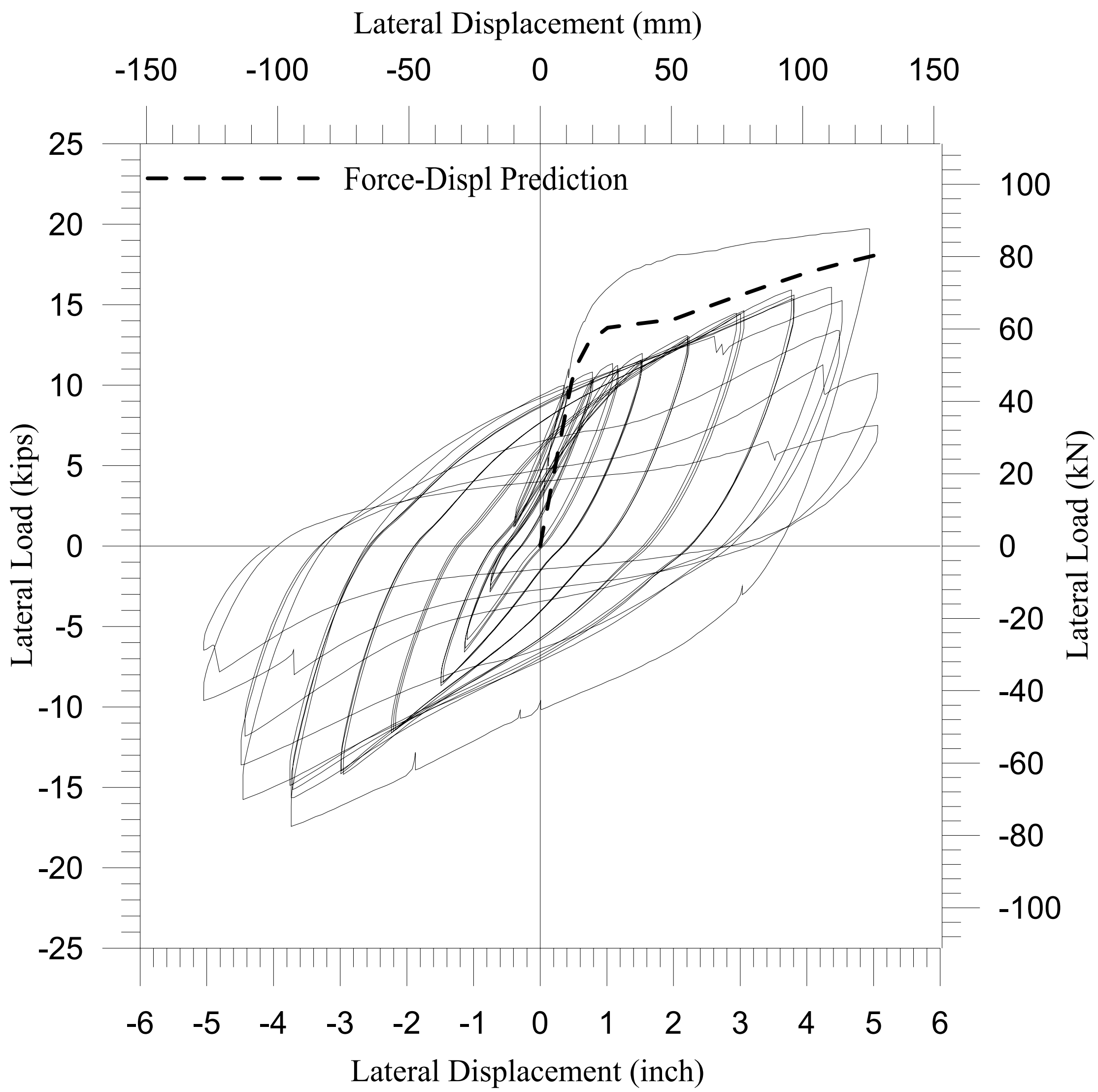

Fig. 5.5 Recorded response of Slow Test with predicted force-displacement

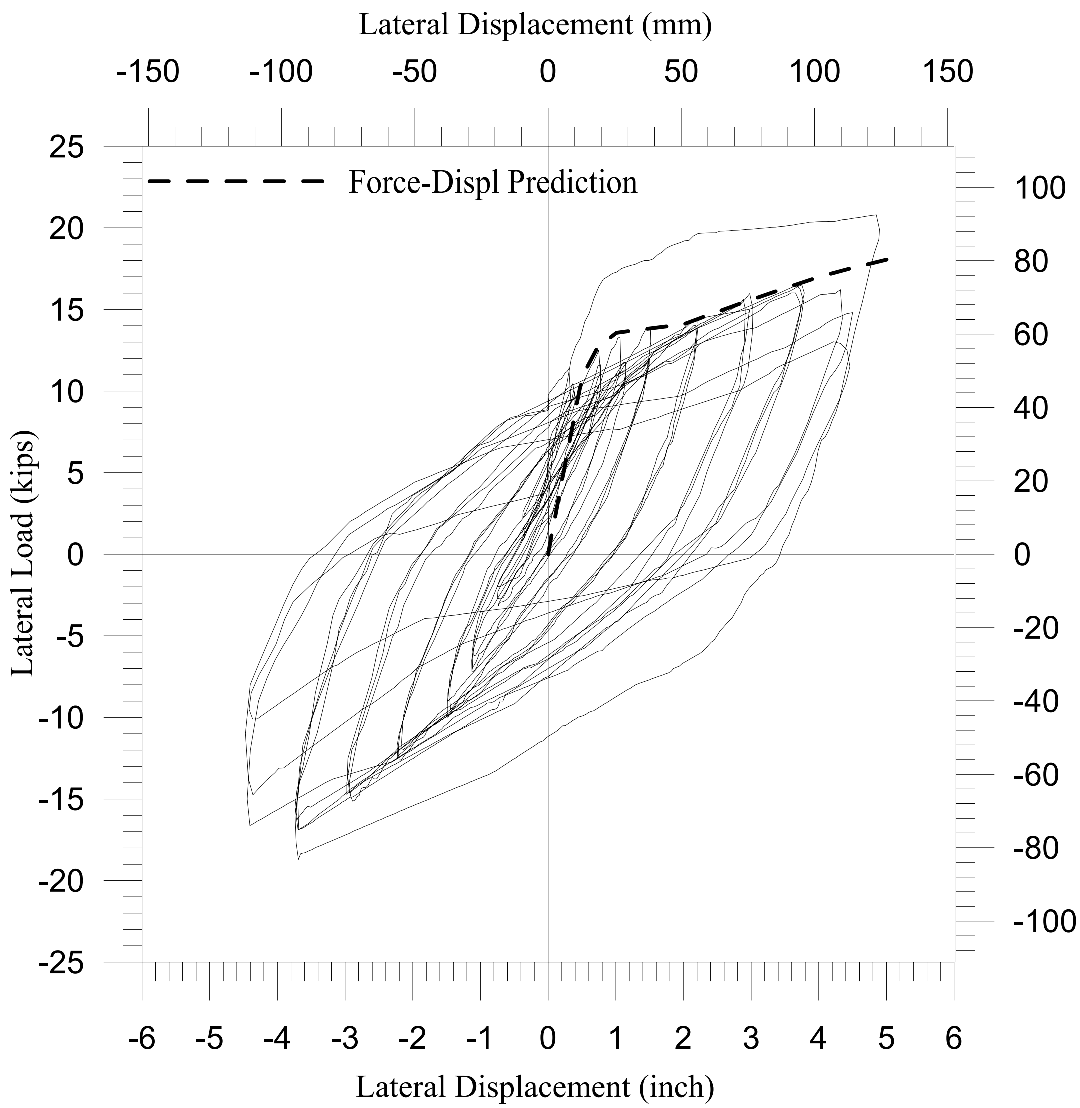

Fig. 5.6 Recorded response of Fast Test with predicted force-displacement

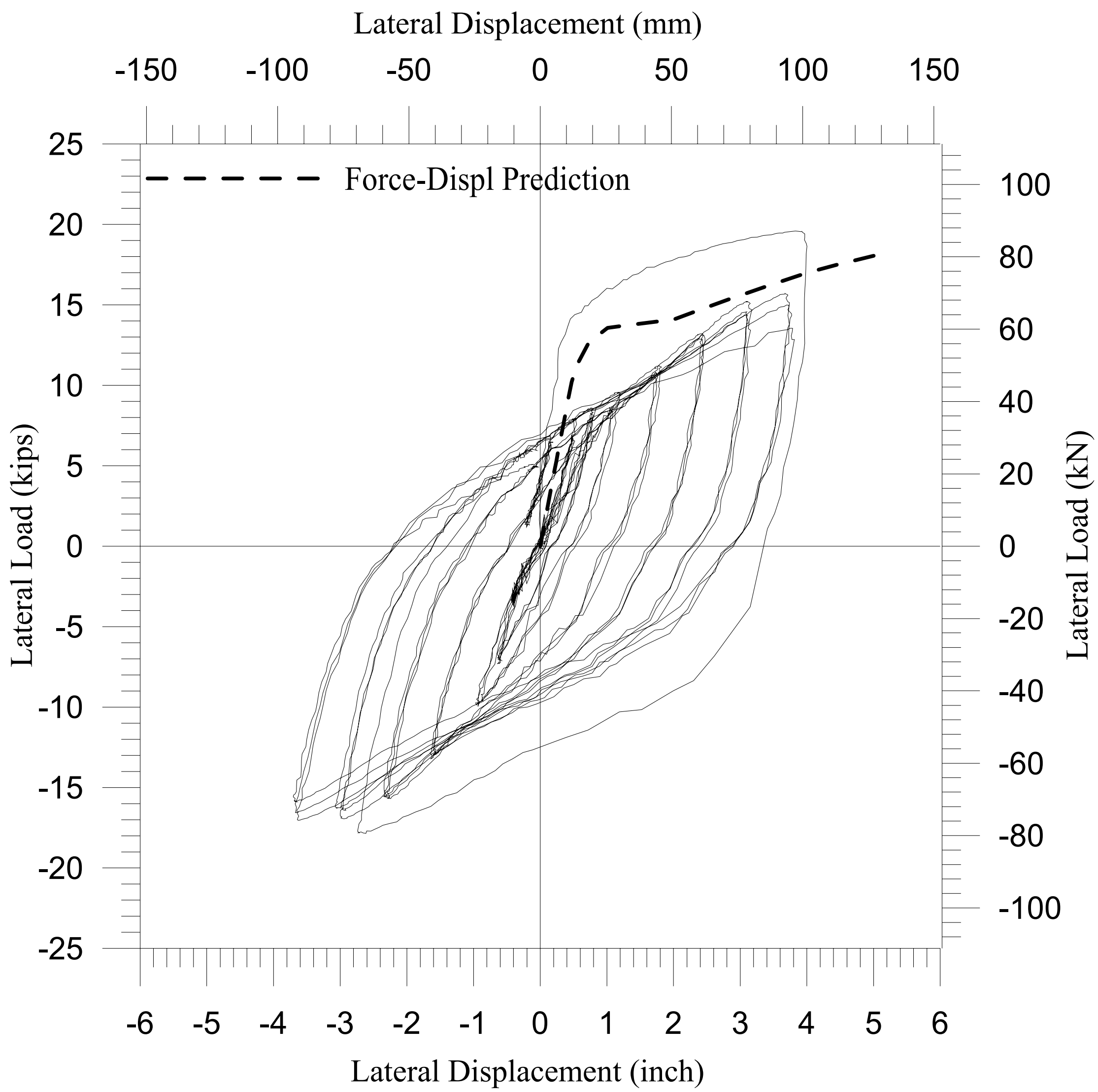

Fig. 5.7 Corrected response of Dynamic Test with predicted force-displacement

5.5 COMPARISON OF TEST RESULTS

To obtain a better understanding the effects of the different loading rates, the three UCSD tests were compared with each other. In order to study the effects of the pulse loading, the three UCSD tests were also compared to the UCI Non-Pulse loading test.

5.5.1 Comparison of Force-Displacements for Three UCSD Tests

A direct comparison of the recorded responses of the Fast Test and Slow Test is provided in Figure 5.8. From this figure, it can be observed that specimen strength of the Fast Test was 10% greater strength than that of the Slow Test during the pulse loading. Another observation is that in the early cycles, greater specimen strength was seen in the Fast Test, but as the cycles progressed, specimen strength in the Slow Test and the Fast Test started to even out.

The next comparison, in Figure 5.9, is of the recorded response of the Fast Test and the corrected response of the Dynamic Test. One conclusion is that the secondary stiffness is greater for the Dynamic than for the Fast Test. Again, the Fast Test had a greater strength in the lower cycles with the strength of the two tests evening out in the later cycles.

The final comparison is of the Slow and Dynamic tests, as shown in Figure 5.10. One conclusion is that the initial stiffness and secondary stiffness are greater for the Dynamic Test than for the Slow Test. In this case, the Slow Test had a greater strength in the lower cycles, but the difference of strength from the two tests leveled off in the later cycles.

The testing procedures may explain the variation of strengths in the three tests. During the Dynamic Test, the footing lifted up, and thus the lateral displacement was not the same for the Dynamic Test as for the Slow and Fast tests. The lateral displacement for the Dynamic Test was the input displacement minus the rigid rotation correction presented in Section 4.4.

Another variable is in the materials and material reactions to the input loading rate. The Slow and Fast tests were constructed side by side and were poured from the same concrete batch. The Dynamic Test was constructed at a later date, where the concrete was delivered with a slump in excess of 180 mm (7 in.). Therefore, the quality of the concrete used in the Dynamic Test varied from that in the Slow and Fast tests. As discussed in Section 5.1, the Fast and Dynamic tests experienced a greater strength due to strain rate. Strain rate effects caused the Fast Test to have an average dynamic amplification factor of 1.2, while that of the Dynamic Test was 1.3. The footing of the Dynamic Test rocked during the test thus comparing the Dynamic Test to the Slow and Fast tests is not a true comparison. The force-displacement correction for the Dynamic Test may overadjust the true force-displacement, thus causing the Dynamic Test to have a strength as low as in the Slow Test.

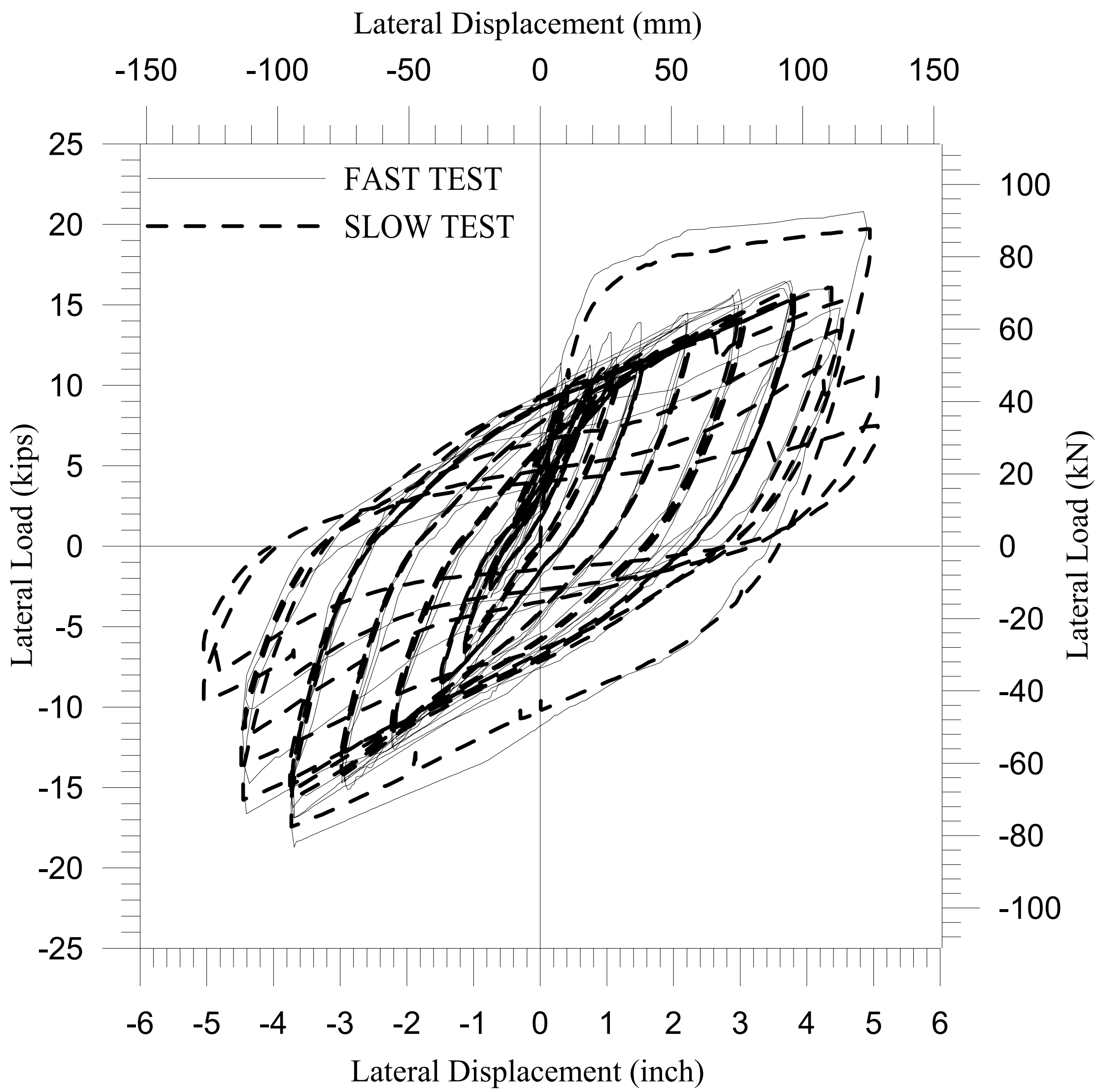

Fig. 5.8 Comparison of Slow Test with Fast Test

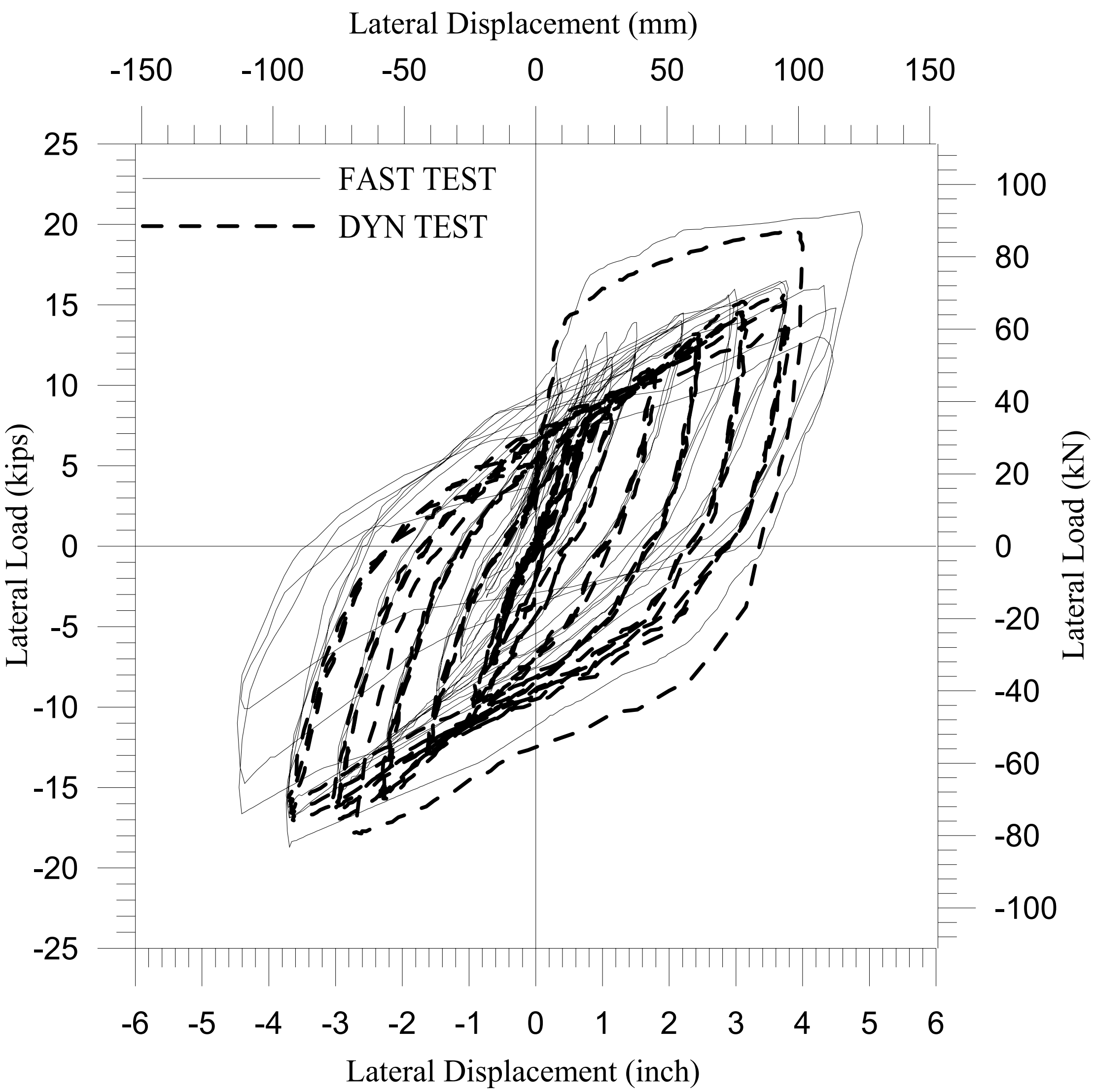

Fig. 5.9 Comparison of Fast Test with Dynamic Test

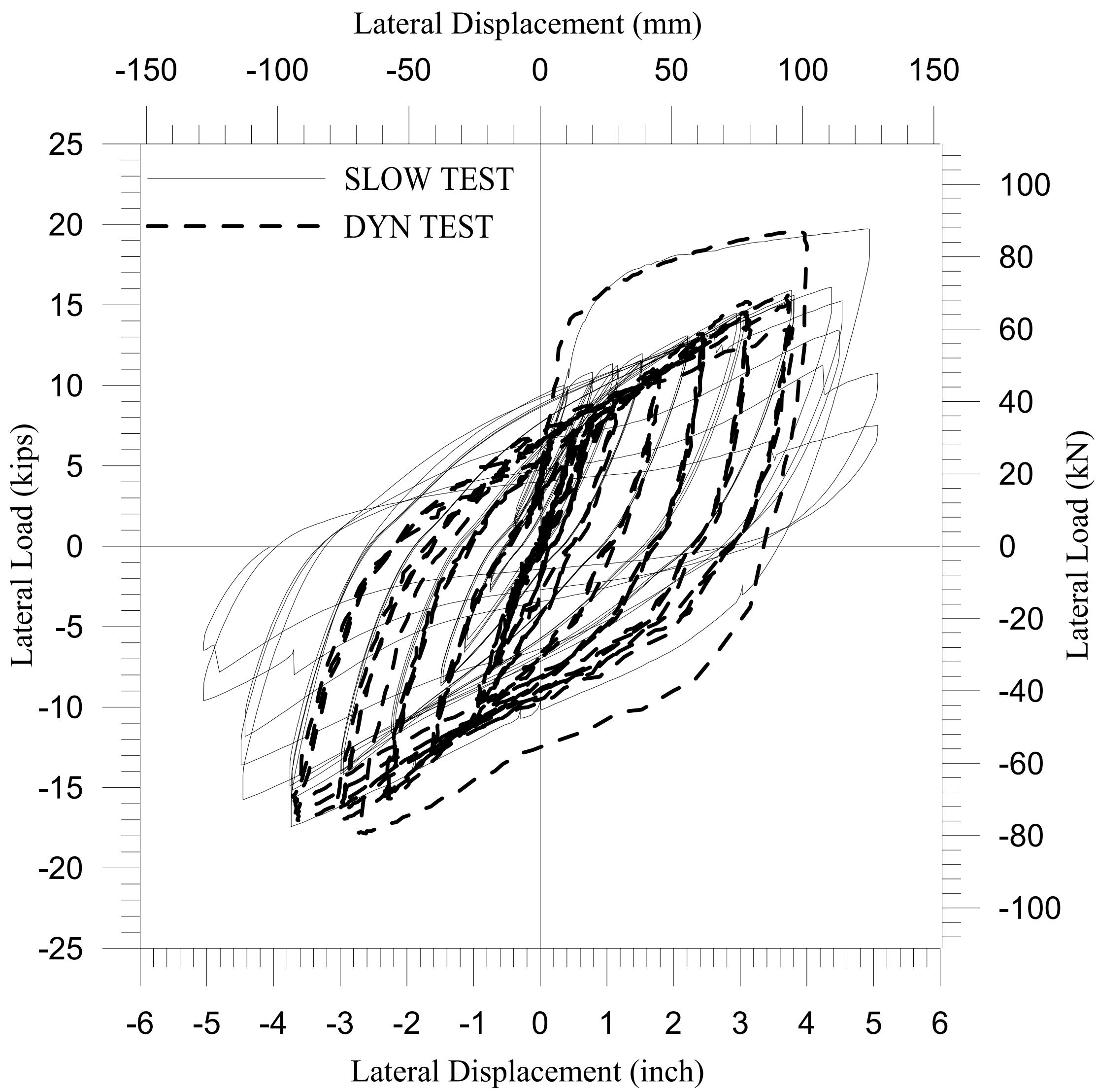

Fig. 5.10 Comparison of Slow Test with Dynamic Test

5.5.2 Comparison of Force-Displacements for UCSD Tests and UCI Non-Pulse Test

To assess the effects of the velocity pulse on the bridge column, the three UCSD tests were compared against the UCI Non-Pulse test. The UCI test was with a bridge column that had the same design parameters and construction as the UCSD test specimens. Furthermore, the UCI test had the same input loading history as UCSD except for the pulse loading. The first comparison is of the recorded response of the Slow Test and the UCI Non-Pulse Test results as provided in Figure 5.11. The next comparison is of the recorded response of the Fast Test versus the UCI Non-Pulse Test as furnished in Figure 5.12. Finally, a comparison of the corrected response for the Dynamic Test and the UCI Non-Pulse Test is provided in Figure 5.13.

In all three comparisons, the UCI Non-Pulse Test results had a greater strength than that of the three UCSD tests in the early cycles. Studying the results of the later cycles, the UCI Non-Pulse Test had a similar strength level if not less than that of the three UCSD specimens. Based on these results, it can be concluded that the pulse has no essential effect on the ultimate performance of the bridge columns. However, it is clear that the pulse did adversely effect the column performance in the early stages of loading. The initial pulse loading on the three UCSD test specimens caused deterioration. Thus the deterioration of the pulse loading on the three UCSD test specimens was not equated in the UCI Non-Pulse Test results until the UCI specimen experienced similar displacement levels as during the initial pulse for the three UCSD test specimens.

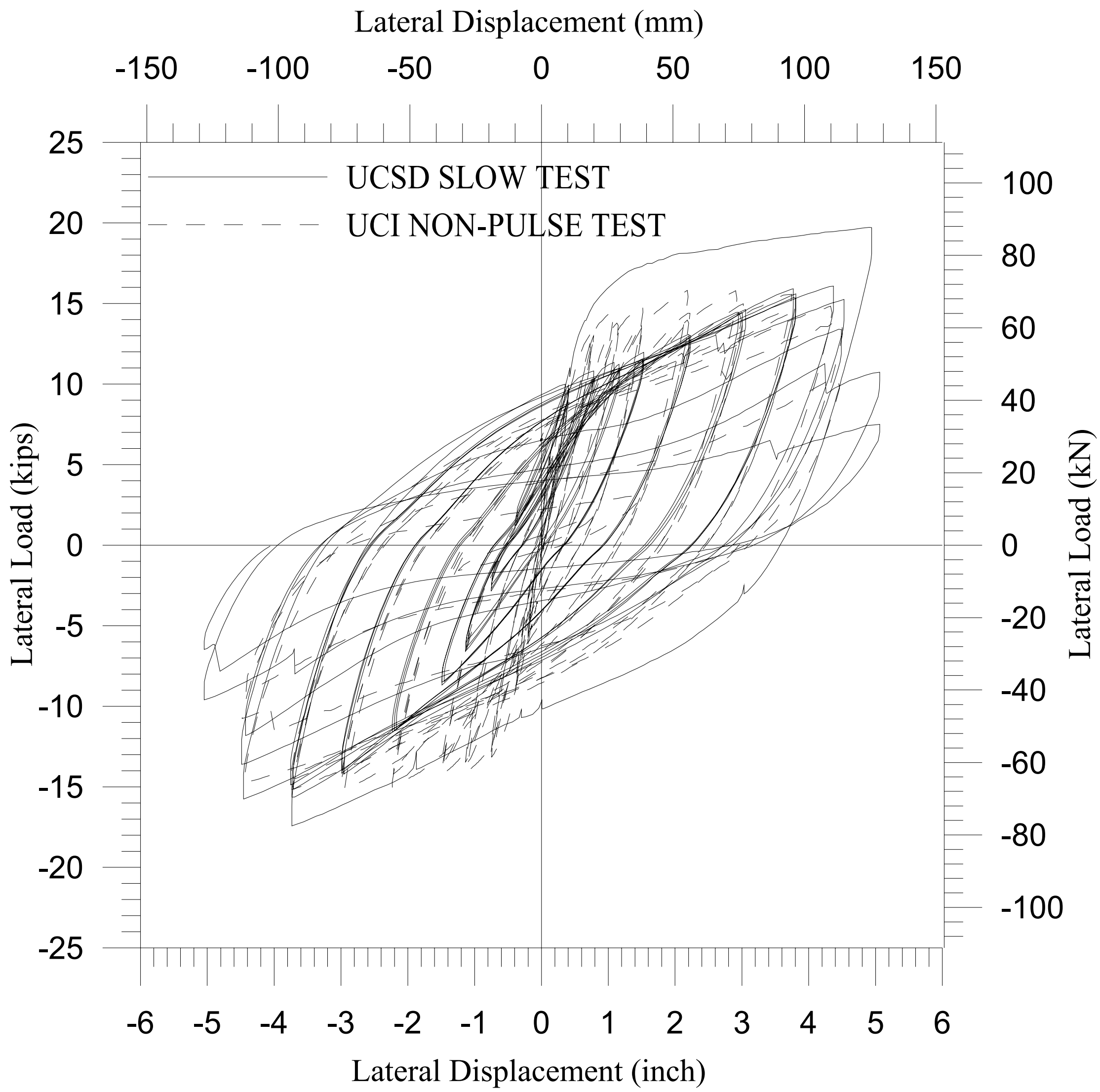

Fig. 5.11 Comparison of UCSD Slow Test and UCI Non-Pulse Test

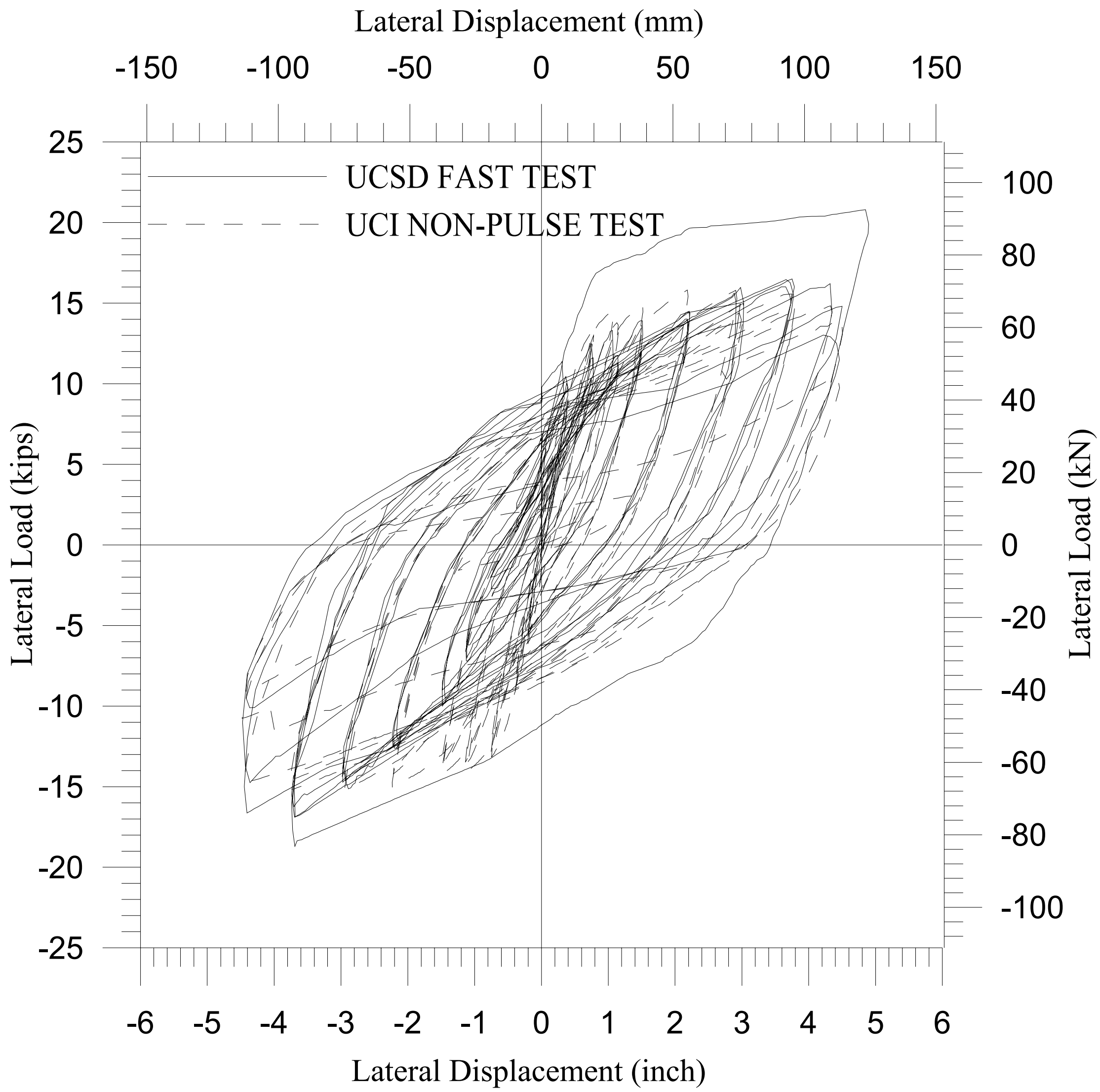

Fig. 5.12 Comparison of UCSD Fast Test and UCI Non-Pulse Test

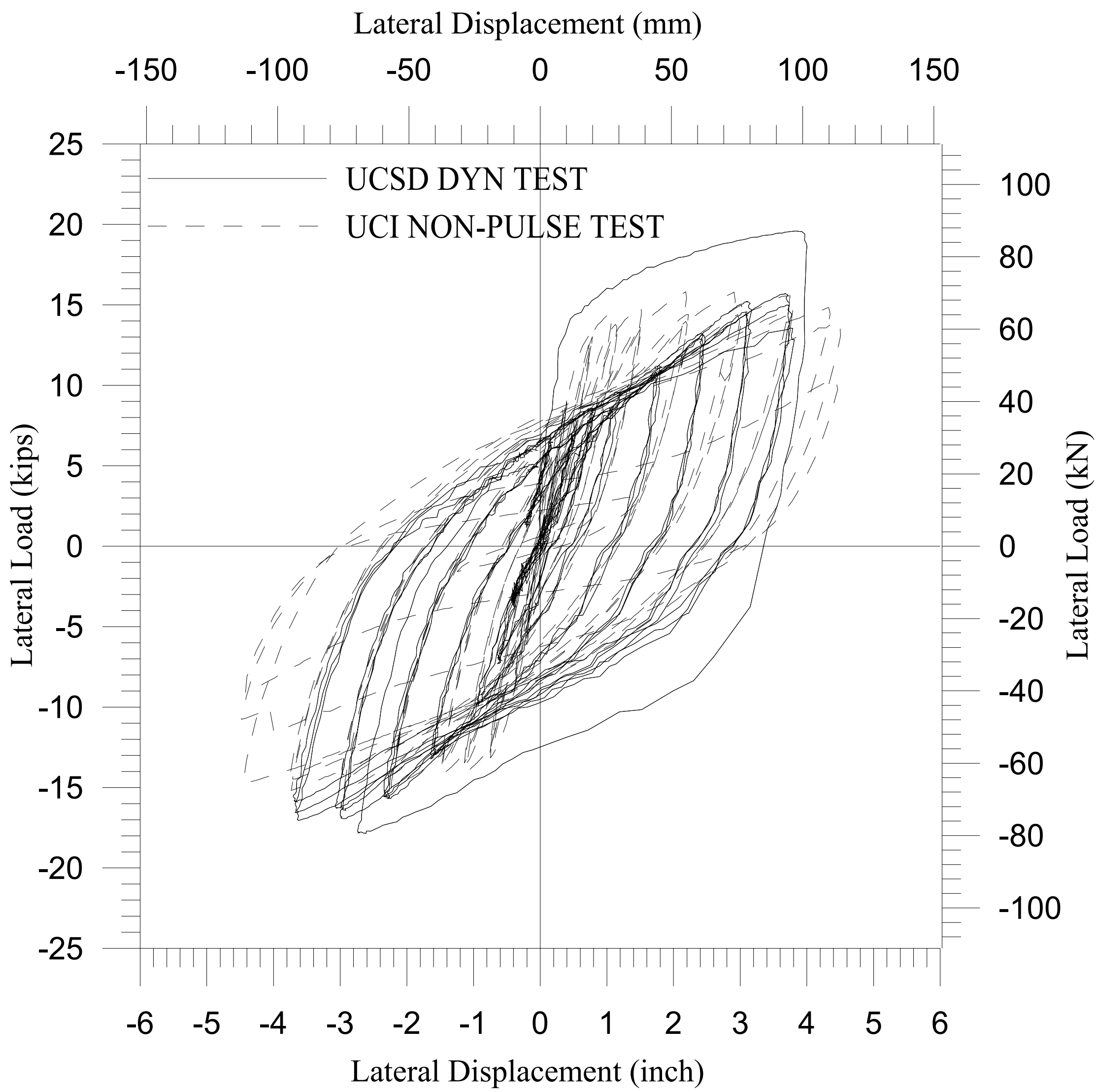

Fig. 5.13 Comparison of UCSD Dynamic Test and UCI Non-Pulse Test

5.5.3 Comparison of Energy Dissipation for Three UCSD Pulse Tests and UCI Non-Pulse Test

Figure 5.14 shows the differences in energy dissipation between the three UCSD tests and the UCI Non-Pulse Test. The energy dissipation was calculated by integrating the recorded force-displacement curves as discussed in Section 5.4. Because the four tests were recorded at different rates, the results needed to be standardized, or multiplied by a factor, in order to equate the loading histories. In addition to standardizing the four tests, the Slow Test energy-dissipation curve contains the energy dissipation up to the 6% drift ratio loading cycle.

The three UCSD tests showed similar effects for the pulse loading and followed a similar pattern throughout the remainder of the loading cycle. Since the UCI test did not have a pulse in the loading history, energy dissipation was slower.

When comparing just the three UCSD tests, the initial energy dissipation during the pulse loading was 30% greater for the Fast Test in comparison to the Slow and Dynamic tests. This can be explained by the fact that the Fast Test had a higher force during the initial pulse loading than did either the Slow or Dynamic test. Between the pulse loading and the final loading, the Slow Test had a greater amount of energy dissipated than during the Fast or Dynamic Test. After the initial pulse loading, the Slow Test dissipated more energy than in the Fast Test because the Fast test had more plastic displacement during the pulse loading. The Dynamic Test had uplifting in the footing, thus providing results that are inconclusive. At the final loading cycle, the Slow and Fast tests were comparable in energy dissipation. Owing to the uplift of the footing for the Dynamic Test, the results are again inconclusive.

The UCI test showed a similar rate of energy dissipation in comparison to the three UCSD tests. However, the final energy dissipation was less than for the Slow or Fast Test by 20%. The difference between the final energy dissipation in the UCI Non-Pulse Test and the UCSD Slow and Fast Tests is approximately the same as the initial energy dissipation during the pulse. Therefore the pulse loading had no effect on the final performance of the bridge columns.

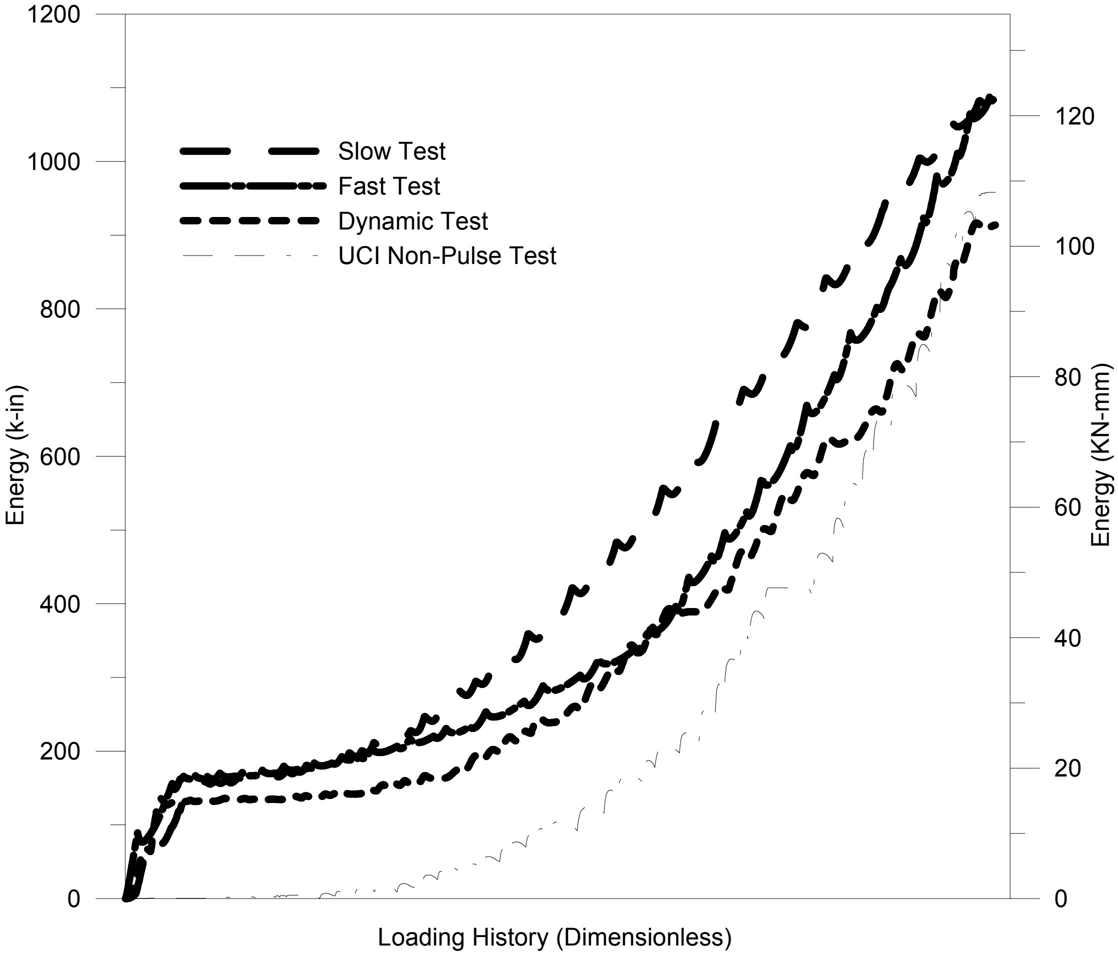

Fig. 5.14 Comparison of energy dissipation for three UCSD Pulse Tests and UCI Non-Pulse Test

6 Post-Diction and Refinement

To better assess the response of the bridge column during the pulse loading, two post-dictions were computed and compared against the recorded responses. The first post-diction employed SEQMC (SC Solutions) with the dynamic amplification factors based on the calculated strain rate and modified plastic hinge length. The second post-diction was based on a dynamic bilinear response developed by Mayes and Shaw (1997) as presented in Section 2.3.

6.1 SEQMC POST-DICTION WITH DYNAMIC AMPLIFICATION FACTORS

To capture the pulse loading responses, the SEQMC program was utilized with a modified plastic hinge length and material properties adjusted for the dynamic amplification factors. The comparison of the SEQMC post-diction against the Fast Test is shown in Figure 6.1. Figure 6.2 displays the comparison of the SEQMC post-diction with the Dynamic Test.

The dynamic amplification factors used in the post-diction for the Fast Test are in Table 5.1. The calculated dynamic amplification factors for the Dynamic Test are in Table 5.2. The dynamic amplification factors were multiplied by the tested properties as presented in Tables 4.2 and 4.3. Then the new modified values were input into the SEQMC program. Finally, the conversion from the moment-curvature output to the predicted force-displacement was performed similarly as before. The difference between the post–diction and prediction is that the plastic hinge length was made equal to the radius of the bridge column, as discussed in Section 5.2. The plastic hinge length equal to the radius of the bridge column is referred to as the "modified plastic hinge length."

The SEQMC post-diction overestimated the yield of the pulse loading for both the Fast and Dynamic tests. In the Fast Test, SEQMC post-diction assessed the initial stiffness well but overestimated the secondary stiffness. For the Dynamic Test, the SEQMC post-diction estimated both the initial and secondary stiffness slopes adequately but overestimated the yield of the recorded response of the bridge column. The strain rate equations used in the SEQMC post-diction were based upon tests that isolated the materials. However, the isolation may not provide an accurate measurement of the interaction effects of the reinforcing, concrete, and confinement of the bridge column and further testing is needed on their combined effects. In the Dynamic Test, the rocking of the footing during the test may have contributed to the overestimation of the yield strength of the bridge column.

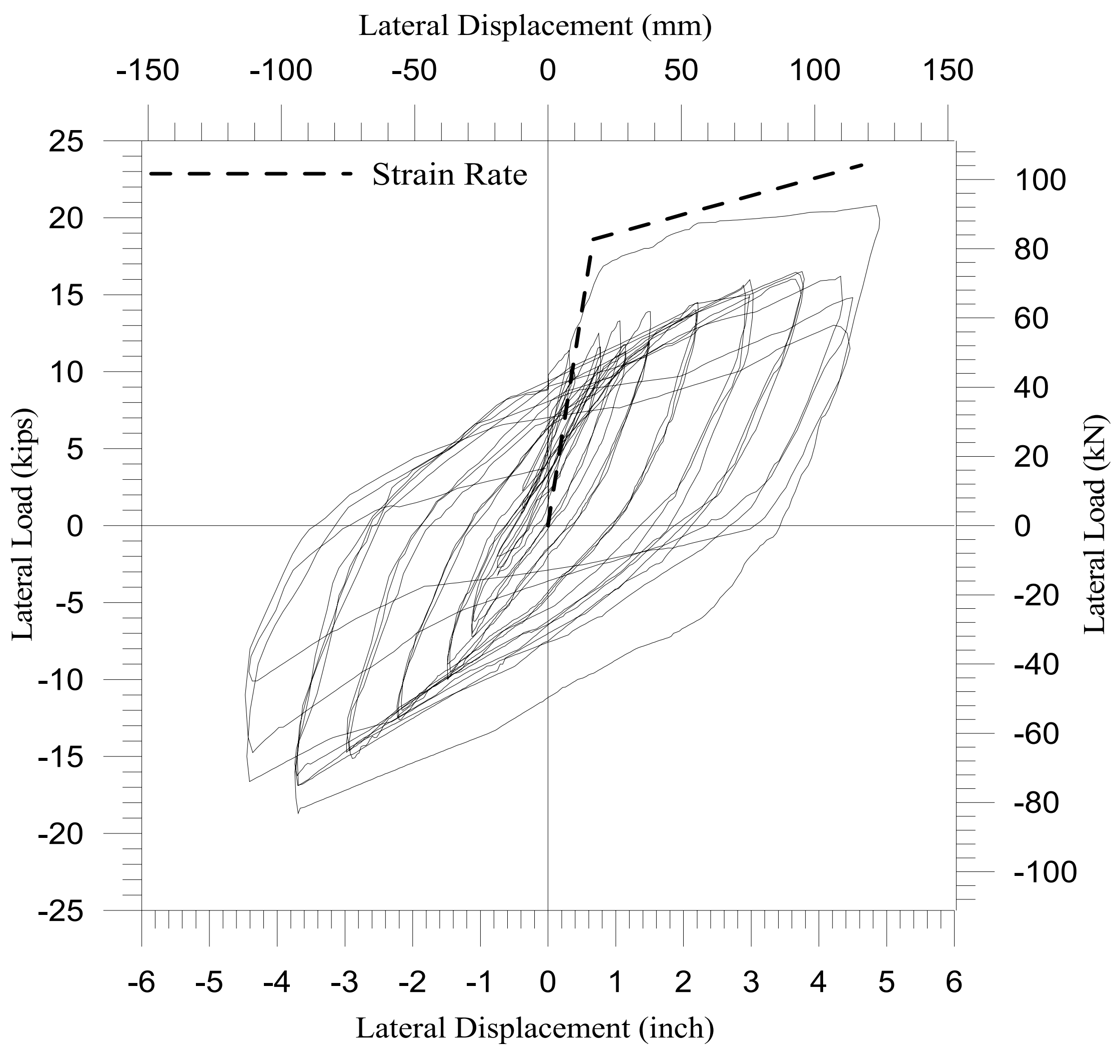

Fig. 6.1 SEQMC post-diction compared to recorded response of Fast Test

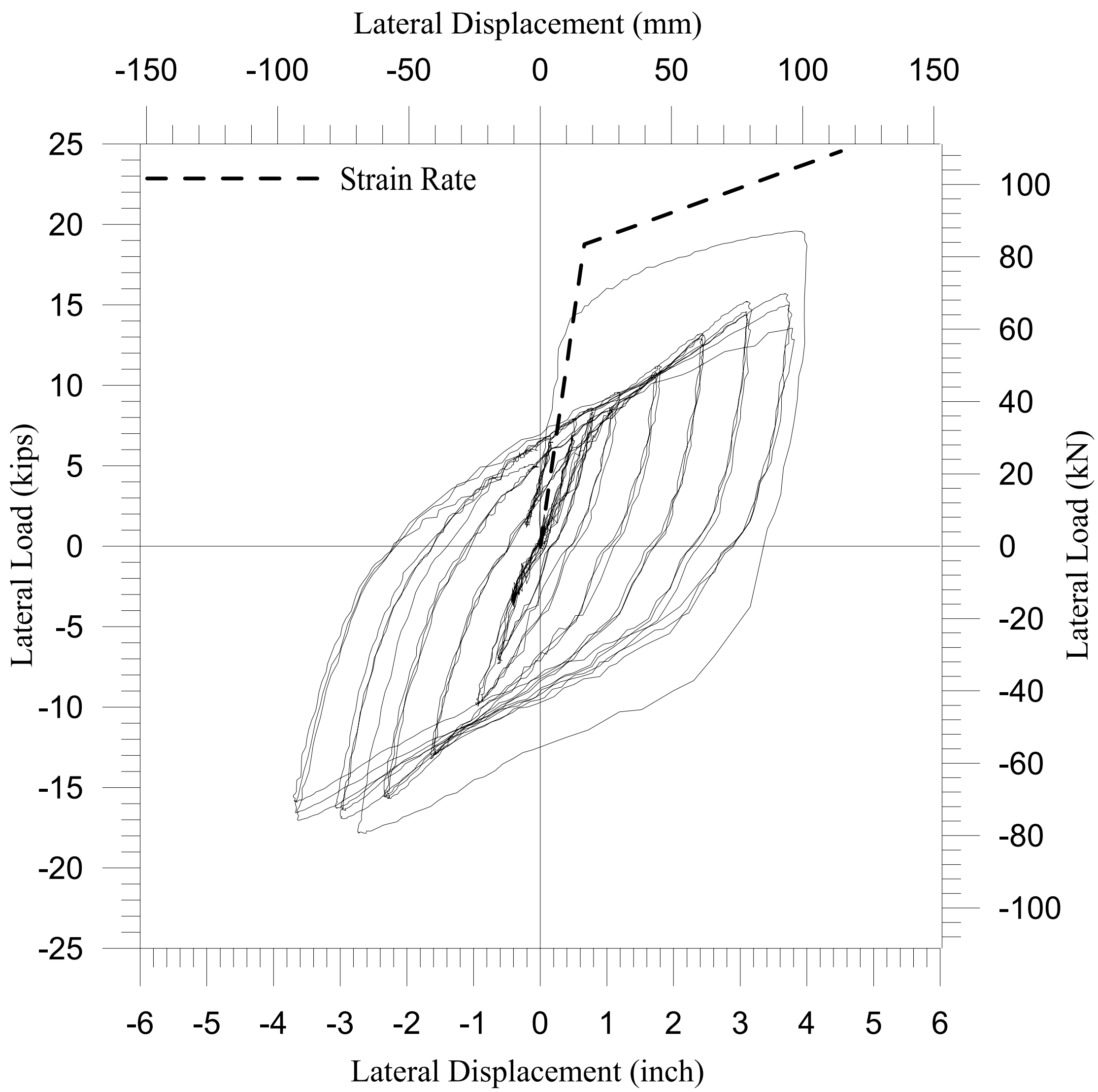

Fig. 6.2 SEQMC post-diction compared to corrected response of Dynamic Test

6.2 BILINEAR HYSTERESIS POST-DICTION

Since the SEQMC post-diction did not estimate the pulse response well, a bilinear hysteresis post-diction was developed to compare with the pulse loading response. The bilinear hysteresis post-diction for the Slow Test is shown in Figure 6.3. Figure 6.4 shows the post-diction for the Fast Test. The bilinear hysteresis post-diction for the Dynamic Test is displayed in Figure 6.5.

In developing the bilinear hysteresis post-diction, Equations 2.7 and 2.8 in Section 2.3 were used as the basis:

$$K_i = 3E_cI_e/L^3$$

$$K_2 = 0.03\ K_i$$

The yield displacement was calculated based on Equation 5.1, where the yield curvature was based on Equation 5.5.

$$\Delta_y = \phi_y L^2/3$$

$$\Phi_y = 2.45 f_{s,} /(E_s \cdot D)$$

The Slow Test bilinear hysteresis post-diction stiffness coefficients are provided in Table 6.1. In the Fast Test, the initial calculations were done for a static-loading scenario. Then the bilinear hysteresis post-diction stiffness coefficients were recalculated with the dynamic amplification factors for the Fast Test from Table 5.1, and were multiplied against the static material properties. Table 6.2 provides the calculated bilinear hysteresis post-diction stiffness coefficient for both the static and dynamic loading conditions of the Fast Test. Similar to the Fast Test, both static and dynamic bilinear hysteresis post-diction stiffness coefficients were calculated for the Dynamic Test. The bilinear hysteresis post-diction stiffness coefficients for the Dynamic Test are given in Table 6.3.

Table 6.1 Bilinear hysteresis post-diction stiffness coefficients for Slow Test

Stiffness	kN/m
K_i	4919
K_2	148

Table 6.2 Bilinear hysteresis post-diction stiffness coefficients for Fast Test

Stiffness	kN/m
$K_{i\ stat}$	4604
$K_{2\ stat}$	138
$K_{i\ dyn}$	5524
$K_{2\ dyn}$	166

Table 6.3 Bilinear hysteresis post-diction stiffness coefficients for Dynamic Test

Stiffness	kN/m
$K_{i\ stat}$	4749
$K_{2\ stat}$	142
$K_{i\ dyn}$	5936
$K_{2\ dyn}$	178

It was observed that the bilinear hysteresis post-diction rendered an excellent match to the bridge column response during the pulse loading for all three tests. Thus, using the appropriate dynamic amplification factors, the bilinear hysteresis post-diction provided a suitable assessment of the performance of the bridge column during the pulse.

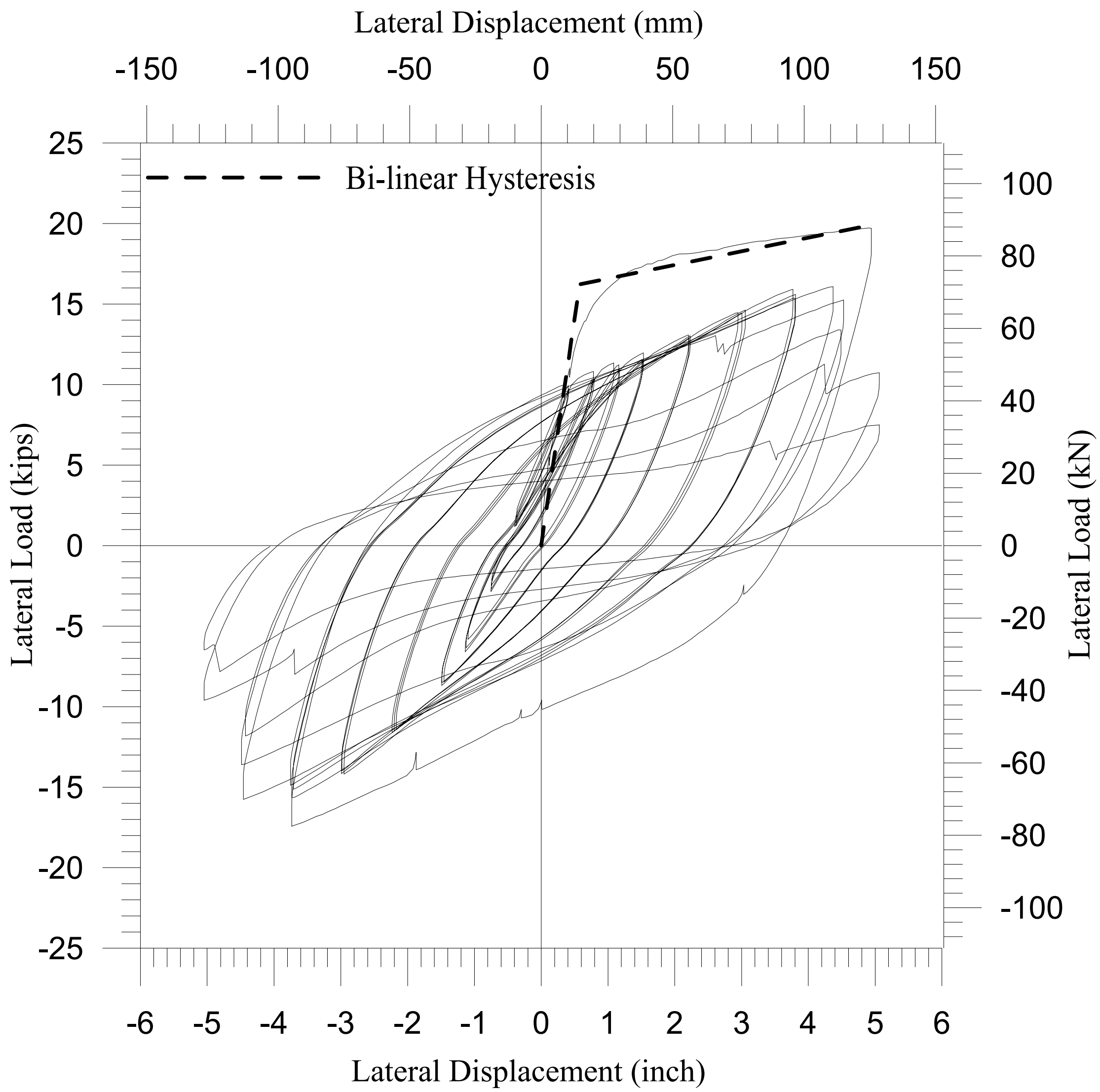

Fig. 6.3 Bilinear hysteresis post-diction compared to recorded response of Slow Test

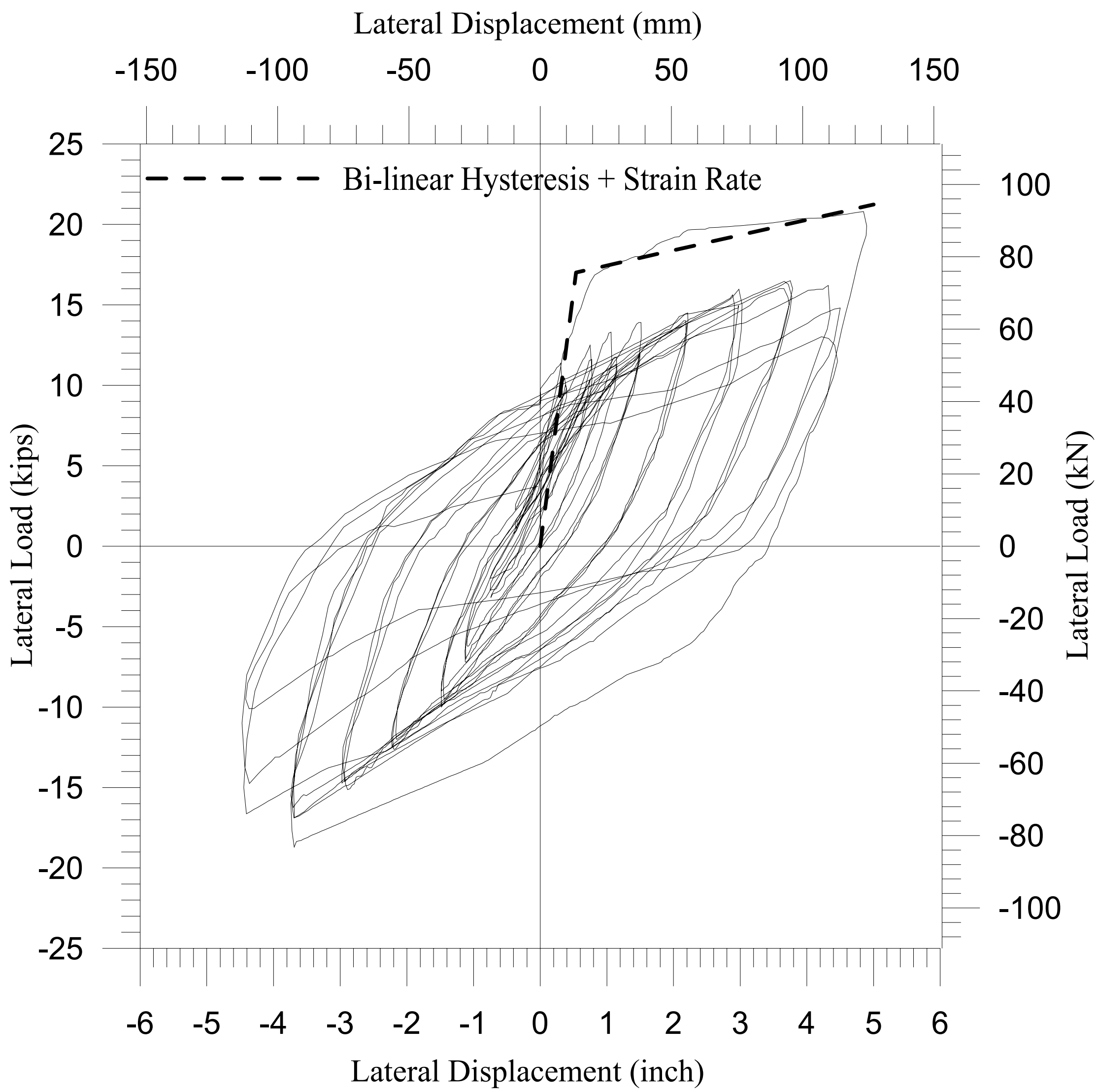

Fig. 6.4 Bilinear hysteresis post-diction compared to recorded response of Fast Test

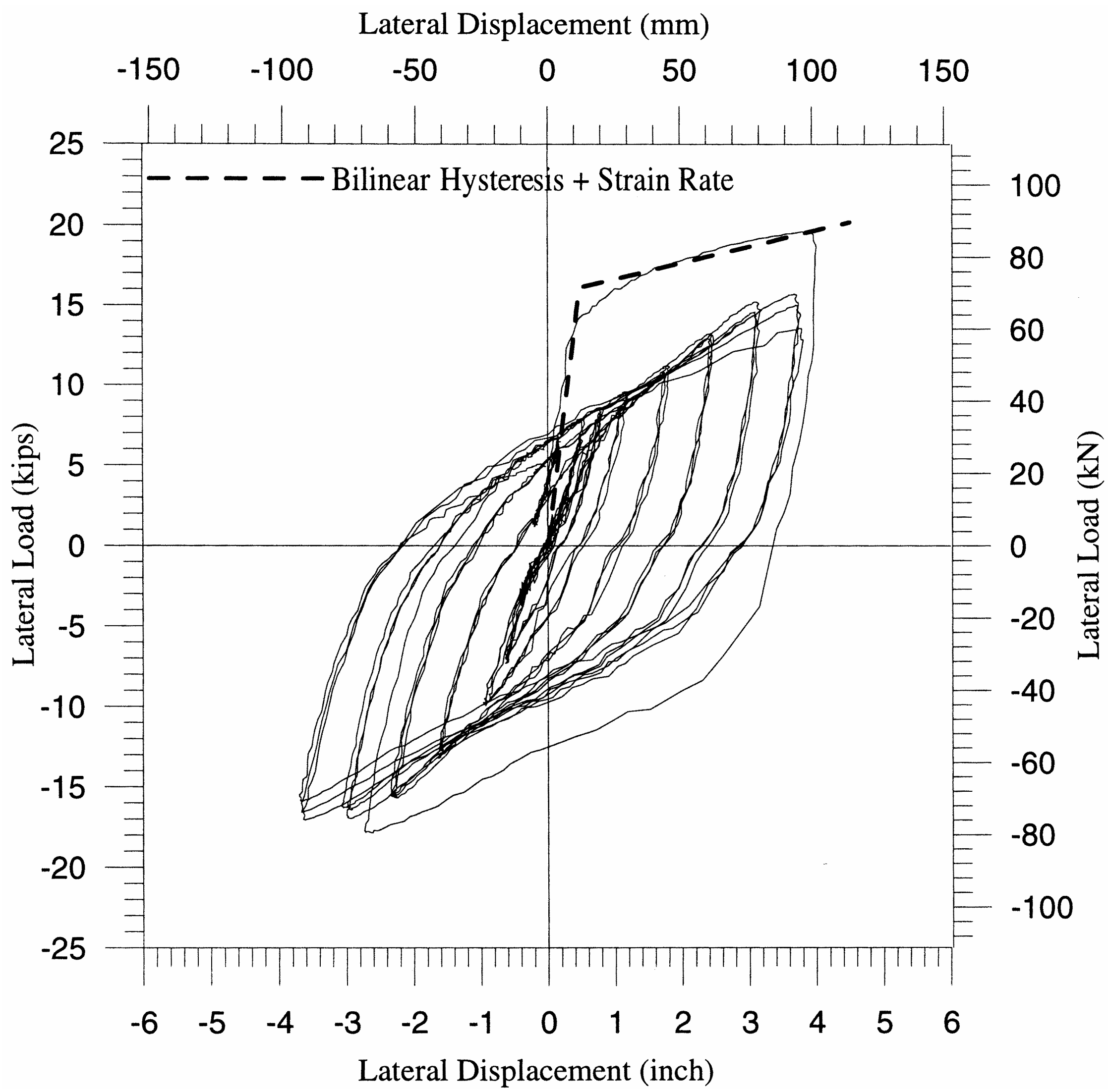

Fig. 6.5 Bilinear hysteresis post-diction compared to corrected response of Dynamic Test

7 Summary and Conclusions

Three identical bridge columns with different loading rates were tested to study the performance of the bridge columns subjected to a large velocity pulse. Two of the three test specimens were loaded by an actuator while the third bridge column was loaded by a shake table. All three tests had the same loading history, but varied in loading rate. For one of the two actuator tests, the Slow Test, the specimen was loaded quasi-statically; for the other actuator, the Fast Test, the input time rate was 0.33 m/s; and during the Dynamic Test on the shake table the input loading rate was 1 m/s.

Within the plastic hinge region of the specimen used in the Fast and Dynamic tests, the strain rate was calculated based on the strains of the longitudinal bars. The Fast Test had a strain rate of 0.05/sec, while the Dynamic Test produced a strain rate of 0.1/sec. Based on available relationships to account for strain rate effects, the dynamic amplification factors for the Fast Test averaged 1.2, and for the Dynamic Test 1.3.

Studying the recorded responses of the Slow and Fast tests with respect to their predicted force-displacement response, the following observations were made:

- The predicted force-displacement response assessed the overall performance of the bridge column relatively well.
- The predicted force-displacement response did not estimate the bridge column response during the initial pulse well.
- Comparing the three specimens tested with pulse loading at UCSD with the bridge columns tested without pulse loading at UCI, the overall performance of the bridge columns was as follows:
- The pulse test caused no significant degradation of the bridge column as compared to the UCI Non-Pulse Test with regard to ultimate performance.

- The pulse loading significantly reduced the performance of the bridge column at low levels of drift.
- Strain rate increased the strength of the bridge column for the Fast Test by 10% to 15%.
- The post-diction refinement utilizing the bilinear hysteresis representations provided a good approximation for predicting the performance of the bridge column during the velocity pulse if the appropriate dynamic multipliers were applied.

In conclusion, the large velocity pulse seems to have little or no effect on the performance of the bridge columns. In terms of predicting the strain rate effects on reinforced concrete, more testing is needed to derive equations that included the interaction effects of the concrete and steel elements because most of the testing and the resulting equations for strain rate effects are based on isolated materials and their strength.

REFERENCES

Abrahamson, N., 1998. Seismological Aspects of Near-Fault Ground Motions, *5th Caltrans Seismic Research Workshop*, Sacramento, California, June.

Al-Haddad, M.S., 1995. Curvature Ductility of Reinforced Concrete Beams under Low and High Strain Rate, *ACI Structural Journal*, Vol.92, pp. 526 – 534.

Ammann, W., and H. Nussbaumer, 1995. Behaviour of Concrete and Steel under Dynamic Actions, *Vibration Problems in Structures*, pp. 177 –183.

Attalla, M. R., T.F. Paret, and S.A. Freeman, 1998. Near-Source Behavior of Buildings under Pulse-Type Earthquakes, *Proceedings of the sixth US National Conference on Earthquake Engineering*, Seattle, Washington.

Bertero, V. V., S.A. Mahin, and R.A. Herrera, 1978. A Seismic Design Implication of Near-fault San Fernando Earthquake Records, *Earthquake Engineering and Structural Dynamics*, Vol. 6, pp. 31-34.

Bischoff, P.H., and S.H. Perry, 1995. Impact Behaviour of Plain Concrete Loaded in Uniaxial Compression, *Journal of Engineering Mechanics, ASCE,* Vol. 121, pp. 685 – 693.

Carr, A.J., 1996. "Ruaumoko – Program for Inelastic Dynamic Analysis," Department of Civil Engineering, University of Canterbury, New Zealand.

Charney, F. A. (1997) "NONLIN Version 5.50" Advanced Structural Concepts, Golden, Colorado

Filiatrault, A., Holleran, M., and Massicotte, B. "Seismic Behaviour of Reinforced Concrete Bridge Piers in Eastern North American under Simulated Winter Conditions," University of Montreal, Canada.

Hall, J. F., and B.T. Aagaard, 1998. Fundamentals of the Near-Source Problem, *5th Caltrans Seismic Research Workshop*, Sacramento, California, June.

Hall, J. F., T.H. Heaton, M.W. Halling, and D.J. Wald, 1995. Near-Source Ground Motion and its Effects on Flexible Buildings, *Earthquake Spectra,* Vol. 11, pp. 569-605.

Hose, Y.D., P. Silva, and F. Seible, 1999. "Performance Library of Concrete Bridge Components, Sub-Assemblages, and Systems under Simulated Seismic Loads," University of California, San Diego, La Jolla.

International Conference of Building Officials, 1997. *Uniform Building Code*, Whitter, California.

Iwan, W.D., 1996. Implications of Measured Near-Field Ground Motion on Structural Response, *Building an International Community of Structural Engineering Proceedings of Structures Congress XIV*, Chicago, Illinois.

Mahin, S., and M. Hachem, 1998. Response of Simple Bridge Structures to Near-Fault Ground Motions, *5th Caltrans Seismic Research Workshop,* Sacramento, California, June.

Mayes, R. L., and A. Shaw, 1997. The Effects of Near Fault Ground Motions on Bridge Columns, *Proceedings of the FHWA/NCEER Workshop on the National Representation of Seismic Ground Motion for New and Existing Highway Facilities.* Burlingame, California, May.

Mander, J.B., M.J.N. Priestley, and R. Park, 1988. Theoretical Stress-Strain Model for Confined Concrete, *Journal of Structural Engineering, ASCE*, Vol. 114, pp. 1804 – 1826.

Paulay, T., and M.J.N Priestley, 1993. *Seismic Design of Concrete & Masonry Structures,* John Wiley & Sons, New York.

Priestley, M.J.N., F. Seible, and E.M. Calvi, 1996. *Seismic Design & Retrofit of Bridges,* John Wiley & Sons, New York.

Restrepo-Posada, J.I. 1993. "Seismic Behaviour of Connections Between Precast Concrete Elements," University of Canterbury, Christchurch, New Zealand.

Restrepo-Posada, J.I., L.L. Dodd, R. Park, and N. Cooke, 1994. Variables Affecting Cyclic Behavior of Reinforcing Steel, *Journal of Structural Engineering, ASCE*, Vol. 120, pp. 3178 – 3196.

SC Solutions, SEQMC SEQad Moment Curvature Analysis, http://www.best.com/~solvers/seqmc.html.

Somerville, P., 1997. The Characteristics and Quantification of Near Fault Ground Motion. *Proceedings of the FHWA/NCEER Workshop on the National Representation of Seismic Ground Motion for New and Existing Highway Facilities.* Burlingame, California, May.

Somerville, P., and R. Graves, 1993. Conditions that Give Rise to Unusually Large Long Period Ground Motions, *The Structural Design of Tall Buildings,* Vol. 2, pp. 211-232.

Tedesco, J.W., A. Ross, and S.T. Kuenneu, 1993. Experimental and Numerical Analysis of High Strain Rate Splitting Tensile Tests, *ACI Materials Journal,* Vol. 90, pp. 162 – 169.

Appendix

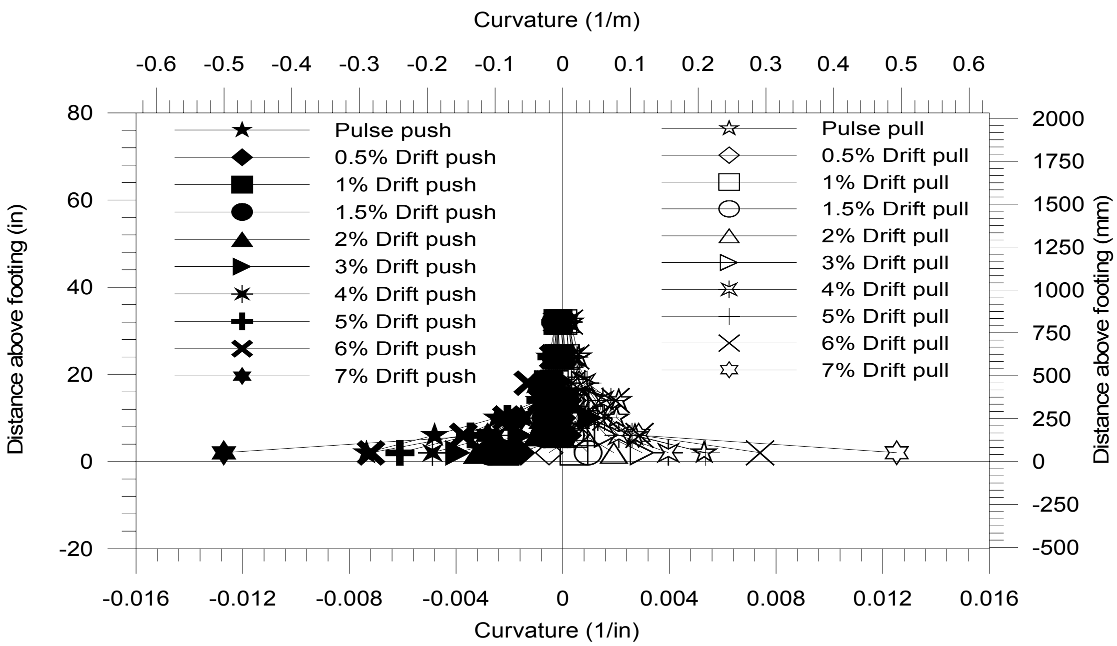

Fig. A.1 Curvature profile using fine discretization of potentiometers for Slow Test

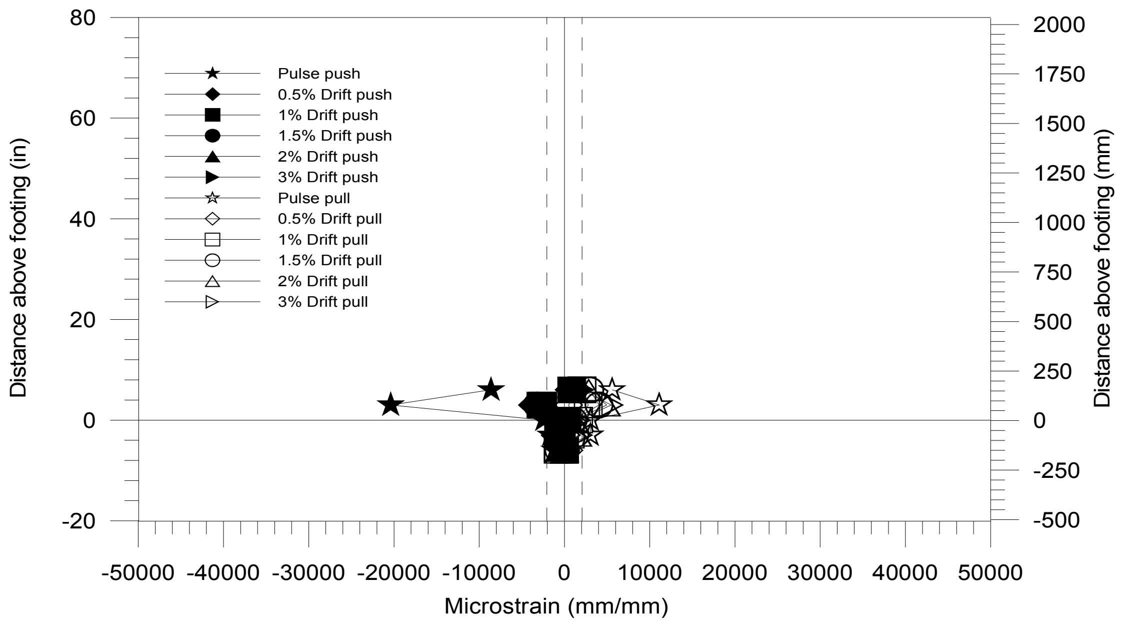

Fig. A.2 Longitudinal Bar A regular-yield for Slow Test

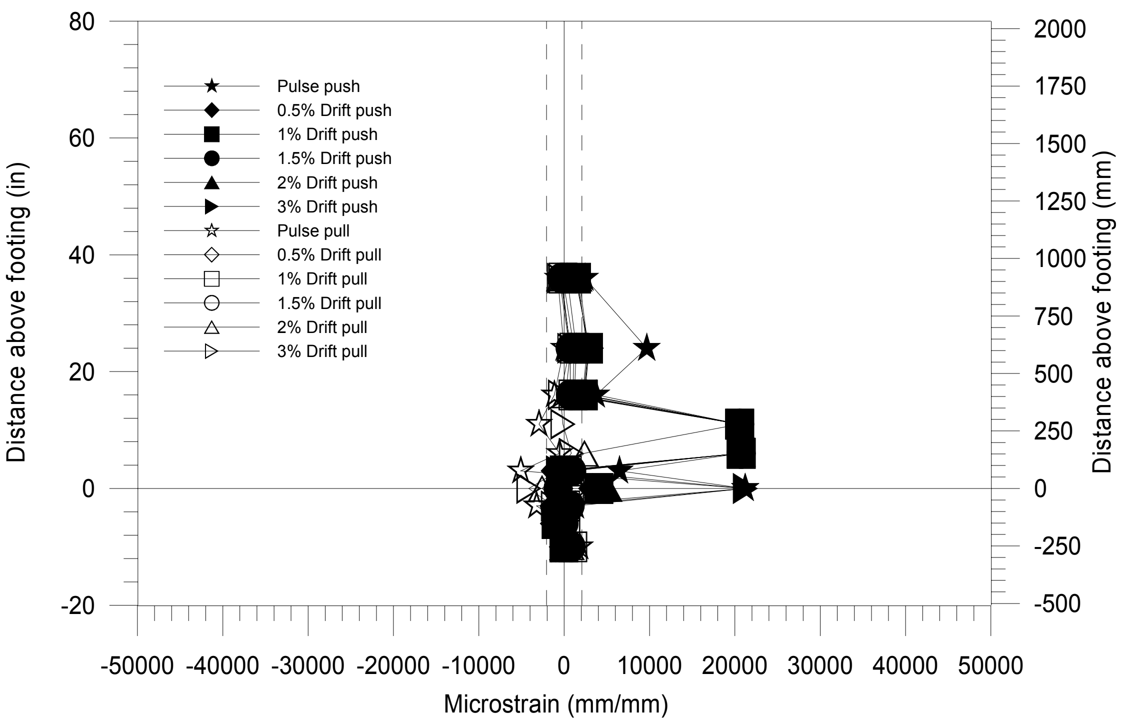

Fig. A.3 Longitudinal Bar C regular-yield for Slow Test

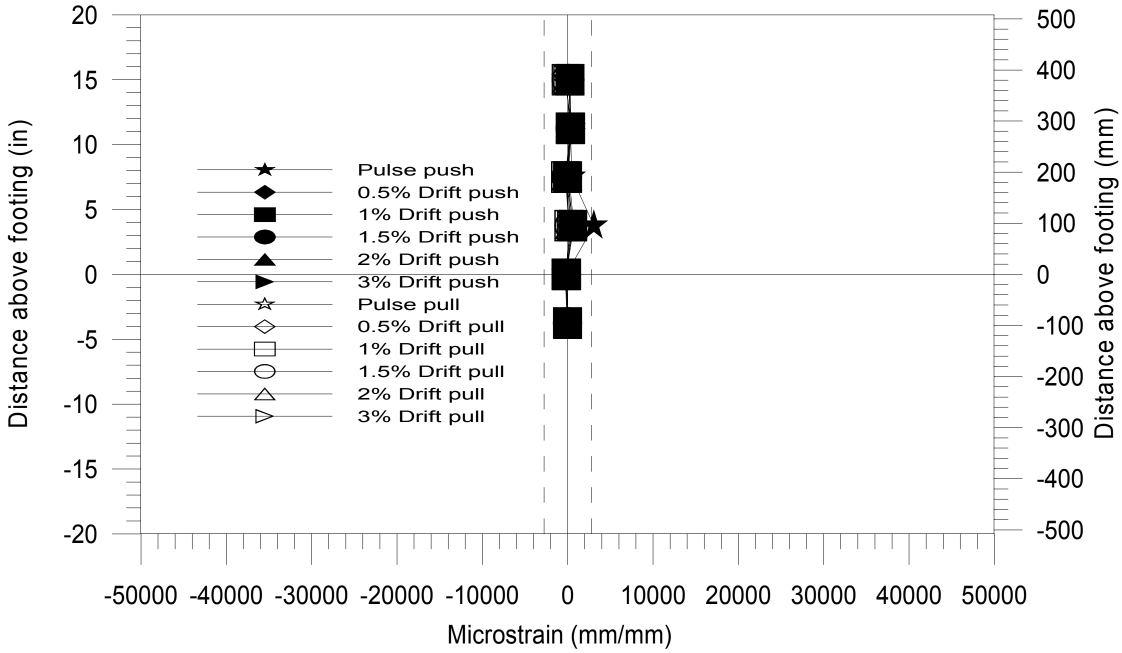

Fig. A.4 Spiral gauges at Location A for Slow Test

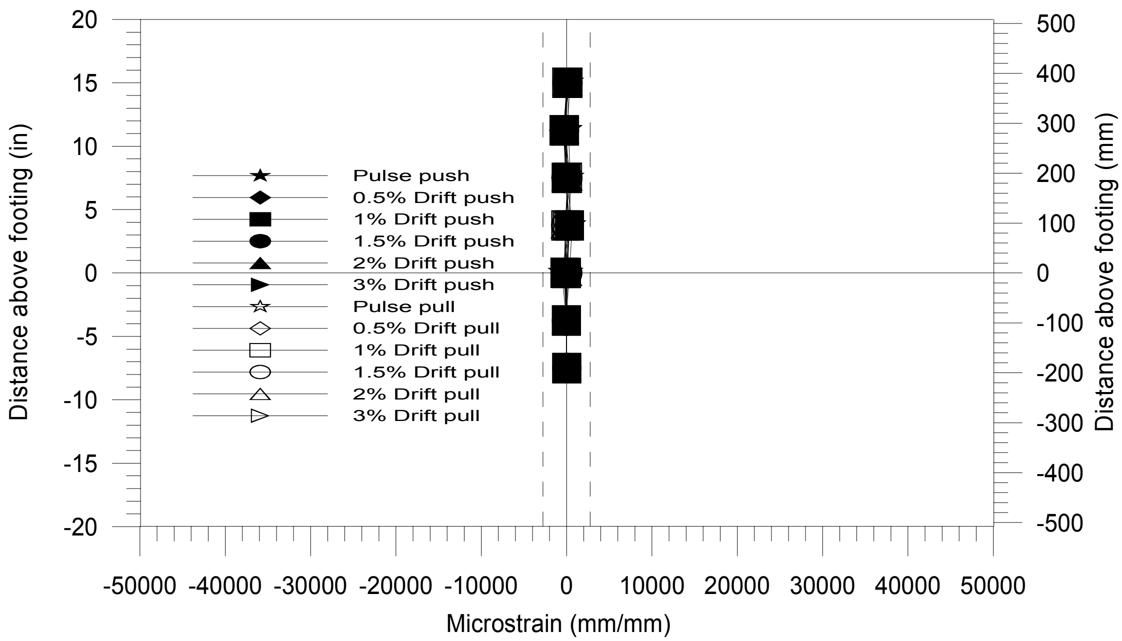

Fig. A.5 Spiral gauges at Location C for Slow Test

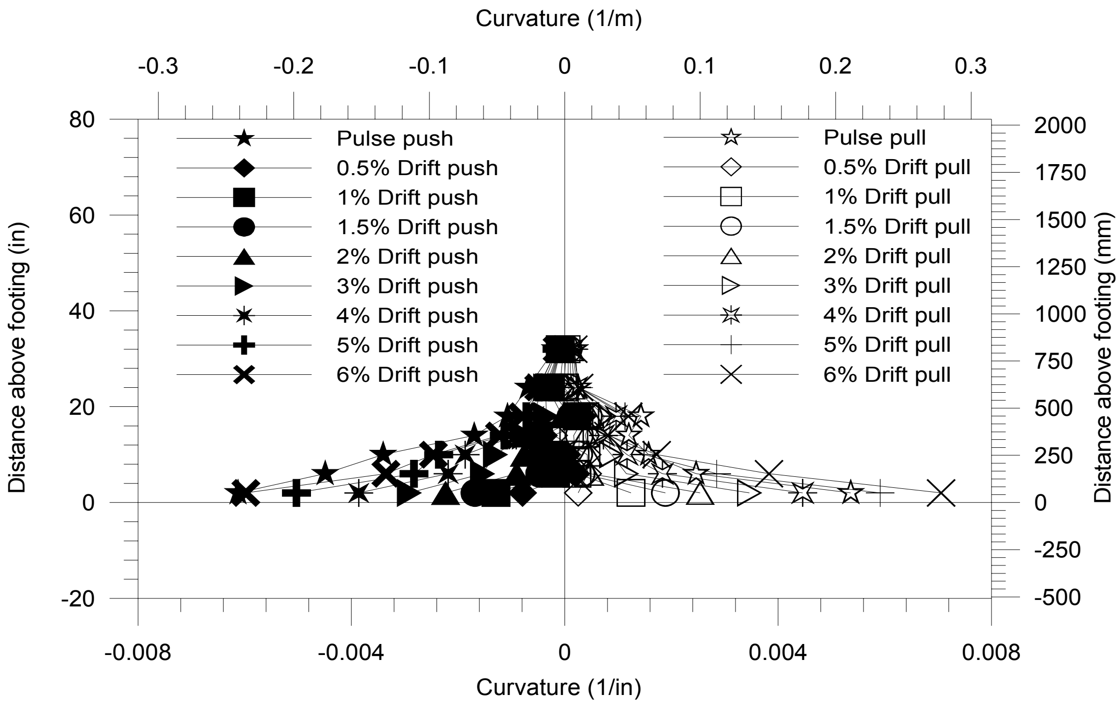

Fig. A.6 Curvature profile using fine discretization of potentiometers for Fast Test

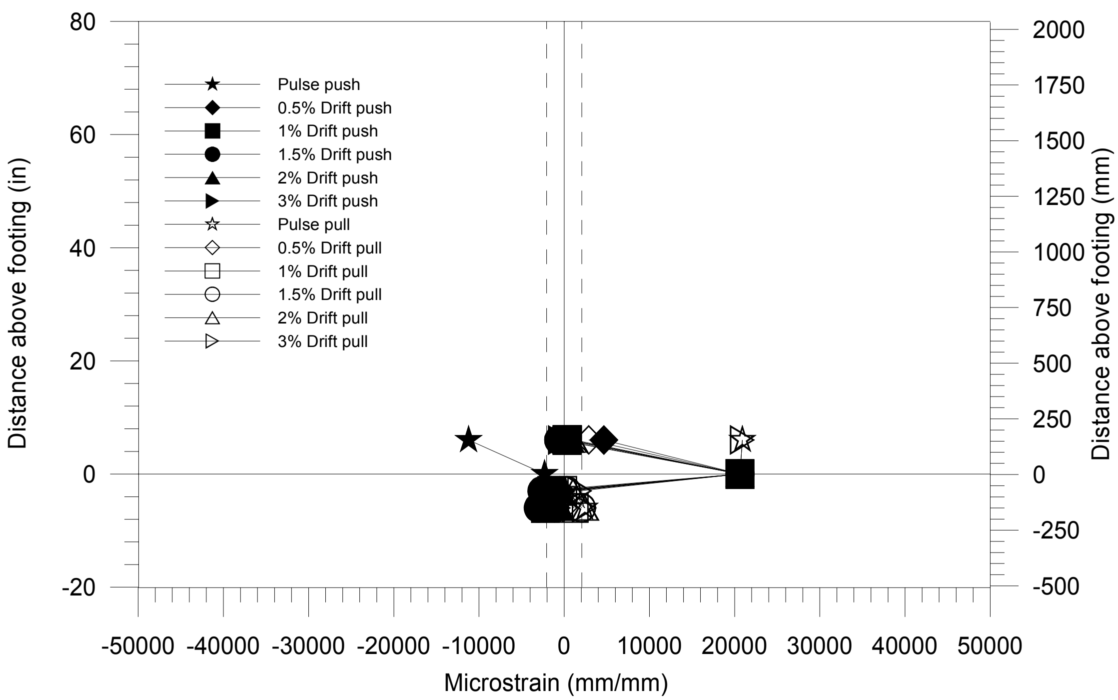

Fig. A.7 Longitudinal Bar A regular-yield for Fast Test

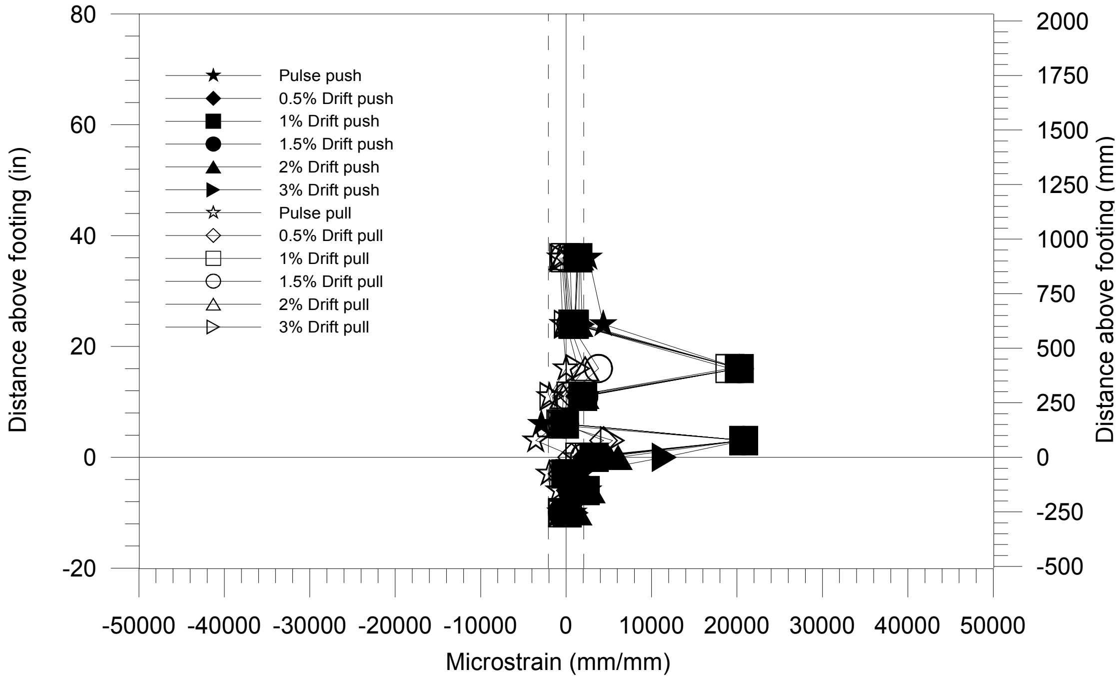

Fig. A.8 Longitudinal Bar C regular-yield for Fast Test

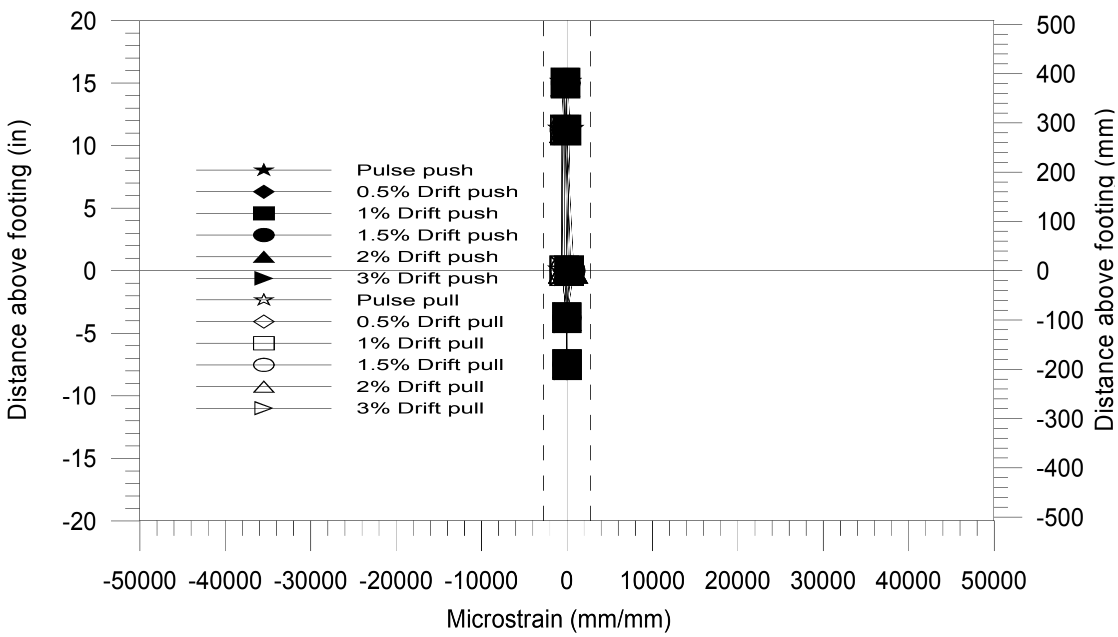

Fig. A.9 Spiral gauges at Location A for Fast Test

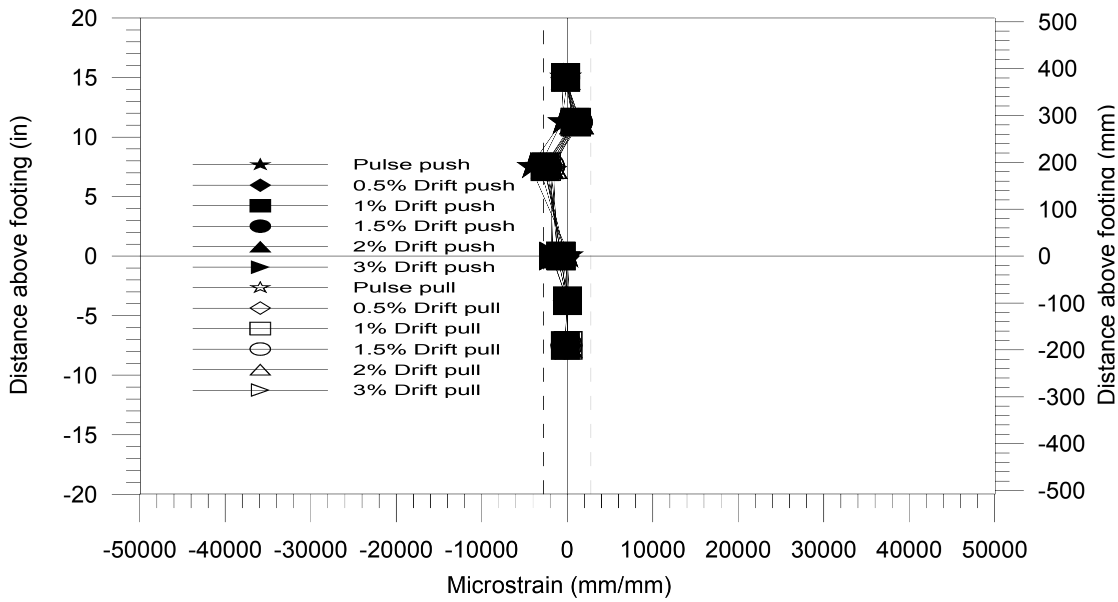

Fig. A.10 Spiral gauges at Location C for Fast Test

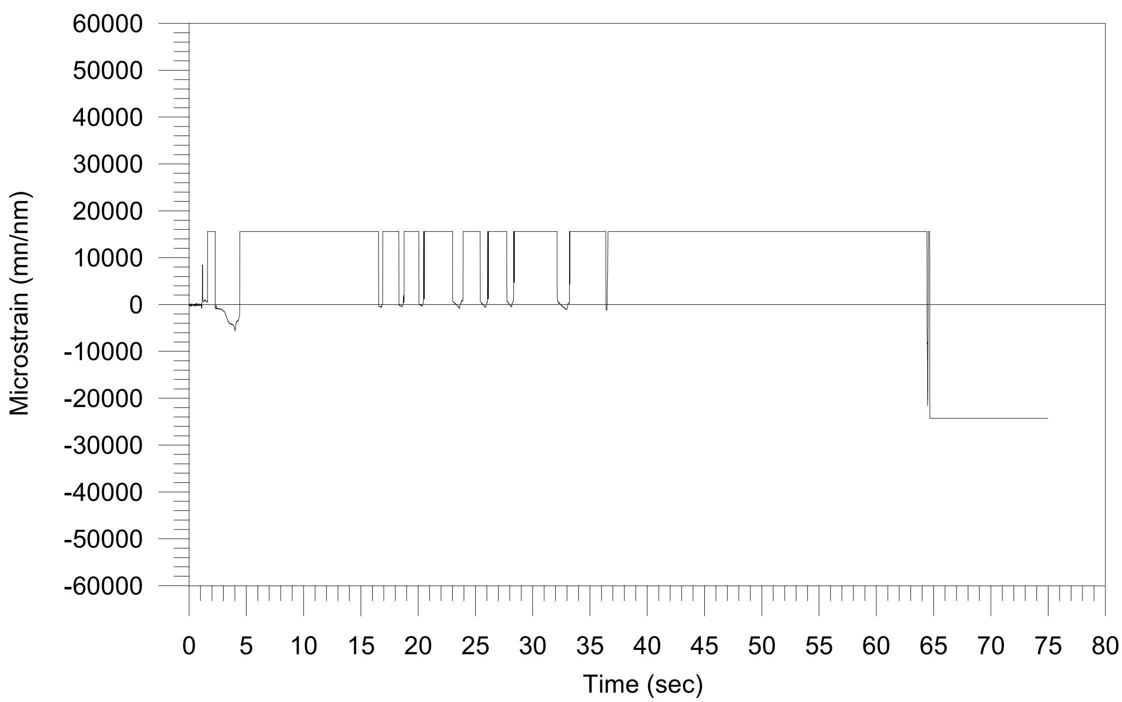

Fig. A.11 Longitudinal strain history Bar D at footing-column interface for Fast Test

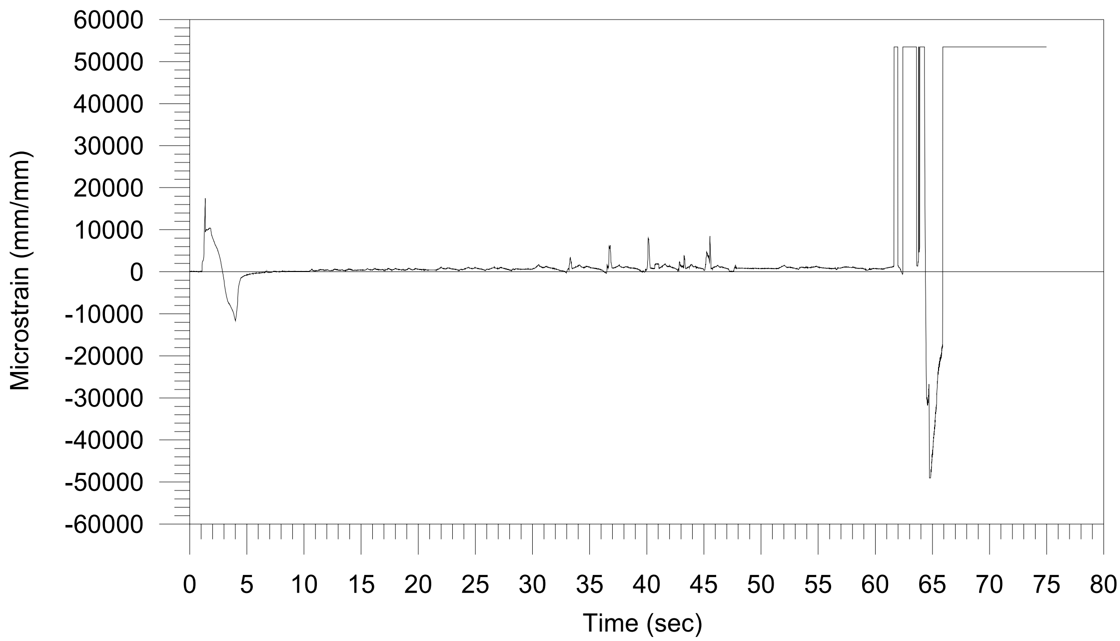

Fig. A.12 Longitudinal strain history Bar D at +76 mm for Fast Test

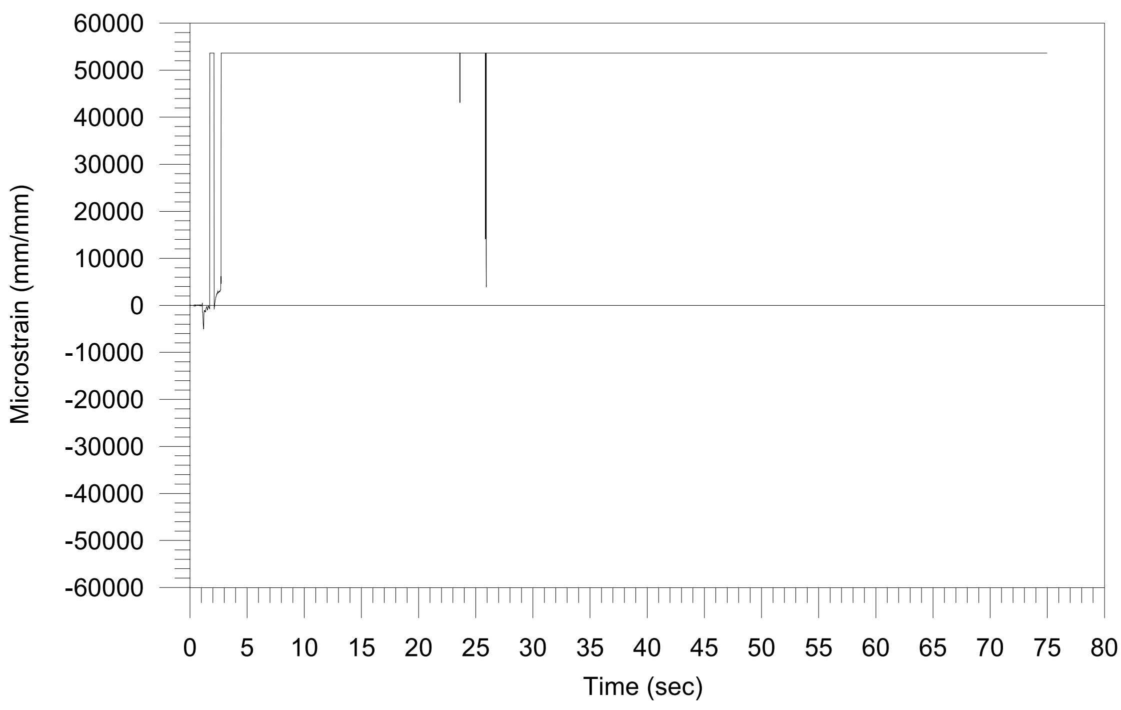

Fig. A.13 Longitudinal strain history Bar D at +152 mm for Fast Test

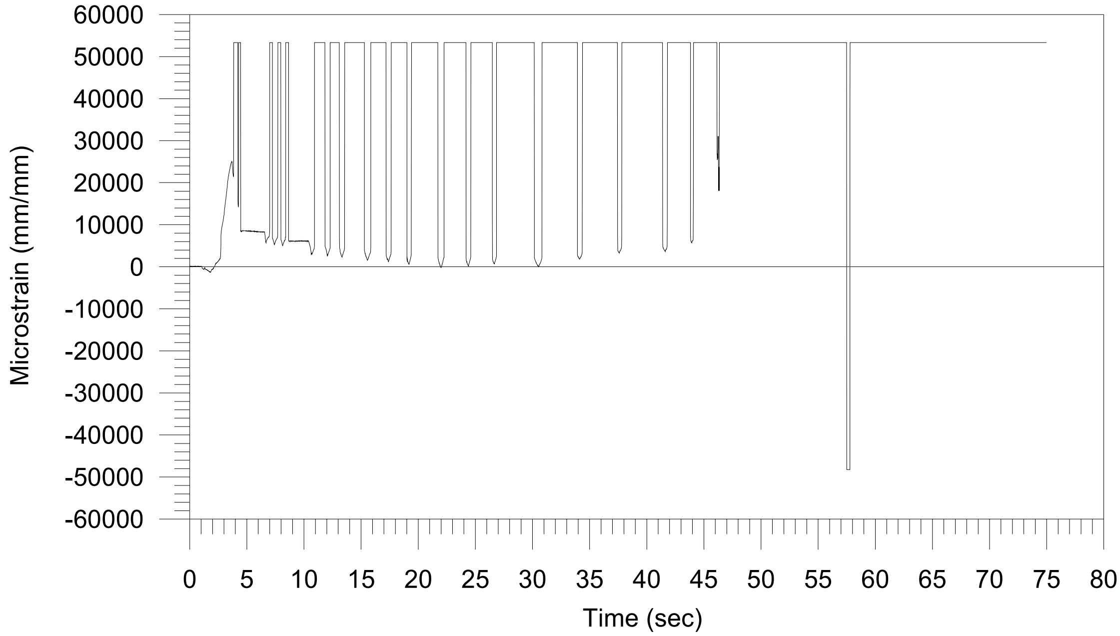

Fig. A.14 Longitudinal strain history Bar F at footing-column interface for Fast Test

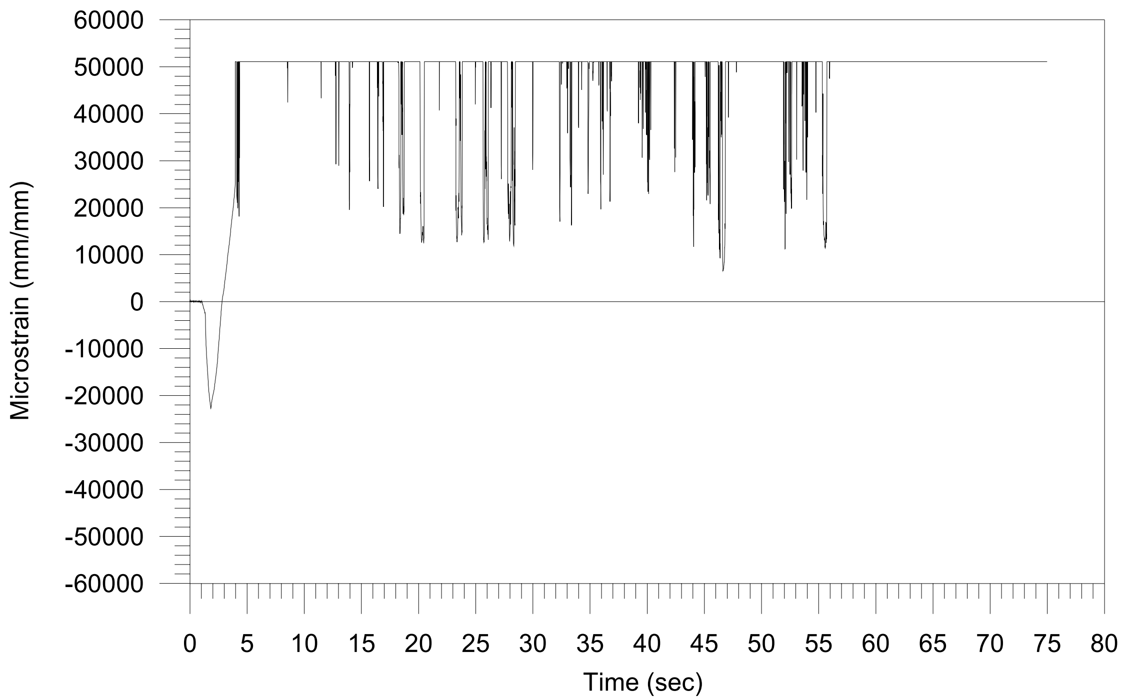

Fig. A.15 Longitudinal strain history Bar F at +76 mm for Fast Test

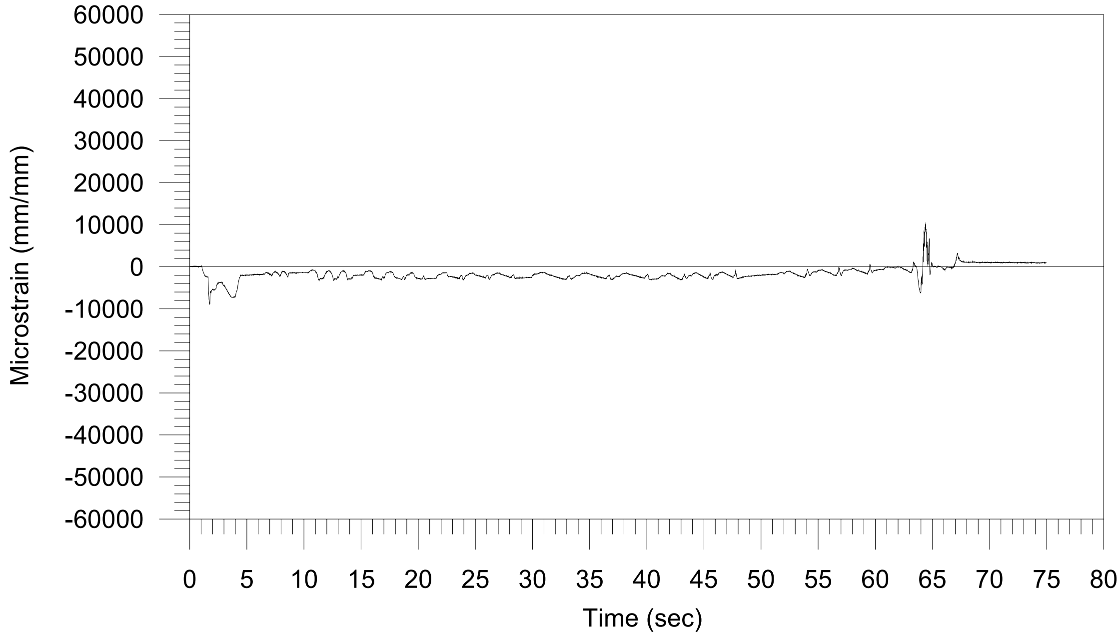

Fig. A.16 Longitudinal strain history Bar F at +152 mm for Fast Test

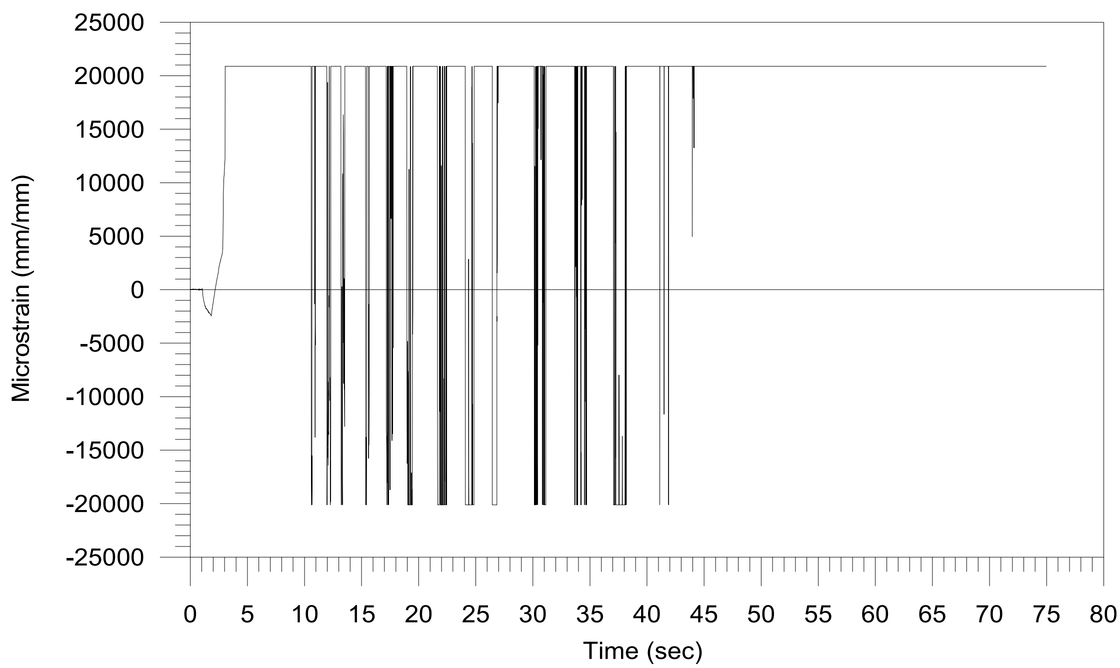

Fig. A.17 Longitudinal strain history Bar F at +279 mm for Fast Test

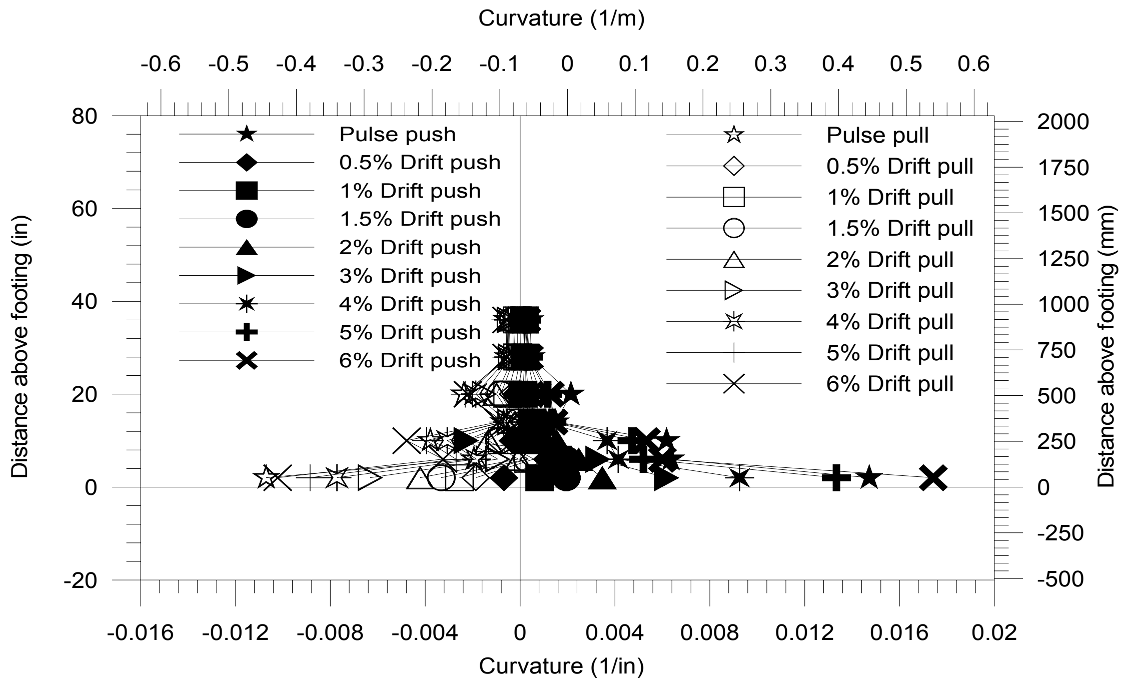

Fig. A.18 Curvature profile using fine discretization of potentiometers for Dynamic Test

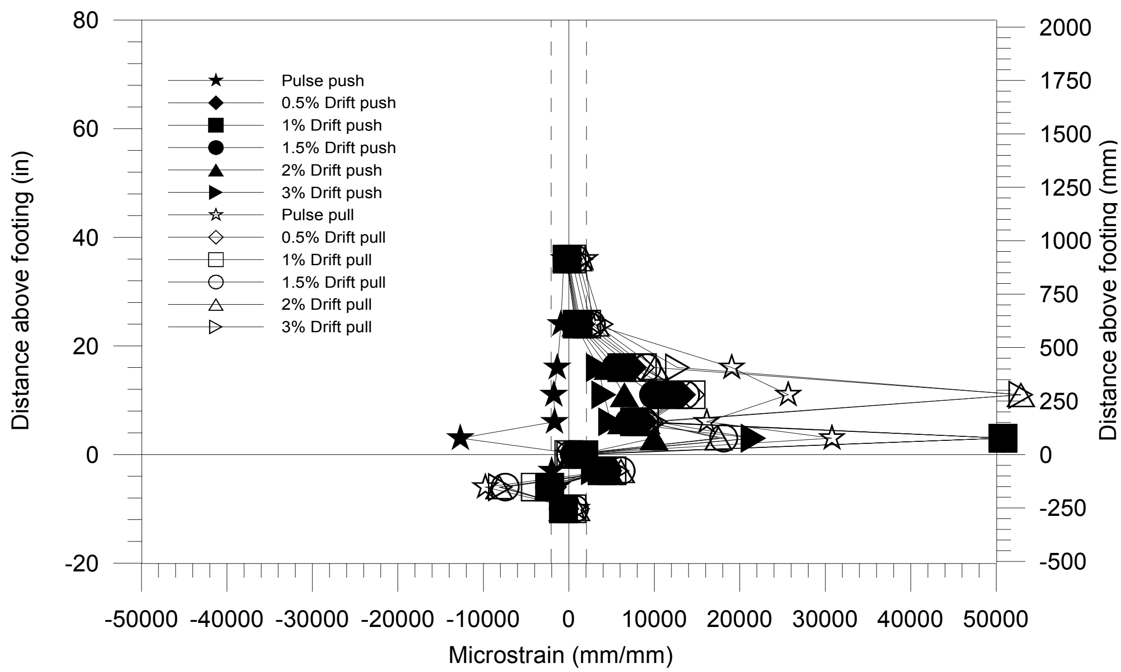

Fig. A.19 Longitudinal Bar D high-yield for Dynamic Test

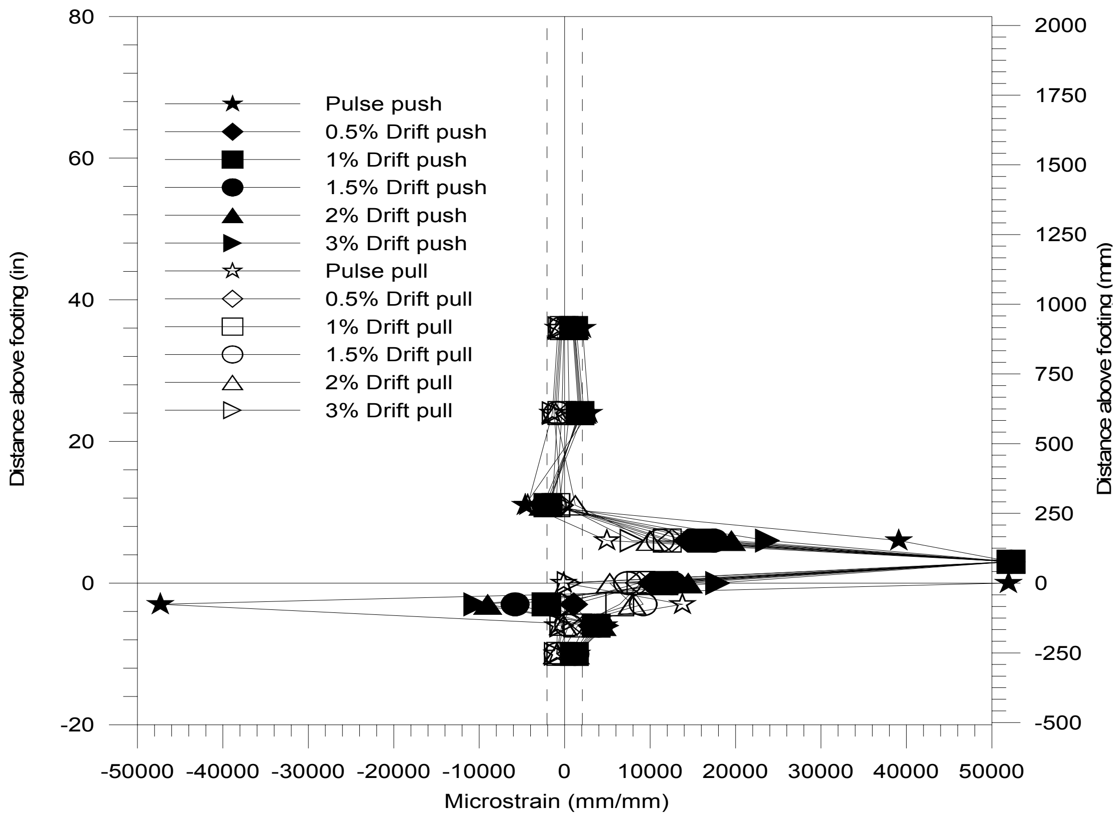

Fig. A.20 Longitudinal Bar F high-yield for Dynamic Test

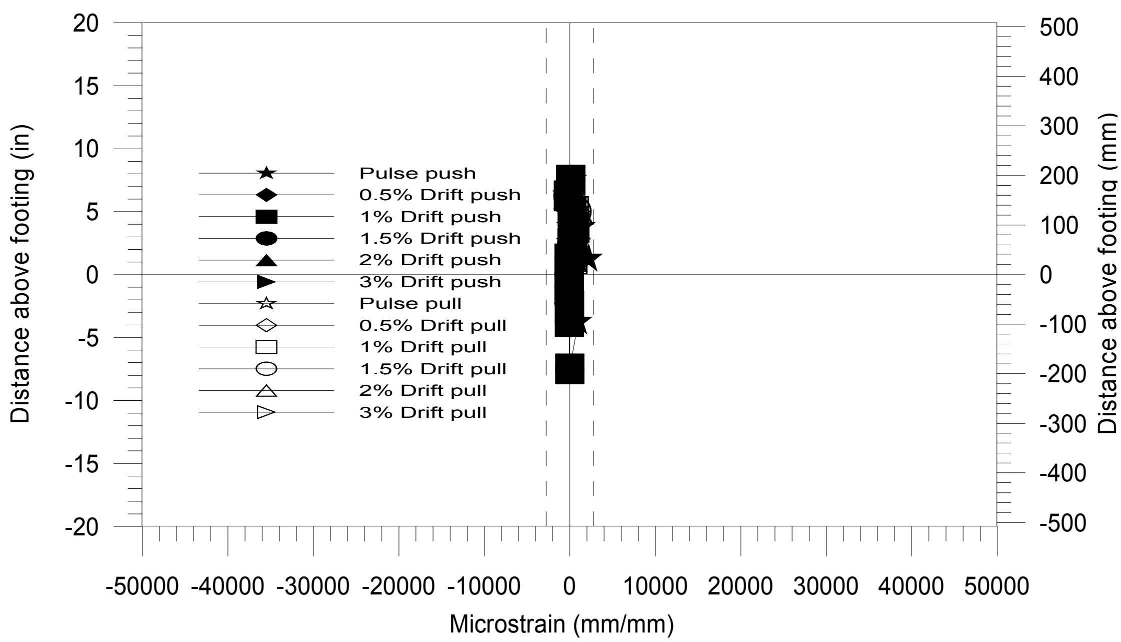

Fig. A.21 Spiral gauges at Location A for Dynamic Test

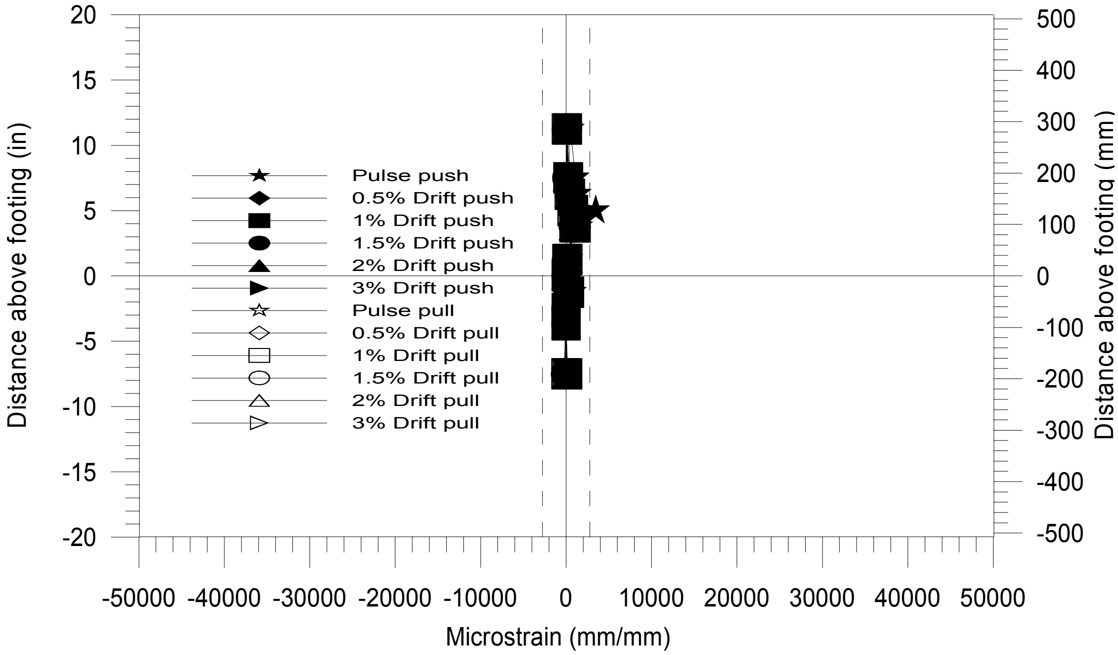

Fig. A.22 Spiral gauges at Location C for Dynamic Test

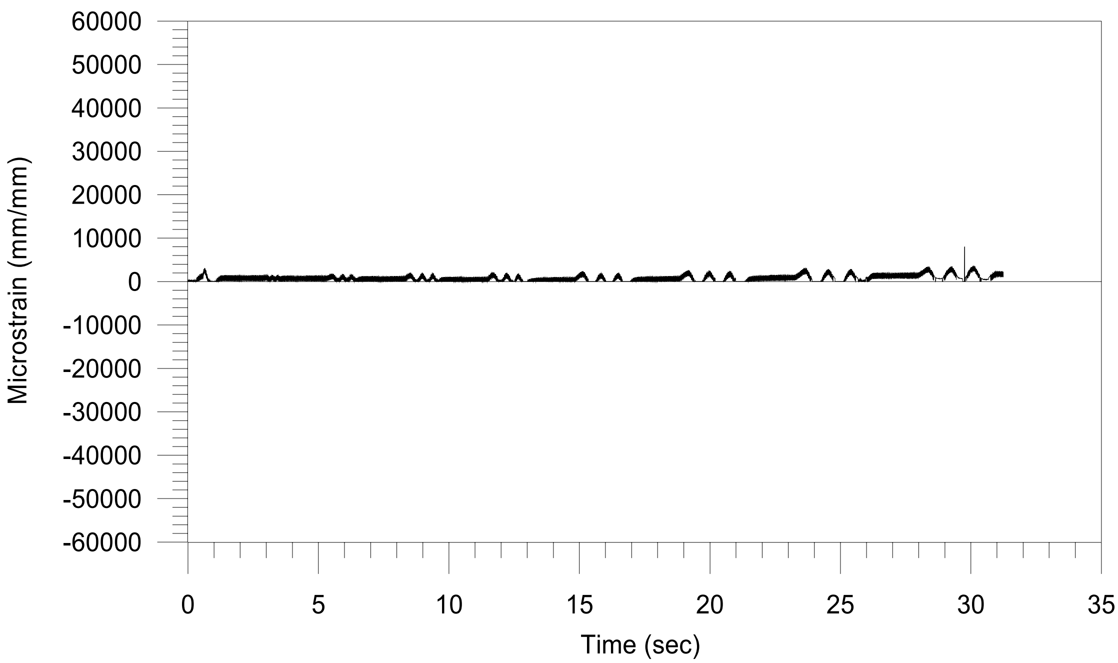

Fig.A.23 Longitudinal strain history Bar D at footing-column interface for Dynamic Test

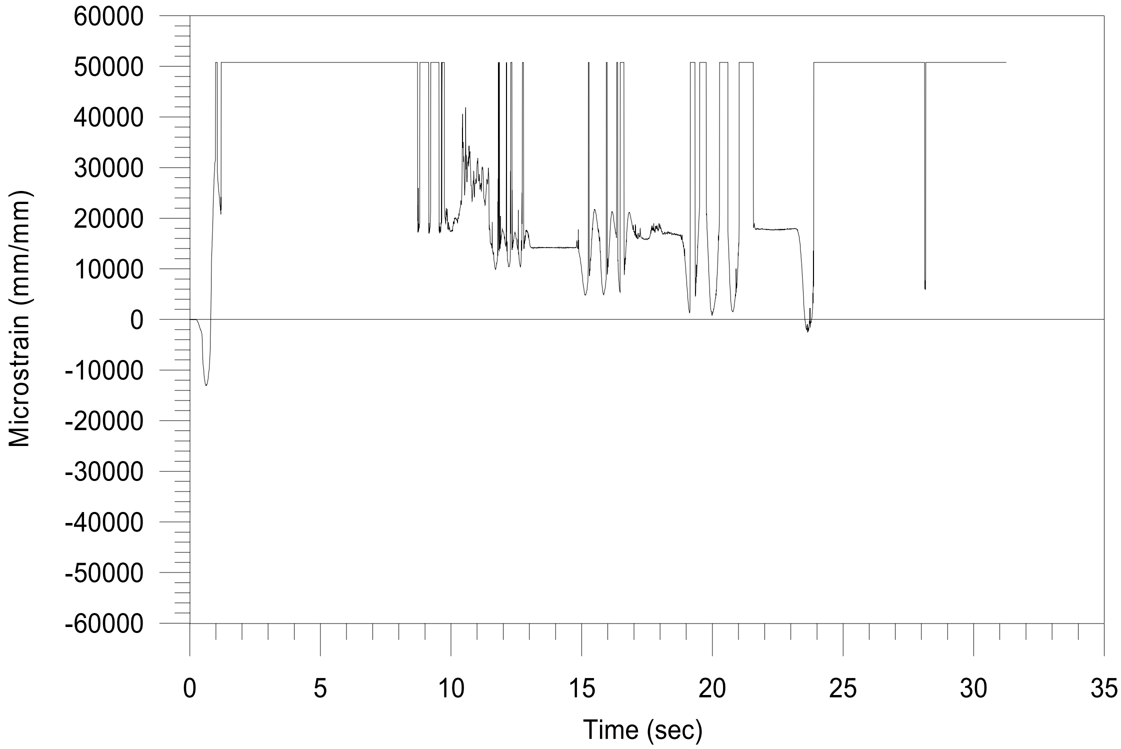

Fig. A.24 Longitudinal strain history Bar D at +76 mm for Dynamic Test

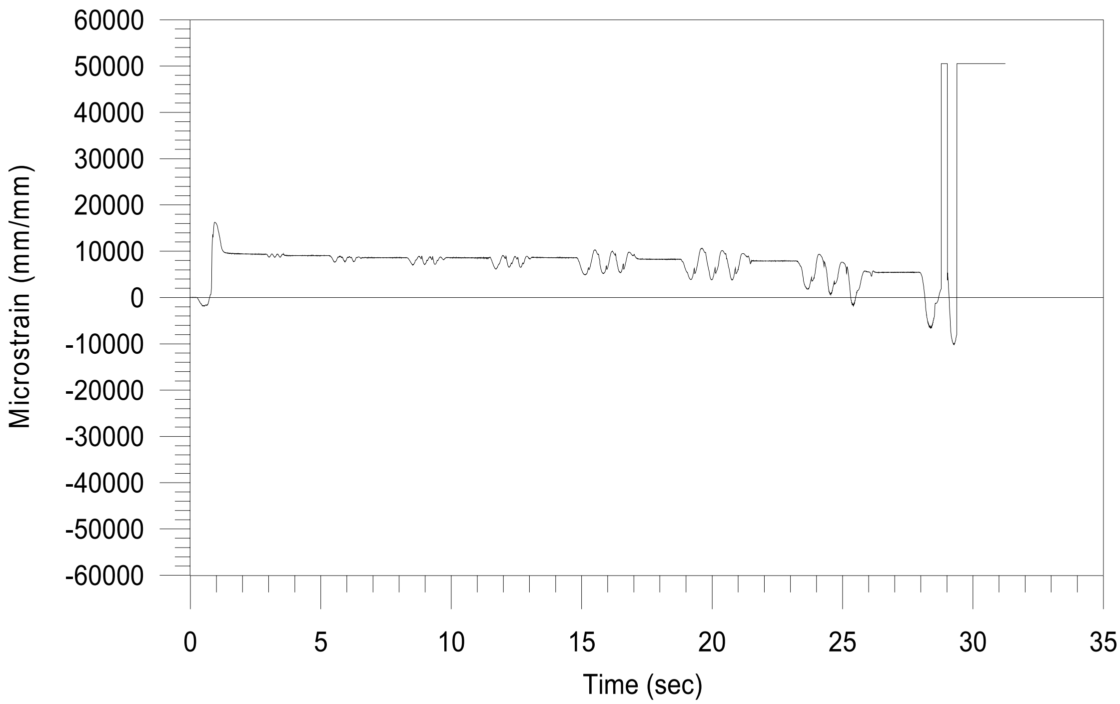

Fig. A.25 Longitudinal strain History Bar D at +152 mm for Dynamic Test

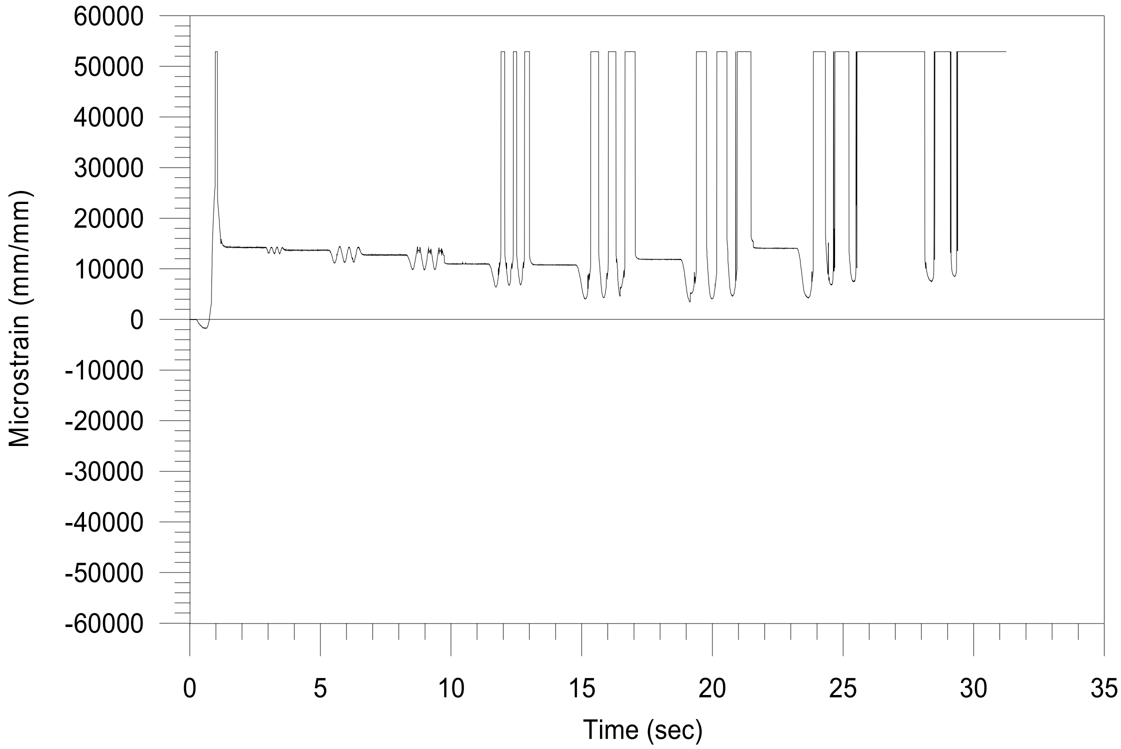

Fig. A.26 Longitudinal strain history Bar D at +279 mm for Dynamic Test

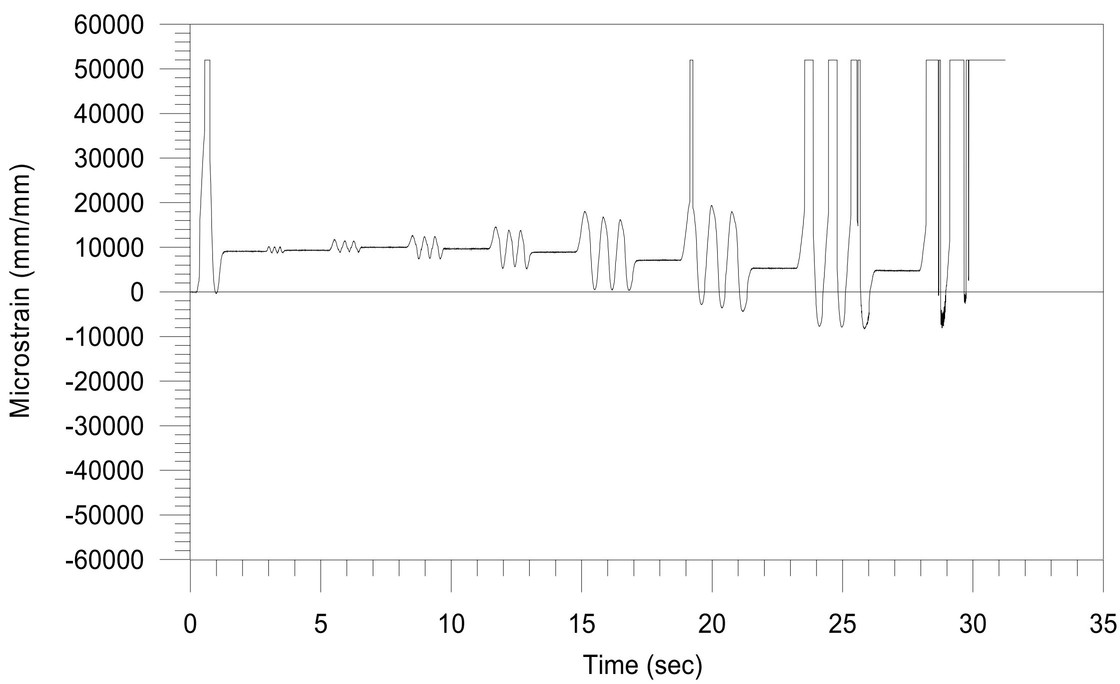

Fig. A.27 Longitudinal strain history Bar F at footing-Column Interface for Dynamic Test

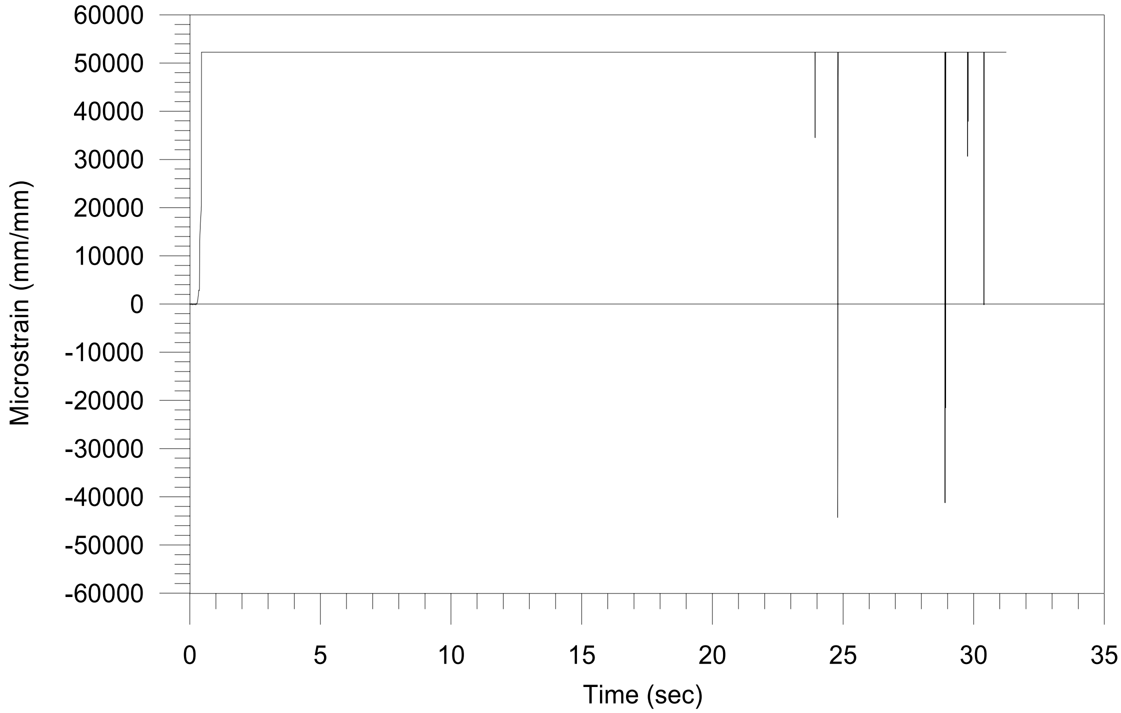

Fig. A.28 Longitudinal strain history Bar F at +76 mm for Dynamic Test

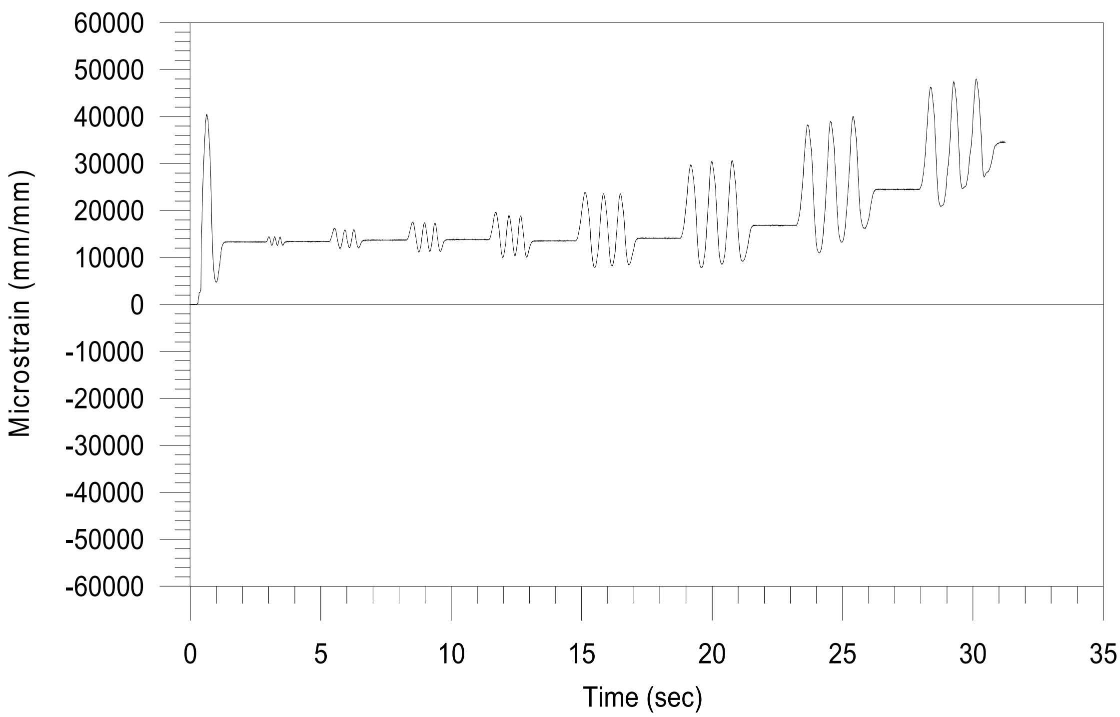

Fig. A.29 Longitudinal strain history Bar F at +152 mm for Dynamic Test

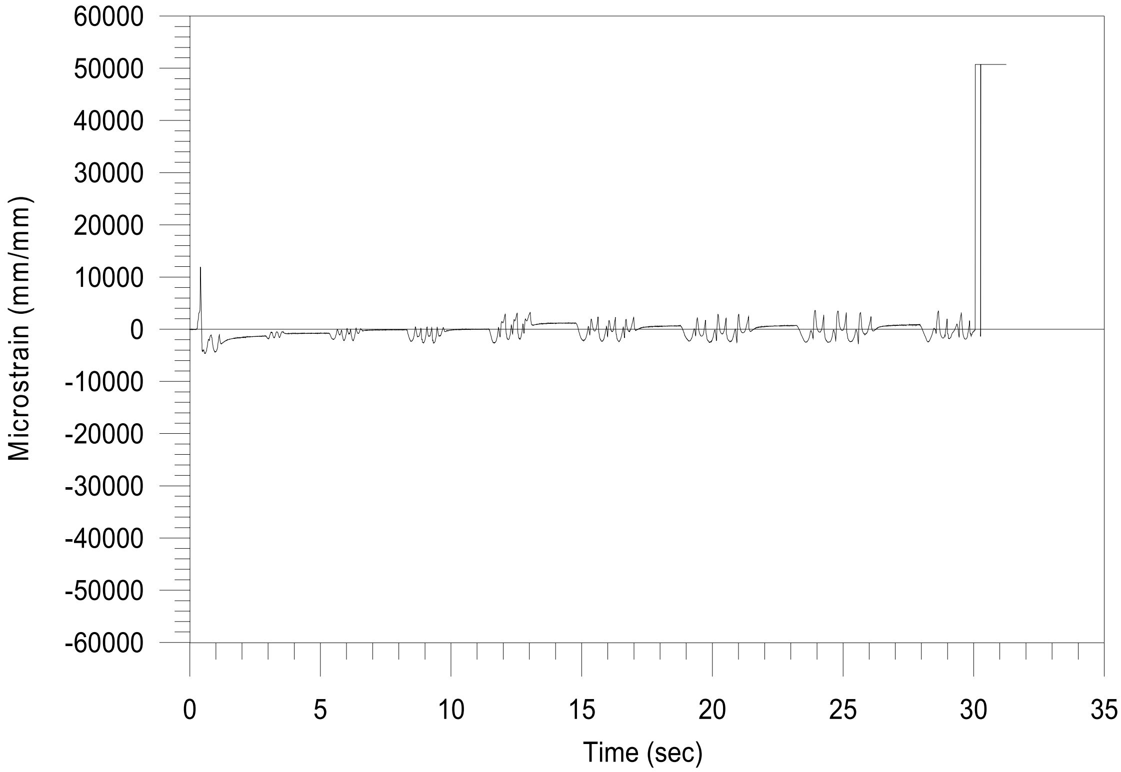

Fig. A.30 Longitudinal strain history Bar F at +279 mm for Dynamic Test

PEER REPORTS

PEER reports are available from the National Information Service for Earthquake Engineering (NISEE). To order PEER reports, please contact the Pacific Earthquake Engineering Research Center, 1301 South 46th Street, Richmond, California 94804-4698. Tel.: (510) 231-9468; Fax: (510) 231-9461.

PEER 2002/23 *Effects of Large Velocity Pulses on Reinforced Concrete Bridge Columns.* Greg L. Orozco and Scott A. Ashford. April 2002.

PEER 2002/22 *Characterization of Large Velocity Pulses for Laboratory Testing.* Kenneth E. Cox and Scott A. Ashford. April 2002.

PEER 2002/21 *Fourth U.S.-Japan Workshop on Performance-Based Earthquake Engineering Methodology for Reinforced Concrete Building Structures.* December 2002.

PEER 2002/20 *Barriers to Adoption and Implementation of PBEE Innovations.* Peter J. May. August 2002.

PEER 2002/19 *Economic-Engineered Integrated Models for Earthquakes: Socioeconomic Impacts.* Peter Gordon, James E. Moore II, and Harry W. Richardson. July 2002.

PEER 2002/18 *Assessment of Reinforced Concrete Building Exterior Joints with Substandard Details.* Chris P. Pantelides, Jon Hansen, Justin Nadauld, and Lawrence D. Reaveley. May 2002.

PEER 2002/17 *Structural Characterization and Seismic Response Analysis of a Highway Overcrossing Equipped with Elastomeric Bearings and Fluid Dampers: A Case Study.* Nicos Makris and Jian Zhang. November 2002.

PEER 2002/16 *Estimation of Uncertainty in Geotechnical Properties for Performance-Based Earthquake Engineering.* Allen L. Jones, Steven L. Kramer, and Pedro Arduino. December 2002.

PEER 2002/15 *Seismic Behavior of Bridge Columns Subjected to Various Loading Patterns.* Asadollah Esmaeily-Gh. and Yan Xiao. December 2002.

PEER 2002/14 *Inelastic Seismic Response of Extended Pile Shaft Supported Bridge Structures.* T.C. Hutchinson, R.W. Boulanger, Y.H. Chai, and I.M. Idriss. December 2002.

PEER 2002/13 *Probabilistic Models and Fragility Estimates for Bridge Components and Systems.* Paolo Gardoni, Armen Der Kiureghian, and Khalid M. Mosalam. June 2002.

PEER 2002/12 *Effects of Fault Dip and Slip Rake on Near-Source Ground Motions: Why Chi-Chi Was a Relatively Mild M7.6 Earthquake.* Brad T. Aagaard, John F. Hall, and Thomas H. Heaton. December 2002.

PEER 2002/11 *Analytical and Experimental Study of Fiber-Reinforced Strip Isolators*. James M. Kelly and Shakhzod M. Takhirov. September 2002.

PEER 2002/10 *Centrifuge Modeling of Settlement and Lateral Spreading with Comparisons to Numerical Analyses***.** Sivapalan Gajan and Bruce L. Kutter. January 2003.

PEER 2002/09 *Documentation and Analysis of Field Case Histories of Seismic Compression during the 1994 Northridge, California, Earthquake.* Jonathan P. Stewart, Patrick M. Smith, Daniel H. Whang, and Jonathan D. Bray. October 2002.

PEER 2002/08 *Component Testing, Stability Analysis and Characterization of Buckling-Restrained Unbonded Braces™.* Cameron Black, Nicos Makris, and Ian Aiken. September 2002.

PEER 2002/07 *Seismic Performance of Pile-Wharf Connections.* Charles W. Roeder, Robert Graff, Jennifer Soderstrom, and Jun Han Yoo. December 2001.

PEER 2002/06 *The Use of Benefit-Cost Analysis for Evaluation of Performance-Based Earthquake Engineering Decisions*. Richard O. Zerbe and Anthony Falit-Baiamonte. September 2001.

PEER 2002/05 *Guidelines, Specifications, and Seismic Performance Characterization of Nonstructural Building Components and Equipment*. André Filiatrault, Constantin Christopoulos, and Christopher Stearns. September 2001.

PEER 2002/04 *Consortium of Organizations for Strong-Motion Observation Systems and the Pacific Earthquake Engineering Research Center Lifelines Program: Invited Workshop on Archiving and Web Dissemination of Geotechnical Data, 4–5 October 2001*. September 2002.

PEER 2002/03 *Investigation of Sensitivity of Building Loss Estimates to Major Uncertain Variables for the Van Nuys Testbed.* Keith A. Porter, James L. Beck, and Rustem V. Shaikhutdinov. August 2002.

PEER 2002/02 *The Third U.S.-Japan Workshop on Performance-Based Earthquake Engineering Methodology for Reinforced Concrete Building Structures*. July 2002.

PEER 2002/01 *Nonstructural Loss Estimation: The UC Berkeley Case Study. Mary C. Comerio and John C. Stallmeyer.* December 2001.

PEER 2001/16 *Statistics of SDF-System Estimate of Roof Displacement for Pushover Analysis of Buildings.* Anil K. Chopra, Rakesh K. Goel, and Chatpan Chintanapakdee. December 2001.

PEER 2001/15 *Damage to Bridges during the 2001 Nisqually Earthquake.* R. Tyler Ranf, Marc O. Eberhard, and Michael P. Berry. November 2001.

PEER 2001/14 *Rocking Response of Equipment Anchored to a Base Foundation.* Nicos Makris and Cameron J. Black. September 2001.

PEER 2001/13 *Modeling Soil Liquefaction Hazards for Performance-Based Earthquake Engineering.* Steven L. Kramer and Ahmed-W. Elgamal. February 2001.

PEER 2001/12 *Development of Geotechnical Capabilities in OpenSees.* Boris Jeremic. September 2001.

PEER 2001/11 *Analytical and Experimental Study of Fiber-Reinforced Elastomeric Isolators*. James M. Kelly and Shakhzod M. Takhirov. September 2001.

PEER 2001/10 *Amplification Factors for Spectral Acceleration in Active Regions.* Jonathan P. Stewart, Andrew H. Liu, Yoojoong Choi, and Mehmet B. Baturay. December 2001.

PEER 2001/09 *Ground Motion Evaluation Procedures for Performance-Based Design.* Jonathan P. Stewart, Shyh-Jeng Chiou, Jonathan D. Bray, Robert W. Graves, Paul G. Somerville, and Norman A. Abrahamson. September 2001.

PEER 2001/08 *Experimental and Computational Evaluation of Reinforced Concrete Bridge Beam-Column Connections for Seismic Performance*. Clay J. Naito, Jack P. Moehle, and Khalid M. Mosalam. November 2001.

PEER 2001/07 *The Rocking Spectrum and the Shortcomings of Design Guidelines.* Nicos Makris and Dimitrios Konstantinidis. August 2001.

PEER 2001/06 *Development of an Electrical Substation Equipment Performance Database for Evaluation of Equipment Fragilities*. Thalia Agnanos. April 1999.

PEER 2001/05 *Stiffness Analysis of Fiber-Reinforced Elastomeric Isolators.* Hsiang-Chuan Tsai and James M. Kelly. May 2001.

PEER 2001/04 *Organizational and Societal Considerations for Performance-Based Earthquake Engineering.* Peter J. May. April 2001.

PEER 2001/03 *A Modal Pushover Analysis Procedure to Estimate Seismic Demands for Buildings: Theory and Preliminary Evaluation.* Anil K. Chopra and Rakesh K. Goel. January 2001.

PEER 2001/02 *Seismic Response Analysis of Highway Overcrossings Including Soil-Structure Interaction.* Jian Zhang and Nicos Makris. March 2001.

PEER 2001/01 *Experimental Study of Large Seismic Steel Beam-to-Column Connections.* Egor P. Popov and Shakhzod M. Takhirov. November 2000.

PEER 2000/10 *The Second U.S.-Japan Workshop on Performance-Based Earthquake Engineering Methodology for Reinforced Concrete Building Structures.* March 2000.

PEER 2000/09 *Structural Engineering Reconnaissance of the August 17, 1999 Earthquake: Kocaeli (Izmit), Turkey.* Halil Sezen, Kenneth J. Elwood, Andrew S. Whittaker, Khalid Mosalam, John J. Wallace, and John F. Stanton. December 2000.

PEER 2000/08 *Behavior of Reinforced Concrete Bridge Columns Having Varying Aspect Ratios and Varying Lengths of Confinement.* Anthony J. Calderone, Dawn E. Lehman, and Jack P. Moehle. January 2001.

PEER 2000/07 *Cover-Plate and Flange-Plate Reinforced Steel Moment-Resisting Connections.* Taejin Kim, Andrew S. Whittaker, Amir S. Gilani, Vitelmo V. Bertero, and Shakhzod M. Takhirov. September 2000.

PEER 2000/06 *Seismic Evaluation and Analysis of 230-kV Disconnect Switches.* Amir S. J. Gilani, Andrew S. Whittaker, Gregory L. Fenves, Chun-Hao Chen, Henry Ho, and Eric Fujisaki. July 2000.

PEER 2000/05 *Performance-Based Evaluation of Exterior Reinforced Concrete Building Joints for Seismic Excitation.* Chandra Clyde, Chris P. Pantelides, and Lawrence D. Reaveley. July 2000.

PEER 2000/04 *An Evaluation of Seismic Energy Demand: An Attenuation Approach.* Chung-Che Chou and Chia-Ming Uang. July 1999.

PEER 2000/03 *Framing Earthquake Retrofitting Decisions: The Case of Hillside Homes in Los Angeles.* Detlof von Winterfeldt, Nels Roselund, and Alicia Kitsuse. March 2000.

PEER 2000/02 *U.S.-Japan Workshop on the Effects of Near-Field Earthquake Shaking.* Andrew Whittaker, ed. July 2000.

PEER 2000/01 *Further Studies on Seismic Interaction in Interconnected Electrical Substation Equipment.* Armen Der Kiureghian, Kee-Jeung Hong, and Jerome L. Sackman. November 1999.

PEER 1999/14 *Seismic Evaluation and Retrofit of 230-kV Porcelain Transformer Bushings*. Amir S. Gilani, Andrew S. Whittaker, Gregory L. Fenves, and Eric Fujisaki. December 1999.

PEER 1999/13 *Building Vulnerability Studies: Modeling and Evaluation of Tilt-up and Steel Reinforced Concrete Buildings.* John W. Wallace, Jonathan P. Stewart, and Andrew S. Whittaker, editors. December 1999.

PEER 1999/12 *Rehabilitation of Nonductile RC Frame Building Using Encasement Plates and Energy-Dissipating Devices.* Mehrdad Sasani, Vitelmo V. Bertero, James C. Anderson. December 1999.

PEER 1999/11 *Performance Evaluation Database for Concrete Bridge Components and Systems under Simulated Seismic Loads.* Yael D. Hose and Frieder Seible. November 1999.

PEER 1999/10 *U.S.-Japan Workshop on Performance-Based Earthquake Engineering Methodology for Reinforced Concrete Building Structures.* December 1999.

PEER 1999/09 *Performance Improvement of Long Period Building Structures Subjected to Severe Pulse-Type Ground Motions*. James C. Anderson, Vitelmo V. Bertero, and Raul Bertero. October 1999.

PEER 1999/08 *Envelopes for Seismic Response Vectors.* Charles Menun and Armen Der Kiureghian. July 1999.

PEER 1999/07 *Documentation of Strengths and Weaknesses of Current Computer Analysis Methods for Seismic Performance of Reinforced Concrete Members.* William F. Cofer. November 1999.

PEER 1999/06 *Rocking Response and Overturning of Anchored Equipment under Seismic Excitations.* Nicos Makris and Jian Zhang. November 1999.

PEER 1999/05 *Seismic Evaluation of 550 kV Porcelain Transformer Bushings.* Amir S. Gilani, Andrew S. Whittaker, Gregory L. Fenves, and Eric Fujisaki. October 1999.

PEER 1999/04 *Adoption and Enforcement of Earthquake Risk-Reduction Measures.* Peter J. May, Raymond J. Burby, T. Jens Feeley, and Robert Wood.

PEER 1999/03 *Task 3 Characterization of Site Response General Site Categories*. Adrian Rodriguez-Marek, Jonathan D. Bray, and Norman Abrahamson. February 1999.

PEER 1999/02 *Capacity-Demand-Diagram Methods for Estimating Seismic Deformation of Inelastic Structures: SDF Systems*. Anil K. Chopra and Rakesh Goel. April 1999.

PEER 1999/01 *Interaction in Interconnected Electrical Substation Equipment Subjected to Earthquake Ground Motions.* Armen Der Kiureghian, Jerome L. Sackman, and Kee-Jeung Hong. February 1999.

PEER 1998/08 *Behavior and Failure Analysis of a Multiple-Frame Highway Bridge in the 1994 Northridge Earthquake.* Gregory L. Fenves and Michael Ellery. December 1998.

PEER 1998/07 *Empirical Evaluation of Inertial Soil-Structure Interaction Effects.* Jonathan P. Stewart, Raymond B. Seed, and Gregory L. Fenves. November 1998.

PEER 1998/06 *Effect of Damping Mechanisms on the Response of Seismic Isolated Structures.* Nicos Makris and Shih-Po Chang. November 1998.

PEER 1998/05 *Rocking Response and Overturning of Equipment under Horizontal Pulse-Type Motions.* Nicos Makris and Yiannis Roussos. October 1998.

PEER 1998/04 *Pacific Earthquake Engineering Research Invitational Workshop Proceedings, May 14–15, 1998: Defining the Links between Planning, Policy Analysis, Economics and Earthquake Engineering.* Mary Comerio and Peter Gordon. September 1998.

PEER 1998/03 *Repair/Upgrade Procedures for Welded Beam to Column Connections.* James C. Anderson and Xiaojing Duan. May 1998.

PEER 1998/02 *Seismic Evaluation of 196 kV Porcelain Transformer Bushings.* Amir S. Gilani, Juan W. Chavez, Gregory L. Fenves, and Andrew S. Whittaker. May 1998.

PEER 1998/01 *Seismic Performance of Well-Confined Concrete Bridge Columns.* Dawn E. Lehman and Jack P. Moehle. December 2000.